Phase Transitions in Classical Systems: Anisotropic Models, Computational Methods, and Universality Predictions

Von der Fakultät für Mathematik, Informatik und Naturwissenschaften der RWTH Aachen University zur Erlangung des akademischen Grades eines Doktors der Naturwissenschaften genehmigte Dissertation

vorgelegt von

Florian Kischel, M.Sc.

aus

Essen, Deutschland

Berichter: Univ.-Prof. Stefan Weßel, Ph.D.
Prof. Dr. rer. nat. Moritz Helias

Tag der mündlichen Prüfung: 14.06.2024

Abstract

This thesis is mostly concerned with phase transitions in classical systems, with a focus on the anisotropic Ising model in two dimensions and on parallelogram lattices. After first discussing the history of phase transitions and specifically how anisotropies were treated in the renormalization group approach, an introduction to multi-parameter universality is given. This is followed by a derivation, using anti-commuting Grassmann variables, of the exact solution of the fully anisotropic $2d$ Ising model on a finite parallelogram lattice for all temperatures and couplings; from there, the scaling function near the critical point in the ferromagnetic regime is recovered. Additionally, some predictions made by multi-parameter universality regarding non-universal prefactors, modular invariance and behavior at criticality are confirmed. Finally, the strip limit of the model is discussed and connections to previous results of more restricted cases are made.

In the next chapter, the investigation of anisotropic systems in $2d$ is continued, now by discussing the q-state Potts model and attempting to measure its angle dependent correlation lengths, a characterizing quantity according to multi-parameter universality, via an tensor network approach. More specifically, the Corner Transfer Matrix Renormalization Group (CTMRG) algorithm is used to numerically extract the quantities of interest. A range of checks and comparisons to the few exactly known results are made to ensure a continued high accuracy of the simulation method.

Finally, the discrete to continuous crossover behavior in a modified $3d$ clock model, a relative of the Potts model, is investigated. This model exhibits a first order phase transition between an ordered and disordered phase and, based on prior work, predictions can be made for how much the phases contribute at the transition point when the clock has either three different states or, on the other extreme, infinitely many. This behavior is simulated at and between these extremes using the Wang-Landau Monte Carlo algorithm, which is very well suited for systems that exhibit complicated energy distributions, as present near and at first order phase transitions. A wide range of system sizes are simulated and care is taken to carefully determine the bulk transition temperature on which the accuracy of the final results depends very crucially.

Zusammenfassung

Diese Arbeit beschäftigt sich mit Phasenübergängen in klassischen Systemen mit Schwerpunkt auf dem anisotropen Ising-Modell in zwei Dimensionen auf Parallelogramm-Gittern. Nach einer ersten Diskussion der Forschungshistorie von Phasenübergänge und speziell wie Anisotropien in der Renormierungsgruppentheorie behandelt wurden, wird eine Einführung in die Mehrparameter-Universalität (multi-parameter universality) gegeben. Es folgt die Ableitung der exakten Lösung des vollständig anisotropen $2d$-Ising-Modells auf einem endlichen Parallelogramm-Gitter bei allen Temperaturen und Kopplungen mit Hilfe von nicht-kommutierenden Grassmann-Variablen. Von dort wird die Skalierungsfunktion in der Nähe des kritischen Punktes im ferromagnetischen Bereich hergeleitet. Zusätzlich werden einige Vorhersagen der Mehrparameter-Universalität in Bezug auf nicht-universelle Vorfaktoren, modulare Invarianz und Verhalten direkt am kritischen Punkt bestätigt. Schließlich wird der Streifenlimes des Modells diskutiert und Verbindungen zu vorherigen Ergebnissen von Spezialfällen hergestellt.

Im nächsten Kapitel wird die Untersuchung von anisotropen Systemen in $2d$ durch die Diskussion des Potts-Modells mit q Zuständen fortgesetzt und der Versuch seine winkelabhängigen Korrelationslängen, eine charakterisierende Größe gemäß der Mehrparameter-Universalität, über einen Tensor-Netzwerk-Ansatz zu bestimmen, präsentiert. Genauer gesagt, wird der Corner Transfer Matrix Renormalization Group (CTMRG) Algorithmus verwendet, um die relevanten Größen numerisch zu extrahieren. Eine Reihe von Überprüfungen und Vergleichen mit den wenigen, exakten Ergebnissen werden durchgeführt, um die fortlaufend hohe Genauigkeit der Simulationsmethode zu gewährleisten.

Schließlich wird das Übergangsverhalten von diskreten zu kontinuierlichen Freiheitsgeraden in einem modifizierten $3d$-Uhren-Modell (Clock model), einem Verwandten des Potts-Modells, untersucht. Dieses Modell zeigt einen Phasenübergang erster Ordnung zwischen einer geordneten und einer ungeordneten Phase und, basierend auf vorherigen Arbeiten, können Vorhersagen gemacht werden, in welchem Umfang die Phasen am Übergangspunkt beitragen, wenn die Uhr entweder drei verschiedene Zustände hat oder, am anderen Extrem, unendlich viele. Dieses Verhalten wird an und zwischen diesen Extremen mit dem Wang-Landau-Monte-Carlo-Algorithmus simuliert, der sehr gut für Systeme geeignet ist, welche komplizierte Energieverteilungen aufweisen, wie sie in der Nähe und bei Übergängen erster Ordnung auftreten. Eine breite Palette von Systemgrößen wird simuliert und besondere Sorgfalt wird darauf verwendet, den Übergangspunkt im thermodynamischen Limes sorgfältig zu bestimmen, da von diesem die Genauigkeit der Endresultate stark abhängt.

Eidesstattliche Erklärung

Florian Kischel erklärt hiermit, dass diese Dissertation und die darin dargelegten Inhalte die eigenen sind und selbstständig, als Ergebnis der eigenen originären Forschung, generiert wurden.

Hiermit erkläre ich an Eides statt

1. Diese Arbeit wurde vollständig oder größtenteils in der Phase als Doktorand dieser Fakultät und Universität angefertigt;
2. Sofern irgendein Bestandteil dieser Dissertation zuvor für einen akademischen Abschluss oder eine andere Qualifikation an dieser oder einer anderen Institution verwendet wurde, wurde dies klar angezeigt;
3. Wenn immer andere eigene- oder Veröffentlichungen Dritter herangezogen wurden, wurden diese klar benannt;
4. Wenn aus anderen eigenen- oder Veröffentlichungen Dritter zitiert wurde, wurde stets die Quelle hierfür angegeben. Diese Dissertation ist vollständig meine eigene Arbeit, mit der Ausnahme solcher Zitate;
5. Alle wesentlichen Quellen von Unterstützung wurden benannt;
6. Wenn immer ein Teil dieser Dissertation auf der Zusammenarbeit mit anderen basiert, wurde von mir klar gekennzeichnet, was von anderen und was von mir selbst erarbeitet wurde;

Ein Teil oder Teile dieser Arbeit wurden zuvor veröffentlicht und zwar in: [1],[2] und [3].

Aachen, 19. August 2024

Contents

Abstract i

Zusammenfassung iii

Eidesstattliche Erklärung v

Contents viii

1 Universality in critical systems 1
- 1.1 Two-scale-factor universality . . . 1
- 1.2 Multi-parameter universality . . . 4

2 The Ising model 9
- 2.1 Definition of the model . . . 9
- 2.2 Exact solution . . . 10
  - 2.2.1 Grassmann variables . . . 12
  - 2.2.2 Mixed representation of the spin polynomial . . . 12
  - 2.2.3 Boundary conditions . . . 16
  - 2.2.4 Fermionic representation . . . 16
- 2.3 The ferromagnetic regime . . . 19
- 2.4 Correlation function at criticality . . . 19
- 2.5 Singular bulk free energy . . . 24
  - 2.5.1 Identifying the reduced anisotropy matrix . . . 24
  - 2.5.2 Solving the integral . . . 25
  - 2.5.3 Scaling behavior near T_c . . . 25
- 2.6 Scaling function of the excess free energy . . . 27
  - 2.6.1 Derivation of the scaling function . . . 29
  - 2.6.2 Modular invariance of $\mathcal{F}_{\text{ex}}^{\text{trIs}}$ . . . 33
  - 2.6.3 Behavior at criticality . . . 35
- 2.7 Visualizations . . . 36
- 2.8 Comparison with [50] . . . 41
  - 2.8.1 Proof for $n = 0$ . . . 41
  - 2.8.2 Proof for $n \neq 0$ . . . 44
- 2.9 Strip limit . . . 46
  - 2.9.1 Limit $\rho_p \to \infty$ . . . 46
  - 2.9.2 Limit $\rho_p \to 0$ . . . 48
  - 2.9.3 Limit $x \to 0$ . . . 49
- 2.10 Comparison to previous results . . . 49
  - 2.10.1 Isotropic couplings . . . 49
  - 2.10.2 Rectangular, anisotropic couplings . . . 51

2.11 Conclusions 54

3 Numerical study of non-universal critical behavior 55
3.1 Overview and notation 56
3.2 Bulk tensor of the q-state Potts model 58
3.3 The CTMRG algorithm 60
3.3.1 The original projector 60
3.3.2 A more advanced projector 63
3.3.3 Initializing the environment 63
3.3.4 Convergence 63
3.4 Calculating the correlation length 63
3.5 Comparison with exact results 65
3.6 Predictions for the corner free energy 73
3.7 Conclusions 74

4 Crossover in models with discrete and continuous variables 75
4.1 First order phase transitions 75
4.2 Clock model with biquadratic term 78
4.3 Estimating the transition point 80
4.4 The Wang-Landau algorithm 81
4.5 Simulation results 83
4.6 Conclusions 89

Publications 91

Bibliography 93

Acknowledgments 99

Chapter 1

Universality in critical systems

One of this thesis's focal point are continuous phase transitions in anisotropic, finite systems in the scaling limit. To this end, in this first chapter the history of universal behavior and scaling in critical thermodynamic systems is given a brief review. First, the well known theory of two-scale-factor universality is discussed, in which the general form of the free energy at and near the critical temperature in terms of the scaling function is explained, followed by an introduction to multi-parameter universality where differences that arise in weakly anisotropic systems are elaborated on.

1.1 Two-scale-factor universality

The phenomenon of phase transitions has been studied, from a theoretical perspective, extensively since the description of real fluids by van der Waals [4], which aided in, for example, explaining liquid-gas coexistence at first order transitions of fluids. Later Landau's theory of phase transitions [5] gave insight into the phenomenon of universality by explaining how two seemingly different systems can exhibit the same behavior near the critical point. These comparisons are usually done by looking at the critical exponents of certain observables, such as the liquid-gas density difference

$$|\rho_+ - \rho_-| \propto |T - T_c|^\beta \tag{1.1}$$

and compressibility

$$\kappa \propto |T - T_c|^{-\gamma} \tag{1.2}$$

in fluids or magnetization

$$M \propto |T - T_c|^\beta \tag{1.3}$$

and susceptibility

$$\chi \propto |T - T_c|^{-\gamma} \tag{1.4}$$

in magnetic systems near the critical temperature T_c. For example, one finds experimentally for the liquid-gas density difference of sulfur hexafluoride $\beta = 0.350 \pm 0.001$ and $\gamma = 1.24 \pm 0.02$ [6] and for the magnetization of $CrBr_3$ a value of $\beta = 0.365 \pm 0.015$ and $\gamma = 1.20 \pm 0.08$ [7]. It is surprising how these very different materials and phases result in experimentally compatible critical exponents – and this is not an accident. Over the last decades a wide range of materials have been examined and many classes of shared critical exponents were found. However, even though the aforementioned theories by van

der Waals and Landau predict that these exponents should be equal, they predict values of $\beta = 1/2$ and $\gamma = 1$ [8]. This is because they are both mean field theories, i.e., they ignore thermal fluctuations, which turn out to be critical for the full explanation of phase transitions and the correct prediction of critical exponents.

One of the biggest discoveries that followed was that of phenomenological scaling laws by Widom and others [9, 10], which demonstrates that the function (equation of state)

$$H = f(M, t) \tag{1.5}$$

that relates the external magnetic field H to the magnetization M and reduced temperature $t = (T - T_c)/T_c$, which depends on two parameters, can actually be expressed through a function Φ of a single parameter in conjunction with the critical exponents:

$$H = M^{\delta}\ \Phi\left(\frac{|t|}{M^{1/\delta}}\right) \tag{1.6}$$

It was discovered that not only is Φ valid for a range of materials with the appropriate T_c and critical exponents, but also that, as a consequence of the above functional dependence, not all critical exponents are independent; one finds the relations

$$\alpha = 2 - \nu\, d \tag{1.7}$$

$$\gamma = \beta(\delta - 1) = \nu(2 - \eta) \tag{1.8}$$

where d is the dimensionality of the system, α is the critical exponent of the specific heat ($C \propto |t|^{-\alpha}$), δ for the equation of state ($H \propto M^{\delta}$), η for the correlation function, ν for the correlation length ($\xi \propto |t|^{-\nu}$). Finally β and γ are the critical exponents of the order parameter and susceptibility, as above. It also possible to define the scaling function for the free energy density[1]. More specifically, the singular part of the bulk free energy behaves as

$$f_{b,s}(t, h) = |t|^{2-\alpha} F_{\pm}\left(\frac{h}{|t|^{2-\alpha-\beta}}\right) \tag{1.9}$$

where $h = H/(k_b T)$ with the Boltzmann constant k_b and $\pm$ indicates $t > 0$ (+) or $t < 0$ (–). Here the notation and naming of the physical observables were chosen based on a typical magnetic systems, since this is what this work is focused on; but, as mentioned above, the results are of course more general.

It was Kadanoff [11, 12] however, who proposed a theoretical approach that thought to explain the origins of scaling laws. His idea was initially limited to spin models with constraints on the type of interactions, but was able to explain scaling by combining neighboring spins successively into large and large block spins and thus, step by step, integrating out the microscopic details that are distinct for a specific model. Implied in the procedure, also called coarse graining, is the concept of scale invariance – since in every step more spins are combined but the functional form of the resulting Hamiltonian remains, the system seems to be the same on all length scales and the resulting functional dependence is exactly that of (1.6). One consequence of this procedure is that the couplings, external fields and temperature now depend on the current scale of the system.

This was the basis for Wilson [13] who generalized this approach and made it applicable to a wide range of models with short range interactions; he also formalized the procedure into what is called the renormalization group (RG). A lot of the details are quite technical,

[1] The bulk free energy density f_b is to be understood as free energy $\mathcal{F}$ per system volume V as $V \to \infty$; singular in this context refers to the part that exhibits singular behavior at the critical point.

but suffice to say, that one of the generalization steps he achieved was to go from discrete increments in system size when integrating out the microscopic details to a continuous length scale ℓ, where $\ell = 1$ represents the original microscopic system. It is then possible to define the RG transformation R_ℓ, the explicit form of which may be very complicated, that takes the initial, microscopic parameters K_i to their coarse grained form at scale ℓ with

$$\{K_i'\} = R_\ell[\{K_i\}]. \tag{1.10}$$

Here K_i can consist for example out of the nearest and next-nearest neighbor couplings, temperature, external magnetic field, etc. Of special interest are certain parameter sets that are invariant under the RG transform

$$\{K_i^*\} = R_\ell[\{K_i^*\}] \tag{1.11}$$

called fixed points. Since ℓ rescales all length scales one finds that the correlation length ξ, which would usually transform like

$$\xi[\{K_i'\}] = \xi[\{K_i\}]/\ell \tag{1.12}$$

has to be either zero or infinity at a fixed point. Fixed points with $\xi = \infty$ are called critical, those with $\xi = 0$ trivial. One usually proceeds by linearizing the RG transform around a fixed point – there are then eigenvalues and eigenvectors associated with the linear RG transform which influence the RG flow near the fixed point. More precisely, if λ_n are these eigenvalues and $\boldsymbol{a}_n$ the eigenvectors, then if

(1) $|\lambda_n| > 1$: $\boldsymbol{a}_n$ represents a relevant direction

(2) $|\lambda_n| < 1$: $\boldsymbol{a}_n$ represents a irrelevant direction

(3) $|\lambda_n| = 1$: $\boldsymbol{a}_n$ represents a marginal direction

because as ℓ increases, only the directions of case (1) will remain important. From here, one can then derive exactly both the correct critical exponents and the scaling laws that were discussed earlier [8]. Furthermore, it is possible to show that all universal quantities (scaling functions, critical exponents and amplitude ratios) can be divided into universality classes (d, n) based on the dimensionality d of the system and the number n of order parameters components [14]. These results will become significant below, when the impact of anisotropy on critical behavior is discussed.

But first, it is instructive to briefly discuss the effects of the finite system size on scaling [15–17]. In a strict sense, there are no phase transitions in finite systems, since it is the thermodynamic limit that allows the appearance of the characteristic singularities. However, it can be shown that the inverse of the linear system size $1/L$ is a relevant perturbation in the RG sense and thus has to be tuned, similar to for example the reduced temperature t or external magnetic field h, to zero at a critical fixed point. As a result, the scaling function of the singular free energy density, in a finite system, can be shown to be of the form

$$f_s(t, L) = |t|^{2-\alpha} \tilde{F}_\pm \left(\frac{\xi(t)}{L} \right) \tag{1.13}$$

where $\xi(t) \propto |t|^{-\nu}$. It is clear, that the true critical regime is only reached in case of $L \to \infty$ or correspondingly, $x \to 0$ in $\tilde{F}_\pm(x)$; implying that $L \gg \xi(t)$ or, in other words, that the correlation length should not be influenced by the boundaries of the system. In the opposite case, where the correlation length dominates, instead of the usual singularities close to $|t| = 0$, one observes a rounding off of these features and a shift of the peak away from the singularity, as can be seen in fig. 1.1 for the heat capacity [8].

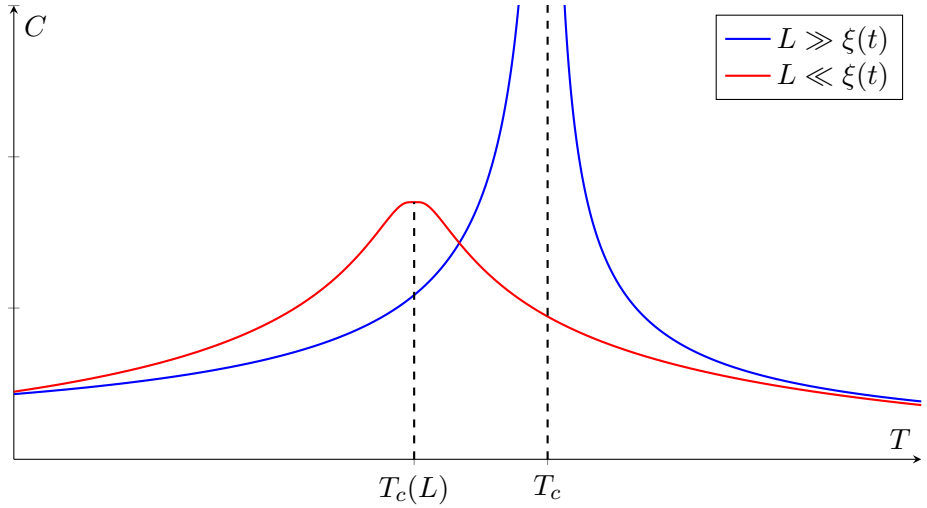

Figure 1.1: The heat capacity C is sketched as a function of the temperature; both in a finite system as well as in the thermodynamic limit.

In contrast to finite system size, anisotropy was considered relatively unimportant for the nature of phase transitions [18–20]; for example it was shown in [18] that the anisotropy parameter

$$f_0 = (J_1 - J_2)/J_1 \tag{1.14}$$

of a d-dimensional continuous spin model, with couplings J_1 within a $(d-1)$-dimensional plane and J_2 perpendicular to that plane, is either only a marginal variable in the renormalization group flow or, depending on the exact parameters of the model, would tend to a stable fixed point with $f^* = 0$, i.e., the isotropic case, and that there is no other stable fixed point with $f^* < 1$. Similarly in [21] the pure and diluted, anisotropic transverse Ising model were studied via a real space renormalisation group scheme and no change in the critical behavior due to anisotropy was found until dimensional crossover effects were detected. Dimensional crossover here refers to an reduction in a system's dimensionality when one or more couplings between (hyper)-planes dominate over the other such that these become effectively decoupled.

1.2 Multi-parameter universality

However, further investigations of anisotropy in systems far way from dimensional crossover effects, via the $O(n)$ symmetric φ^4 theory showed [22], that universality was absent in a range of physical observables. More specifically, it was found that the Hamiltonian

$$H_{\varphi^4} = \int_V \mathrm{d}^d x \left(\frac{r_0}{2}\varphi^2 + \sum_{\alpha,\beta}^{d} \frac{A_{\alpha,\beta}}{2} \frac{\partial\varphi}{\partial x_\alpha} \frac{\partial\varphi}{\partial x_\beta} + u_0(\varphi^2)^2 \right) \tag{1.15}$$

with n component fields $\varphi \equiv \varphi(\boldsymbol{x})$ and anisotropy matrix $A_{\alpha,\beta} = (\boldsymbol{A})_{\alpha,\beta}$, after going to the continuum limit, results in the bulk correlation function near the critical point

$$G(\boldsymbol{x}, \boldsymbol{A}, u_0) \equiv \langle \varphi(\boldsymbol{x})\varphi(0)\rangle \tag{1.16}$$

$$= \frac{A_G(\det \boldsymbol{A})^{-1/2}}{|\boldsymbol{\lambda}^{-1/2}\boldsymbol{U}\boldsymbol{x}|^{d+\eta-1}}\Phi(|\boldsymbol{\lambda}^{-1/2}\boldsymbol{U}\boldsymbol{x}|/\xi') \tag{1.17}$$

where ξ' is the mean correlation length, A_G is a non-universal amplitude, $\boldsymbol{\lambda}$ the diagonal matrix of eigenvalues and $\boldsymbol{U}$ the unitary matrix associated with the eigenvalue problem of $\boldsymbol{A}$. This form is quite interesting, since the transform $\boldsymbol{x'} \equiv \boldsymbol{\lambda}^{-1/2}\boldsymbol{U}\boldsymbol{x}$ of the lattice vectors can be interpreted as transforming the system to an isotropic one with $\boldsymbol{A} = 1$, since

$$\frac{\partial\varphi}{\partial x_\alpha} = \frac{\partial x'_\alpha}{\partial x_\alpha}\frac{\partial\varphi}{\partial x'_\alpha} = (\boldsymbol{\lambda}^{-1/2}\boldsymbol{U})_\alpha \ \frac{\partial\varphi}{\partial x'_\alpha} \tag{1.18}$$

where x_α is a component of $\boldsymbol{x}$ with $\alpha = 1, 2, \ldots, d$ and thus

$$\sum_{\alpha,\beta}^{d} \frac{A_{\alpha,\beta}}{2}\frac{\partial\varphi}{\partial x_\alpha}\frac{\partial\varphi}{\partial x_\beta} = \sum_{\alpha,\beta}^{d} \frac{(\boldsymbol{\lambda}^{-1/2}\boldsymbol{U})_\alpha A_{\alpha,\beta}(\boldsymbol{U}^T\boldsymbol{\lambda}^{-1/2})_\beta}{2} \ \frac{\partial\varphi}{\partial x'_\alpha} \ \frac{\partial\varphi}{\partial x'_\beta} \tag{1.19}$$

$$= \sum_{\alpha,\beta}^{d} \frac{1}{2}\frac{\partial\varphi}{\partial x'_\alpha}\frac{\partial\varphi}{\partial x'_\beta} \tag{1.20}$$

while simultaneously deforming the lattice. From there it can be seen that even though the scaling function Φ itself remains universal and independent of $\boldsymbol{A}$, its argument does not, since it explicitly depends on the $d(d-1)/2$ parameters of the anisotropy matrix and thus the microscopic details of the model. Additionally, two-scale factor universality cannot be restored by a scale transform in confined systems if $\boldsymbol{A}$ has off-diagonal elements, since the principles axis of $\boldsymbol{A}$ and the boundaries of the system are generally not aligned. Similar behavior was found in the finite size scaling functions of the free energy, Binder cumulant and Casimir amplitude [22].

In a follow up work[23] it was discussed how exactly the previously derived transform deforms the original lattice, by investigating an anisotropic rectangular lattice φ^4 theory with the Hamiltonian

$$H_{\text{Lattice}} = v\left[\sum_{i=1}^{N}\left(\frac{r_0}{2}\varphi_i^2 + u_0(\varphi_i^2)^2 - h\varphi_i\right) + \sum_{i,j=1}^{N}\frac{K_{i,j}}{2}(\varphi_i - \varphi_j)^2\right] \tag{1.21}$$

with φ_i again being an n-component field on N lattice points $\boldsymbol{x}_i$ in d dimensions. Here $v = V/N$ is the volume per lattice site and $K_{i,j}$ are the anisotropic couplings. In Fourier space, the interactions as a function of the wave vector $\boldsymbol{k}$ have the form

$$\hat{K}(\boldsymbol{k}) = N^{-1}\sum_{i,j}^{N} K_{i,j}e^{-i\boldsymbol{k}\cdot(\boldsymbol{x}_i - \boldsymbol{x}_j)} \tag{1.22}$$

with the long wavelength contribution $\delta\hat{K}(\boldsymbol{k}) \equiv 2[\hat{K}(\boldsymbol{0}) - \hat{K}(\boldsymbol{k})]$ given by

$$\delta\hat{K}(\boldsymbol{k}) = \sum_{\alpha,\beta=1}^{d} A_{\alpha,\beta} \ k_\alpha k_\beta + \sum_{\alpha,\beta,\gamma,\delta}^{d} B_{\alpha,\beta,\gamma,\delta} \ k_\alpha k_\beta k_\gamma k_\delta + \mathcal{O}(k^6), \tag{1.23}$$

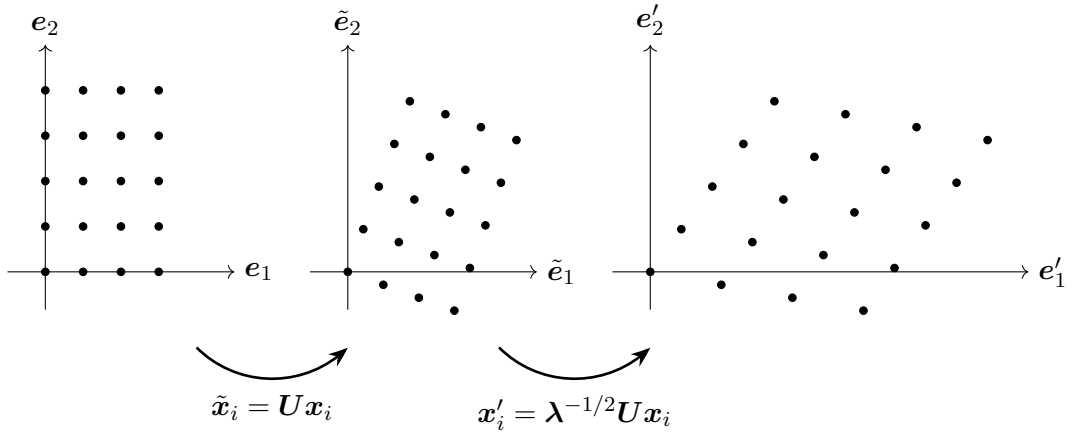

Figure 1.2: Visualization of the lattice transform in $d = 2$ going from an anisotropic to an isotropic system.

where k_i are the components of the wave vector and $A_{i,j}$ is once again the anisotropy matrix that was introduced above. In real space the explicit formula

$$A_{\alpha,\beta} = \frac{1}{N} \sum_{i,j=1}^{N} (x_{i,\alpha} - x_{j,\alpha})(x_{i,\beta} - x_{j,\beta}) K_{i,j} \tag{1.24}$$

is obtained. From here, the lattice transform $\boldsymbol{x}' \equiv \boldsymbol{\lambda}^{-1/2}\boldsymbol{U}\boldsymbol{x}$, that transforms the correlation function to an anisotropic one, can be recovered, or alternatively in reciprocal space, $\boldsymbol{k}' \equiv \boldsymbol{\lambda}^{1/2}\boldsymbol{U}\boldsymbol{k}$. Geometrically this shear transform is depicted in fig. 1.2, where the two steps of first applying the rotation via $\boldsymbol{U}$ of the anisotropic system on a rectangular lattice, followed by a rescaling via $\boldsymbol{\lambda}^{-1/2}$ along the principles axis, defined by the eigenvectors of $\boldsymbol{A}$, into an isotropic, parallelepiped lattice, are shown. These results reveal, that a lattice Hamiltonian in the long wavelength limit, i.e., near the critical point, can be brought into an approximately isotropic form, where the same isotropic scaling function remains. The universality class, however, is augmented by an additional $d(d-1)/2$ parameters, that require knowledge of the microscopic details. A RG approach to this problem, with focus on the thermodynamic Casimir force, can be found in [24–26].

Furthermore, the physical interpretation of the anisotropy matrix was elaborated on in [27–29] for $2d$ systems. In this special case, as the anisotropic correlation function gets transformed into an isotropic one, the lattice turns into a $2d$ parallelepiped, also known as a parallelogram, with internal angles α and $\pi - \alpha$ as well as aspect ratio ρ_p. The eigenvalues of the reduced anisotropy matrix $\bar{\boldsymbol{A}} = \boldsymbol{A}/\sqrt{\det \boldsymbol{A}}$, λ_1 and λ_2, can be identified as being proportional to the square of the correlation length amplitude

$$\xi_{0\pm}^{(1)} \propto \sqrt{\lambda_1}, \quad \xi_{0\pm}^{(2)} \propto \sqrt{\lambda_2} \tag{1.25}$$

in the principle directions given by the two eigenvectors $\boldsymbol{e}^{(i)}$ of $\bar{\boldsymbol{A}}$ above (+) and below (–) the critical point; the geometric mean of both then yields the mean correlation length amplitude

$$\bar{\xi}_{0\pm} \equiv \left[\xi_{0\pm}^{(1)} \xi_{0\pm}^{(2)}\right]^{1/2}. \tag{1.26}$$

This allows the correlation function to be written, similar to (1.17), with the susceptibility

amplitude Γ_+, as:

$$G_\pm(\boldsymbol{x},t) = \frac{\Gamma_+(\bar{\xi}_{0+})^{-7/4}}{[\boldsymbol{x}\cdot\bar{\boldsymbol{A}}^{-1}\boldsymbol{x}]^{1/8}}\ \Psi_\pm\left(\frac{[\boldsymbol{x}\cdot\bar{\boldsymbol{A}}^{-1}\boldsymbol{x}]^{1/2}}{\bar{\xi}_\pm(t)}\right) \tag{1.27}$$

More specifically, the contours with a fixed value of the correlation function are given by the ellipsis equation $\boldsymbol{x}\cdot\bar{\boldsymbol{A}}^{-1}\boldsymbol{x} = \text{const}$. The ellipsis parameters are chosen as

$$q = \xi^{(1)}_{0\pm}/\xi^{(2)}_{0\pm}, \tag{1.28}$$

which is related to the eccentricity, and the rotation angle Ω, which can be extracted from the eigenvectors

$$\boldsymbol{e}^{(1)} = \begin{pmatrix}\cos\Omega\\ \sin\Omega\end{pmatrix}, \quad \boldsymbol{e}^{(2)} = \begin{pmatrix}-\sin\Omega\\ \cos\Omega\end{pmatrix}. \tag{1.29}$$

of $\bar{\boldsymbol{A}}$. In turn, this means that the reduced anisotropy matrix can be expressed through these ellipsis parameters, as

$$\bar{\boldsymbol{A}} = \begin{pmatrix} q c_\Omega^2 + q^{-1}s_\Omega^2 & (q-q^{-1})c_\Omega s_\Omega \\ (q-q^{-1})c_\Omega s_\Omega & q s_\Omega^2 + q^{-1}c_\Omega^2\end{pmatrix}, \tag{1.30}$$

with $c_\Omega = \cos\Omega$ and $s_\Omega = \sin\Omega$. Even though these relations were derived in the context of a φ^4 model, it was conjectured that this form would hold more generally [28], which was proven recently in [30, 31].

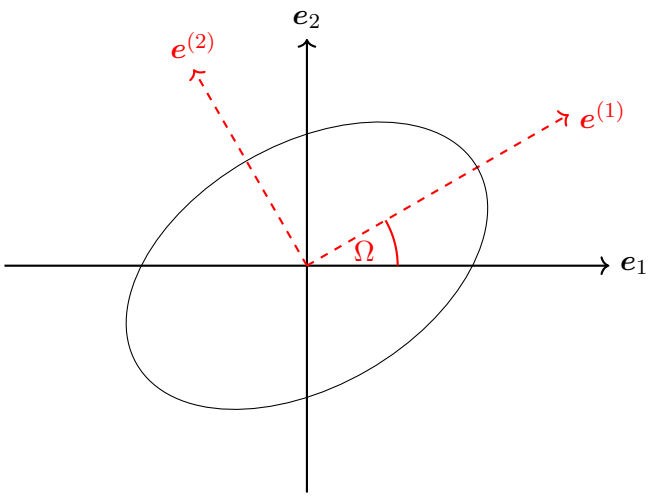

Figure 1.3: Correlation ellipsis at constant $G_\pm(\boldsymbol{x},t)$ with the principle axis $\boldsymbol{e}^{(i)}$ in red.

These quantities were then specifically studied in the context of the $2d$ Ising model [28, 29], with the Hamiltonian ($\sigma = \pm 1$)

$$\beta H^{\text{trIs}} = -\beta\sum_{m,n} E_1\sigma_{m,n}\sigma_{m+1,n} + E_2\sigma_{m+1,n}\sigma_{m+1,n+1} + E_3\sigma_{m,n}\sigma_{m+1,n+1}, \tag{1.31}$$

and its correlation function on the square ($E_3 = 0$) and triangular lattice with arbitrary diagonal next-nearest neighbor couplings [32]. It was found that for the triangular Ising model

$$q(E_1,E_2,E_3) = \frac{2+\hat{S}_1^2+\hat{S}_2^2+[(\hat{S}_1^2+\hat{S}_2^2)^2+4(1-2\hat{S}_1\hat{S}_2)]^{1/2}}{2(\hat{S}_1+\hat{S}_2)} \tag{1.32}$$

$$\tag{1.33}$$

and

$$\tan 2\Omega = \frac{2\hat{S}_3}{\hat{S}_1 - \hat{S}_2} \quad \text{for } E_1 \neq E_2 \tag{1.34}$$

$$\Omega = \pi/4 \qquad \text{for } E_1 = E_2 \tag{1.35}$$

with $\hat{S}_i = \sinh(2\beta_c E_i)$ or, alternatively, the reduced anisotropy matrix can directly be expressed through the couplings as

$$\bar{\boldsymbol{A}} = \begin{pmatrix} \hat{S}_1 + \hat{S}_3 & \hat{S}_3 \\ \hat{S}_3 & \hat{S}_2 + \hat{S}_3 \end{pmatrix}. \tag{1.36}$$

Furthermore, it was shown in [29–31], that the resulting isotropic parallelogram that emerges after the shear transform, can be characterized through the correlation ellipsis parameters by its internal angle α and aspect ratio ρ_p, which take the explicit form:

$$\cot \alpha(q, \Omega) = -\bar{\boldsymbol{A}}(q, \Omega)_{12} \ = (q^{-1} - q)\cos\Omega \sin\Omega \tag{1.37}$$

$$[\rho_p(\rho, q, \Omega)]^2 = \rho^2 \frac{\bar{\boldsymbol{A}}(q, \Omega)_{11}}{\bar{\boldsymbol{A}}(q, \Omega)_{22}} = \rho^2 \frac{\tan^2\Omega + q^2}{1 + q^2 \tan^2\Omega}. \tag{1.38}$$

Here ρ is the aspect ratio of the original rectangular lattice and q, Ω the ellipsis parameters as discussed above. It was then found [29–31], that this can be used in conjunction with the conformal field theory (CFT) solution for the critical $2d$ Ising model partition function

$$Z^{\mathrm{CFT}}(\tau) = \frac{1}{2^{2/3}} \frac{|\theta_2(\tau)| + |\theta_3(\tau)| + |\theta_4(\tau)|}{|\theta_2(\tau)\theta_3(\tau)\theta_4(\tau)|^{1/3}} \tag{1.39}$$

by expressing the modular parameter $\tau = \rho_p \exp(i\alpha)$ through these quantities. Here $\theta_i(\tau)$ are the Jacobi theta functions [33]. This approach is quiet elegant, since the application of conformal field theory requires the system under consideration to be conformal invariant, which implies, among others, isotropy and thus multi-parameter universality is a gateway to apply the rich body of work in CFT to anisotropic systems. Additionally, the critical Ising partition function above exhibits something called modular invariance, which means it does not change under certain transformations of the modular parameter ($\tau \to \tau + 1$, $\tau \to -1/\tau$), details of which will be discussed later on.

In the following chapter, the results obtained by Dohm, Chen, Wessel et al. that were discussed above, will be expanded upon to include the Ising model in finite systems and in the scaling limit, i.e, in the region near the critical point where universal behavior is to be expected. This extension aims to explore the presence of multi-parameter universality and modular invariance within such systems by specifically investigating the free energy scaling function and later on, the heat capacity and strip limit. Furthermore, the connection to previously known more restricted cases is made to validate the results.

Similarly, Chapter 3 introduces a numerical analysis of the $2d$ Potts model, with the objective of identifying any departures from two-scale factor universality. This is of interest since for one, the $q = 2$ state Potts model is equivalent to the Ising model and thus makes it easy to cross-check results. Additionally, the $q = 3, 4$ Potts model both exhibit continuous phase transitions and are of a different universality class, making them good subjects to further study multi-parameter universality.

The final chapter delves into the investigation of first-order transitions in $3d$ systems by utilizing Monte Carlo simulations. This approach seeks to observe crossover phenomena during the transition from discrete to continuous degrees of freedom and aims to shed light on how different coexisting phases contribute to the behavior at the first order transition point.

Chapter 2

The Ising model

The Ising model, a cornerstone in statistical mechanics and condensed matter theory, has undergone significant theoretical developments since its inception. The two-dimensional ($2d$) Ising model, in particular, has been a rich area of study. Onsager's seminal work in 1944 [34] on the $2d$ ferromagnetic Ising model marked a milestone by rigorously computing the partition function for the case of a vanishing field, which unveiled the model's order-disorder transition. This work established the mathematical framework crucial for further advancements in understanding critical phenomena in statistical mechanics. Further significant contributions were made by Kaufman [35], who, alongside Onsager, developed a simpler derivation and extended the solution to include finite systems.

In this chapter, the anisotropic Ising model on a finite, parallelogram lattice is examined by expanding on Plechkos approach [36–38], which is centered around the use of integrals over anticommuting Grassmann variables and the mirror-ordered factorization concepts for the $2d$ Ising partition function. This non-combinatorial fermionic approach offers a distinct perspective on the model, particularly in handling anisotropic bond coupling parameters across various lattices.

Furthermore, the free energy scaling function near the critical point is derived, and the well-known conformal field theory (CFT) results [39] for the critical $2d$ Ising model are recovered, while placing these results in the context of multi-parameter universality [28, 29]. It is demonstrated that there is a dependency on microscopical quantities at and near criticality.

2.1 Definition of the model

A $2d$ parallelogram lattice with periodic boundary conditions, spanned by two vectors $\boldsymbol{L}_i = N_i \boldsymbol{a}_i$ $(i = 1, 2)$, is considered, where N_i represents the number of unit cells in the i-th direction and the two vectors $\boldsymbol{a}_i$ span a unit cell. The lattice constants are denoted as $a_i = |\boldsymbol{a}_i|$. The total area of the system is given by $V = N_1 N_2 v$, where $v = a_1 a_2 \sin\vartheta$ is the area of a primitive cell, with the angle ϑ being spanned by $\boldsymbol{L}_1$ and $\boldsymbol{L}_2$; additionally the aspect ratio of the parallelogram is defined as $\rho_p = |\boldsymbol{L}_2|/|\boldsymbol{L}_1|$. It is specified that each lattice site contains a spin $\sigma_{m,n} = \pm 1$ at the location $\boldsymbol{x}_{m,n} = m\boldsymbol{a}_1 + n\boldsymbol{a}_2$, with the Hamiltonian being

$$\beta H^{\mathrm{Is}} = -\beta \sum_{(i,j),(m,n)} E_{(i,j),(m,n)} \sigma_{i,j} \sigma_{m,n} \tag{2.1}$$

and the inverse temperature $\beta = 1/(k_b T)$. The partition function thus follows as

$$Z^{\mathrm{Is}} = \sum_{\{\sigma\}} \exp\left(-\beta H^{\mathrm{Is}}\right) \tag{2.2}$$

with the total free energy given by

$$\mathcal{F}^{\mathrm{Is}}_{\mathrm{tot}} = -\ln Z^{\mathrm{Is}} \tag{2.3}$$

which is split into a singular $\mathcal{F}^{\mathrm{Is}}_{\mathrm{s}}$ and non-singular $\mathcal{F}^{\mathrm{Is}}_{\mathrm{ns}}$ part. The associated densities are defined as

$$f^{\mathrm{Is}} = \mathcal{F}^{\mathrm{Is}}_{\mathrm{tot}}/V = f^{\mathrm{Is}}_{\mathrm{s}} + f^{\mathrm{Is}}_{\mathrm{ns}}. \tag{2.4}$$

The bulk contribution to the free energy density f_b is also considered, which is the value of the free energy in the thermodynamic limit

$$f^{\mathrm{Is}}_{b} = \lim_{V\to\infty} f^{\mathrm{Is}} = f^{\mathrm{Is}}_{\mathrm{b,s}} + f^{\mathrm{Is}}_{\mathrm{b,ns}}, \tag{2.5}$$

as well as its complement, the excess free energy density

$$f^{\mathrm{Is}}_{\mathrm{ex}} = f^{\mathrm{Is}} - f^{\mathrm{Is}}_{\mathrm{b}}. \tag{2.6}$$

It can be assumed [17, 24, 40, 41] that for periodic boundary conditions $f^{\mathrm{Is}}_{\mathrm{ns}} = f^{\mathrm{Is}}_{\mathrm{b,ns}}$. Additionally, the reciprocal lattice vectors $\boldsymbol{b}_i$ $(i = 1, 2)$, that obey the relation $\boldsymbol{a}_i \cdot \boldsymbol{b}_j = \delta_{ij}$, are introduced, as well as general reciprocal lattice vector $\boldsymbol{k}_{p,q} = 2\pi p/N_1 \boldsymbol{b}_1 + 2\pi q/N_2 \boldsymbol{b}_2$, which will become important after the move to Fourier space later on.

2.2 Exact solution

To exactly solve the $2d$ Ising model, the focus is narrowed to the case of triangular couplings (trIs), where $E_{(i,j),(i+1,j)} = E_1$, $E_{(i,j),(i,j+1)} = E_2$ and $E_{(i,j),(i+1,j+1)} = E_3$ and make use of the approach proposed by Plechko [36–38], who employs anticommuting Grassmann variables and refines the approach initially conceptualized by Berezin [42], to periodic boundary conditions of finite systems. This is an extension and generalization of the work presented in [43]. It is first noted that the system exhibits a phase transition at the critical temperature β_c, which is determined by the equation

$$\hat{S}^c_1 \hat{S}^c_2 + \hat{S}^c_1 \hat{S}^c_3 + \hat{S}^c_2 \hat{S}^c_3 - 1 = 0 \tag{2.7}$$

where $\hat{S}_j = \sinh 2\beta E_j$ and the superscript c indicates $\beta = \beta_c$. It is worth mentioning that, in the aforementioned description, the two couplings with the largest absolute values are assumed to be positive. Should this not be the case, mappings need to be applied. For more details, refer to [44]. The Hamiltonian now simplifies to

$$\begin{aligned}\beta H^{\mathrm{trIs}} = -\beta \sum_{m,n} & E_1 \sigma_{m,n}\sigma_{m+1,n} + E_2 \sigma_{m+1,n}\sigma_{m+1,n+1} \\ & + E_3 \sigma_{m,n}\sigma_{m+1,n+1}\end{aligned} \tag{2.8}$$

and can be rewritten as the product over the Boltzmann weights of the $N_1 \times N_2$ unit cells of the system:

$$Z^{\text{trIs}} = \sum_{\{\sigma\}} \prod_{m,n=1}^{N_1,N_2} \exp\big(\beta E_1 \sigma_{m,n}\sigma_{m+1,n} + \beta E_2 \sigma_{m+1,n}\sigma_{m+1,n+1} + \beta E_3 \sigma_{m,n}\sigma_{m+1,n+1}\big) \tag{2.9}$$

$$= \sum_{\{\sigma\}} \prod_{m,n=1}^{N_1,N_2} R\ w_{m,n} \tag{2.10}$$

Here $w_{m,n}$ represents the Boltzmann weight of a unit cell and the constant R is introduced, which will be determined in a subsequent step. This unit cell contains spins designated as $\sigma_{m,n} = \sigma_a$, $\sigma_{m+1,n} = \sigma_b$, $\sigma_{m+1,n+1} = \sigma_c$, and $\sigma_{m,n+1} = \sigma_d$, as inferred from the preceding equation. Note that the labeling of spins with letters a, b, c, d is to be interpreted within the context of a unit cell located at position (m, n), signifying relative positions within that cell as specified. By using the property $e^{\pm x} = \cosh x \pm \sinh x = \cosh x\ (1 \pm \tanh x)$ and noting that $\sigma_i\sigma_j = \pm 1$ the Boltzmann weight per unit cell can be expressed as

$$\exp\left(\beta E_1 \sigma_a\sigma_b + \beta E_2 \sigma_b\sigma_c + \beta E_3 \sigma_a\sigma_c\right) \tag{2.11}$$

$$= \cosh(\beta E_1)\cosh(\beta E_2)\cosh(\beta E_3)(1 + \hat{Z}_1\sigma_a\sigma_b)(1 + \hat{Z}_2\sigma_b\sigma_c)(1 + \hat{Z}_3\sigma_a\sigma_c) \tag{2.12}$$

$$= R\Big[(1 + \hat{Z}_1\hat{Z}_2\hat{Z}_3) + (\hat{Z}_1 + \hat{Z}_2\hat{Z}_3)\sigma_a\sigma_b + (\hat{Z}_2 + \hat{Z}_1\hat{Z}_3)\sigma_b\sigma_c + (\hat{Z}_3 + \hat{Z}_1\hat{Z}_2)\sigma_a\sigma_c\Big] \tag{2.13}$$

$$= R\left(\alpha_0 + \alpha_1\sigma_a\sigma_b + \alpha_2\sigma_b\sigma_c + \alpha_3\sigma_a\sigma_c\right) \tag{2.14}$$

$$= R\ w_{m,n} \tag{2.15}$$

where $R = \cosh(\beta E_1)\cosh(\beta E_2)\cosh(\beta E_3)$, $\hat{Z}_\alpha := \tanh(\beta E_\alpha)$ and the constants α_i have been introduced; they take the explicit form:

$$\alpha_0 = 1 + \hat{Z}_1\hat{Z}_2\hat{Z}_3, \quad \alpha_1 = \hat{Z}_1 + \hat{Z}_2\hat{Z}_3 \tag{2.16}$$

$$\alpha_2 = \hat{Z}_2 + \hat{Z}_1\hat{Z}_3, \quad \alpha_3 = \hat{Z}_3 + \hat{Z}_1\hat{Z}_2. \tag{2.17}$$

Additionally the trace symbol is defined

$$\operatorname*{Tr}_{\{\sigma\}}(\ \circ\ ) = \prod_{m,n=1}^{N_1,N_2} \left[\frac{1}{2}\sum_{\sigma_{m,n}=\pm 1}(\ \circ\ )\right] \tag{2.18}$$

from which it is straight forward to see

$$\operatorname*{Tr}_{\{\sigma\}}(1) = 1, \quad \operatorname*{Tr}_{\{\sigma\}}(\sigma_{m,n}) = 0 \tag{2.19}$$

and allows for the partition function to be expressed as

$$Z^{\text{trIs}} = (2R)^{N_1N_2}Q \tag{2.20}$$

with

$$Q = \operatorname*{Tr}_{\{\sigma\}}\left(\prod_{m,n=1}^{N_1,N_2}(\alpha_0 + \alpha_1\sigma_a\sigma_b + \alpha_2\sigma_b\sigma_c + \alpha_3\sigma_a\sigma_c)_{m,n}\right) \tag{2.21}$$

here the factor $2^{N_1N_2}$ was added to balance the factor $1/2$ in the definition of the trace.

2.2.1 Grassmann variables

Let c and c^* be a pair of Grassmann variables, they obey the anticommutation relation

$$\{c, c^*\} = cc^* + c^*c = 0, \quad c^2 = c^{*2} = 0 \tag{2.22}$$

which implies that all functions of this pair have the expansion:

$$f(c, c^*) = \alpha + \beta c + \gamma c^* + \delta cc^*, \quad \alpha, \beta, \gamma, \delta \in \mathbb{C} \tag{2.23}$$

It is also possible to define integration over functions of Grassmann variables as a linear functional onto the complex numbers [42], with the general rules:

$$\int dc\ 1 = 0 \qquad \int dc\ c = 1 \tag{2.24}$$

$$\int dc^*\ 1 = 0 \qquad \int dc^*\ c^* = 1 \tag{2.25}$$

where in the case of higher dimensional integrals, the integration measures dc, dc^* anti-commute with each other and the c, c^*. For N pairs of Grassmann variables c_i, c_j^*, the anti-commutation relations

$$c_i c_j = -c_j c_i, \quad c_i^* c_j^* = -c_j^* c_i^*, \quad c_i c_j^* = -c_j^* c_i \quad (i \neq j) \tag{2.26}$$

hold. Another important result, that will be used later, is the evaluation of Gaussian integrals over Grassmann variables, which have been solved in [42] for the cases of complex fermionic fields

$$\int \prod_{j=1}^{L} dc_j^* dc_j \exp\left(\sum_{i=1}^{L}\sum_{j=1}^{L} c_i A_{i,j} c_j^*\right) = \det A, \tag{2.27}$$

with A an arbitrary matrix, and for real fermionic fields

$$\int \prod_{j=1}^{L} dc_j \exp\left(\frac{1}{2}\sum_{i=1}^{L}\sum_{j=1}^{L} c_i A_{i,j} c_j\right) = \text{pf } A \tag{2.28}$$

where pf denotes the Pfaffian. In case of a skew-symmetric matrix ($A_{i,j} = -A_{j,i}$) the relation $(\det A)^{\frac{1}{2}} = \text{pf } A$ applies.

2.2.2 Mixed representation of the spin polynomial

Up until now, only new notation and a slight reformulation of the original problem was presented; in the following anticommuting Grassmann variables will be introduced and the partition function will be brought into a mixed form that contains both spin and Grassmann variables, reordering the factors and finally tracing out the spins will lead to Gaussian integrals over these anticommuting variables that can be solved easily.

Combining the above results, it is convenient to define the Gaussian average as

$$\underset{\{c\}}{\text{Tr}}(\ \circ\ ) = \int dc^* dc\ e^{\lambda cc^*}(\ \circ\ ) \tag{2.29}$$

$$\underset{\{c\}}{\text{Tr}}(1) = \lambda, \quad \underset{\{c\}}{\text{Tr}}(c) = \underset{\{c\}}{\text{Tr}}(c^*) = 0, \quad \underset{\{c\}}{\text{Tr}}(cc^*) = 1 \tag{2.30}$$

where the identities can be checked easily by noting that $\exp(\lambda cc^*) = 1+\lambda cc^*$. This makes it possible to rewrite the Boltzmann weight of a triangular unit cell as a spin polynomial [37] using $\eta = \alpha_1\alpha_2/\alpha_3$

$$w_{m,n} = \alpha_0 + \alpha_1\sigma_a\sigma_b + \alpha_2\sigma_b\sigma_c + \frac{\alpha_1\alpha_2}{\eta}\sigma_a\sigma_c \tag{2.31}$$

$$= (\alpha_0 - \eta) + \eta\left(\frac{\alpha_1}{\eta}\sigma_a + \sigma_b\right)\left(\sigma_b + \frac{\alpha_2}{\eta}\sigma_c\right) \tag{2.32}$$

$$= \int dc^*dc\; e^{\alpha_0 cc^*}\left(1 + c\frac{\alpha_1}{\sqrt{\eta}}\sigma_a\right)\left(1 + \sqrt{\eta}(c+c^*)\sigma_b\right)\left(1 + c^*\frac{\alpha_2}{\sqrt{\eta}}\sigma_c\right) \tag{2.33}$$

Now $N_1 \times N_2$ pairs of Grassmann variables, $c_{m,n}, c^*_{m,n}$, are introduced, which allows one to bring the above expression in a more convenient form

$$w_{m,n} = \int dc^*_{m,n}dc_{m,n}\; e^{\alpha_0 c_{m,n}c^*_{m,n}}\; A_{m,n}B_{m+1,n}C_{m+1,n+1} \tag{2.34}$$

$$= \operatorname*{Tr}_{\{c\}}\left[A_{m,n}B_{m+1,n}C_{m+1,n+1}\right] \tag{2.35}$$

Note that from now on $\lambda = \alpha_0$ in the definition of the trace (2.29); additionally the symbols, which contain both spin and Grassmann variables, are defined as

$$A^{\pm}_{m,n} = 1 \pm \frac{\alpha_1}{\sqrt{\eta}}c_{m,n}\sigma_{m,n} \tag{2.36}$$

$$B^{\pm}_{m+1,n} = 1 \pm \sqrt{\eta}(c_{m,n} + c^*_{m,n})\sigma_{m+1,n} \tag{2.37}$$

$$C^{\pm}_{m+1,n+1} = 1 \pm \frac{\alpha_2}{\sqrt{\eta}}c^*_{m,n}\sigma_{m+1,n+1}. \tag{2.38}$$

Here the indices of the factors have been chosen to be identical to the spin indices, however, all Grassmann variables on the same unit cell share the same index; additionally, for the above factors, the simplified notation $X_{m,n} \equiv X^+_{m,n}$ will be used to make the equations more readable. The partition function can now be expressed as product of the factors $A_{m,n}B_{m+1,n}C_{m+1,n+1}$ containing the mixed representation

$$Q = \operatorname*{Tr}_{\{\sigma\}}\operatorname*{Tr}_{\{c\}}\left[\prod_{m,n} A_{m,n}B_{m+1,n}C_{m+1,n+1}\right] \tag{2.39}$$

which commute with each other under the trace, since (2.33) can be applied anytime to return to pure spin representation of any unit cell, as long as the factors A, B and C remain next to each other.

Before finally solving the Ising model, some identities for non-commuting elements η_i, θ_i that repeatedly occur in the proof, originally presented in [37], are replicated:

$$\prod_{i=1}^{N}\overrightarrow{\eta_i\theta_{i+1}} = (\eta_1\theta_2)(\eta_2\theta_3)\;...\;(\eta_N\theta_{N+1}) \tag{2.40}$$

$$= \eta_1(\theta_2\eta_2)(\theta_3\eta_3)\;...\;(\theta_N\eta_N)\theta_{N+1} \tag{2.41}$$

$$= \eta_1\left(\prod_{i=2}^{N}\overrightarrow{\theta_i\eta_i}\right)\theta_{N+1} \tag{2.42}$$

Here the arrow indicates in which direction the index increases, since the order is important. Now assume in addition, that the pairs $\eta_i\theta_i$ are totally commuting and mirror ordering can be used to rearrange the factors

$$\prod_{i=1}^{N} \overrightarrow{\eta_i\theta_i}^{i} = (\eta_1\theta_1)(\eta_2\theta_2)\ ...\ (\eta_{N-1}\theta_{N-1})(\eta_N\theta_N) \tag{2.43}$$

$$= (\eta_1(\eta_2\ ...\ (\eta_{N-1}(\eta_N\theta_N)\theta_{N-1})\ ...\ \theta_2)\theta_1) \tag{2.44}$$

$$= \prod_{i=1}^{N} \overrightarrow{\eta_i}^{i} \prod_{i=1}^{N} \overleftarrow{\theta_i}^{i} \tag{2.45}$$

and similarly for the reversed direction:

$$\prod_{i=1}^{N} \overrightarrow{\eta_i\theta_i}^{i} = (\eta_N(\eta_{N-1}\ ...\ (\eta_2(\eta_1\theta_1)\theta_2)\ ...\ \theta_{N-1})\theta_N) \tag{2.46}$$

$$= \prod_{i=1}^{N} \overleftarrow{\eta_i}^{i} \prod_{i=1}^{N} \overrightarrow{\theta_i}^{i} \tag{2.47}$$

These identities will be used to rearrange the factors in (2.39) such that terms with the same spin variables are next to each other, which allows easy evaluation of the trace over the spins.

For this proof, the commutation relation of two functions of Grassmann variables $f^{\pm} = f(\{\pm a_i\})$ and $g^{\pm} = g(\{\pm a_i\})$ is needed, where the $\pm$ indicates the sign of all arguments of the respective function. This relation has been shown in the appendix of [36] and states:

$$\begin{aligned} f^+g^+ &= \frac{1}{2}(g^+f^+ + g^+f^- + g^-f^+ - g^-f^-) \\ &\overset{*}{=} g^{\delta_1}f^{\delta_2} \end{aligned} \tag{2.48}$$

In the last line, the symbol $\overset{*}{=}$ was introduced, which indicates that the real structure of term on the right is as presented in the first line, but only one term is written explicitly and the $\delta_i = \pm$ denote the different signs applied to the Grassmann variables. In the following all operations are assumed to be under the Tr operator, the symbol is omitted to improve readability. In a first step, the boundary weights on the top of the system are reordered

$$\prod_{m=1}^{N_1-1} A_{m,N_2}\, B_{m+1,N_2}\, C_{m+1,N_2+1} \tag{2.49}$$

$$= \prod_{m=1}^{N_1-1} C^-_{m+1,N_2+1}\, A_{m,N_2}\, B_{m+1,N_2} \tag{2.50}$$

$$= \prod_{m=1}^{N_1-1} C^-_{m+1,1}\, A_{m,N_2}\, B_{m+1,N_2} \tag{2.51}$$

as well as at the right edge of the system

$$\prod_{n=1}^{N_2-1} A_{N_1,n}\, B_{N_1+1,n}\, C_{N_1+1,n+1} \tag{2.52}$$

$$= \prod_{n=1}^{N_2-1} B_{N_1+1,n}\, C_{N_1+1,n+1} A^{-}_{N_1,n} \tag{2.53}$$

$$= \prod_{n=1}^{N_2-1} B_{1,n}\, C_{1,n+1} A^{-}_{N_1,n}, \tag{2.54}$$

where in the last step periodic boundary conditions $N_1 + 1 \to 1$ and $N_2 + 1 \to 1$ were applied to the spins. Note that the cell at (N_1, N_2) was left out; this is because it has a special role when combining all the weights, more specifically, it is reordered and, again, the boundary conditions are applied:

$$A_{N_1,N_2}\, B_{N_1+1,N_2}\, C_{N_1+1,N_2+1} = C^{-}_{1,1}\, A_{N_1,N_2}\, B_{1,N_2} \tag{2.55}$$

Next the mirror ordering (2.45) is used on the top (t) boundary weights to split $(C^t A^t B^t)$ into $(C^t)(A^t B^t)$ and the right (r) boundary weights $(B^r C^r A^r)$ into $(B^r C^r)(A^r)$. Here the $(\dots)$ indicate a common product. Taking this together with the corner (c) weights (2.55),

$$(C^t) C^c (B^r C^r)(A^r) A^c B^c (A^t B^t) \tag{2.56}$$

this combined structure is created. The identity (2.48) is then used to swap $(A^r)A^c$ with $B^c(A^t B^t)$ to get

$$(C^t) C^c (B^r C^r) B^c (A^t B^t)(A^r) A^c \tag{2.57}$$

In full notation this looks like

$$\prod_{m=2}^{N_1} \overleftarrow{C^{-}_{m,1}}^{\,m}\; C^{-}_{1,1} \left(\prod_{n=1}^{N_2-1} \overrightarrow{B_{1,n} C_{1,n+1}}^{\,n} \prod_{n=1}^{N_2-1} \overleftarrow{A^{-}_{N_1,n}}^{\,n} \right) A_{N_1,N_2} B_{1,N_2} \prod_{m=1}^{N_1-1} \overrightarrow{A_{m,N_2} B_{m+1,N_2}}^{\,m} \tag{2.58}$$

$$\overset{*}{=} \prod_{m=2}^{N_1} \overleftarrow{C^{-}_{m,1}}^{\,m}\; C^{-}_{1,1} \prod_{n=1}^{N_2-1} \overrightarrow{B_{1,n} C_{1,n+1}}^{\,n} B^{\delta_1}_{1,N_2} \prod_{m=1}^{N_1-1} \overrightarrow{A^{\delta_1}_{m,N_2} B^{\delta_1}_{m+1,N_2}}^{\,m} \prod_{n=1}^{N_2-1} \overleftarrow{A^{-\delta_2}_{N_1,n}}^{\,n} A^{\delta_2}_{N_1,N_2} \tag{2.59}$$

$$\overset{*}{=} \prod_{m=2}^{N_1} \overleftarrow{C^{-}_{m,1}}^{\,m} \left\{ C^{-}_{1,1} \prod_{n=1}^{N_2-1} \overrightarrow{B_{1,n} C_{1,n+1}}^{\,n} B^{\delta_1}_{1,N_2} A^{\delta_1}_{1,N_2} \right\}$$
$$\times \prod_{m=2}^{N_1-1} \overrightarrow{B^{\delta_1}_{m,N_2} A^{\delta_1}_{m,N_2}}^{\,m} B^{\delta_1}_{N_1,N_2} A^{\delta_2\delta_3}_{N_1,N_2} \prod_{n=1}^{N_2-1} \overleftarrow{A^{-\delta_2\delta_4}_{N_1,n}}^{\,n} \tag{2.60}$$

Here the $\overset{*}{=}$ notation introduced in (2.48) was made use of. In the last step, the identity (2.42) was applied to the product over $A^{\delta_1}_{m,N_2} B^{\delta_1}_{m+1,N_2}$ and $A^{\delta_2}_{N_1,N_2}$ was moved to the left of the product over $A^{-\delta_2}_{N_1,n}$ by applying (2.48) once again. Even though this seems complicated, the fact that the expression only depends on δ_1 and the products $\delta_2\delta_3$ as well as $\delta_2\delta_4$ allows the reduction from 16 terms down to only 4. If the label $P(\delta_1, \delta_2\delta_3, \delta_2\delta_4)$ is temporarily assigned to (2.60), the only terms that will remain are:

$$\frac{1}{2}\big(P(1,1,-1) + P(1,-1,1) + P(-1,1,1) - P(-1,-1,-1)\big) \tag{2.61}$$

δ_1	$\delta_2\delta_3$	$\delta_2\delta_4$	x	y
1	1	-1	p	a
1	-1	1	a	a
-1	1	1	a	p
-1	-1	-1	p	p

Table 2.1: This tables shows how the different values of δ_i relate to periodic (p) or anti-periodic (a) boundary conditions of the fermionic fields in the x and y-direction.

The process now begins with the iterative addition of non-boundary weights at the right edge of the expression within the curly braces. Subsequently, the content within the curly braces will represent the columns (y-direction) of the system, where the products to the left and right supply the appropriate boundary terms for the top and bottom of the columns; the final product over A will close the iterations once all internal weights have been utilized. By focusing solely on the contents of the curly braces, the internal weights of the first column are added:

$$C^{-}_{1,1}\prod_{n=1}^{N_2-1}\overrightarrow{B_{1,n}C_{1,n+1}}^{\,n}B^{\delta_1}_{1,N_2}A^{\delta_1}_{1,N_2}\prod_{n=1}^{N_2-1}\overleftarrow{A_{1,n}}^{\,n}\prod_{n=1}^{N_2-1}\overrightarrow{B_{2,n}C_{2,n+1}}^{\,n} \tag{2.62}$$

Now the $C^{-}_{1,1}$ can be absorb into the product to the right, momentarily suppressing the minus sign.

$$\prod_{n=1}^{N_2-1}\overrightarrow{C_{1,n}B_{1,n}C_{1,N_2}}^{\,n}B^{\delta_1}_{1,N_2}A^{\delta_1}_{1,N_2}\prod_{n=1}^{N_2-1}\overleftarrow{A_{1,n}}^{\,n}\prod_{n=1}^{N_2-1}\overrightarrow{B_{2,n}C_{2,n+1}}^{\,n} \tag{2.63}$$

Now it is obvious that all the weights with the same index of the first column are next to each other, making it possible to trace them out using (2.18) and leaving only the product over $B_{2,n}C_{2,n+1}$ behind. Products of the type $C_{m,n}B_{m,n}A_{m,n}$ commute with the rest of the expression, since the trace over $\sigma_{m,n}$ only leaves terms with even powers of the Grassmann numbers. This procedure results in the same starting point as in (2.60), albeit with one column traced out; in the subsequent step $C^{-}_{2,1}$ from the left product and $B^{\delta_1}_{2,N_2}A^{\delta_1}_{2,N_2}$ from the right product can be included and the internal weights of the next column can be added until all weights have been used.

2.2.3 Boundary conditions

The boundary condition of the fermionic fields, given in table 2.1, are obtained by inspecting when the boundary terms to the left and right (top and bottom) in (2.60) have the same (opposite) signs. Together with the permissible combinations of δ_i found in (2.61), the four terms can be associated with different combinations of periodic and anti-periodic boundary conditions in x and y direction.

2.2.4 Fermionic representation

From (2.63), it is observed that the order in which the weights with the same index appear is CBA. Given the known boundary conditions for the fermionic fields, these can be temporarily disregarded and later reintroduced upon transitioning to Fourier space.

The relevant part of the partition function is as follows:

$$Q = \operatorname*{Tr}_{\{c\}} \prod_{m=1}^{N_1} \prod_{n=1}^{N_2} \operatorname*{Tr}_{\{\sigma_{m,n}\}} \left[C_{m,n} B_{m,n} A_{m,n} \right] \tag{2.64}$$

$$= \int \prod_{i=1}^{N_1} \prod_{j=1}^{N_2} dc^*_{i,j} dc_{i,j} \exp \left(\sum_{m=1}^{N_1} \sum_{n=1}^{N_2} \alpha_0 c_{m,n} c^*_{m,n} + (c_{m-1,n} + c^*_{m-1,n})(\alpha_1 c_{m,n} - \alpha_2 c^*_{m-1,n-1}) + \alpha_3 c^*_{m-1,n-1} c_{m,n} \right) \tag{2.65}$$

where in the second step the spins were traced out. Shifting the indices separately in each term accordingly [37], one obtains

$$Q = \int \prod_{i=0}^{N_1-1} \prod_{j=0}^{N_2-1} dc^*_{i,j} dc_{i,j} \exp \left(\sum_{m=0}^{N_1-1} \sum_{n=0}^{N_2-1} \alpha_0 c_{m,n} c^*_{m,n} - \alpha_1 c_{m+1,n} c^*_{m,n} - \alpha_2 c_{m,n+1} c^*_{m,n} - \alpha_3 c_{m+1,n+1} c^*_{m,n} + \alpha_1 c_{m,n} c_{m+1,n} + \alpha_2 c^*_{m,n} c^*_{m,n+1} \right). \tag{2.66}$$

The Fourier transforms for the Grassmann variables take the form

$$c_{m,n} = \frac{1}{\sqrt{N_1 N_2}} \sum_{p=0}^{N_1-1} \sum_{q=0}^{N_2-1} \tilde{c}_{p,q} \; e^{i \boldsymbol{x}_{m,n} \cdot (\boldsymbol{k}_{p,q} + \boldsymbol{u})} \tag{2.67}$$

$$c^*_{m,n} = \frac{1}{\sqrt{N_1 N_2}} \sum_{p=0}^{N_1-1} \sum_{q=0}^{N_2-1} \tilde{c}^*_{p,q} \; e^{-i \boldsymbol{x}_{m,n} \cdot (\boldsymbol{k}_{p,q} + \boldsymbol{u})} \tag{2.68}$$

where $\boldsymbol{u} = 2\pi\Delta_x/N_1 \, \boldsymbol{b}_1 + 2\pi\Delta_y/N_2 \, \boldsymbol{b}_2$ and $\Delta_x, \Delta_y \in \{0, \frac{1}{2}\}$. For $\Delta = 0$ normal periodic boundary conditions are enforced e.g. $c_{m+L,n} = c_{m,n}$ for $\Delta = \frac{1}{2}$, on the other hand, anti-periodic boundary conditions are enforced e.g. $c_{m+L,n} = -c_{m,n}$, which can be checked easily. Plugging in the transformations into Q and making use of Kronecker delta definition in Fourier space, one finds

$$Q_{\Delta_x,\Delta_y} = \int \prod_{i=0}^{N_1-1} \prod_{j=0}^{N_2-1} d\tilde{c}^*_{i,j} d\tilde{c}_{i,j} \exp \left(\sum_{p=0}^{N_1-1} \sum_{q=0}^{N_2-1} \tilde{c}_{p,q} \tilde{c}^*_{p,q} \Big[\alpha_0 - \alpha_1 e^{i\frac{2\pi}{N_1}(p+\Delta_x)} - \alpha_2 e^{i\frac{2\pi}{N_2}(q+\Delta_y)} - \alpha_3 e^{2\pi i \left(\frac{p+\Delta_x}{N_1} + \frac{q+\Delta_y}{N_2} \right)} \Big] - \alpha_1 \tilde{c}_{p,q} \tilde{c}_{N_1-p,N_2-q} e^{i\frac{2\pi}{N_1}(p+\Delta_x)} - \alpha_2 \tilde{c}^*_{p,q} \tilde{c}^*_{N_1-p,N_2-q} e^{i\frac{2\pi}{N_2}(q+\Delta_y)} \right) \tag{2.69}$$

which is a block diagonal form that factorizes into low dimensional integrals; here the boundary conditions were made explicit by introducing $Q = Q_{\Delta_x,\Delta_y}$. From here on, the approach is again very similar to Plechko [37] in defining

$$E_{\pm f} = \alpha_0 - \alpha_1 e^{\pm i\frac{2\pi}{N_1}(p+\Delta_x)} - \alpha_2 e^{\pm i\frac{2\pi}{N_2}(q+\Delta_y)} - \alpha_3 e^{\pm 2\pi i \left(\frac{p+\Delta_x}{N_1} + \frac{q+\Delta_y}{N_2} \right)} \tag{2.70}$$

$$\Omega_f = \alpha_1 (e^{i\frac{2\pi}{N_1}(p+\Delta_x)} - e^{-i\frac{2\pi}{N_1}(p+\Delta_x)}) \tag{2.71}$$

$$\Omega'_f = \alpha_2 (e^{i\frac{2\pi}{N_2}(q+\Delta_y)} - e^{-i\frac{2\pi}{N_2}(q+\Delta_y)}) \tag{2.72}$$

where $f = (p, q)$ and $-f = (N_1 - p, N_2 - q)$ are points in frequency space. It is convenient to define the auxiliary integral

$$(\widetilde{Q}^{(p,q)}_{\Delta_x,\Delta_y})^2 = \int dc^*_f dc_f dc^*_{-f} dc_{-f} \exp\left(E_f c_f c^*_f + E_{-f} c_{-f} c^*_{-f} - \Omega_f c_f c_{-f} - \Omega' f c^*_{-f} c^*_f\right) \tag{2.73}$$

that relates to the original integral via

$$Q^2_{\Delta_x,\Delta_y} = \prod_{p=0}^{M-1} \prod_{q=0}^{N-1} (\widetilde{Q}^{(p,q)}_{\Delta_x,\Delta_y})^2 \tag{2.74}$$

where the square arises because the integral $(\widetilde{Q}^{(p,q)}_{\Delta_x,\Delta_y})^2$ is over $f = (p, q)$ and $-f = (N_1 - p, N_2 - q)$, but since $q, p = 0, 1 \ldots N_i - 1$ one passes over all points twice, from opposite directions. $(\widetilde{Q}^{(p,q)}_{\Delta_x,\Delta_y})^2$ can be solved easily using (2.27), the result is

$$\begin{aligned}(\widetilde{Q}^{(p,q)}_{\Delta_x,\Delta_y})^2 &= E_f E_{-f} + \Omega_f \Omega'_f \qquad (2.75)\\ &= (\alpha_0^2 + \alpha_1^2 + \alpha_2^2 + \alpha_3^2) \\ &\quad - 2(\alpha_0\alpha_1 - \alpha_2\alpha_3)\cos\left(\frac{2\pi(p+\Delta_x)}{N_1}\right) \\ &\quad - 2(\alpha_0\alpha_2 - \alpha_1\alpha_3)\cos\left(\frac{2\pi(q+\Delta_y)}{N_2}\right) \\ &\quad - 2(\alpha_0\alpha_3 - \alpha_1\alpha_2)\cos\left(\frac{2\pi(p+\Delta_x)}{N_1} + \frac{2\pi(q+\Delta_y)}{N_2}\right) \qquad (2.76)\end{aligned}$$

With the above, the total partition function takes the form:

$$Z^{\text{trIs}} = (2R)^{N_1 N_2} \frac{1}{2}\left[Q_{0,\frac{1}{2}} + Q_{\frac{1}{2},\frac{1}{2}} + Q_{\frac{1}{2},0} - \operatorname{sgn}\left(\frac{T - T_c}{T_c}\right) Q_{0,0}\right] \tag{2.77}$$

The sign term in front of $Q_{0,0}$ follows from the integration over the zero-mode $p = q = 0$ in case of ferromagnetic couplings[1]. To understand this, consider the integral (2.69) with $\Delta_x = \Delta_y = 0$ only for the mode $p = q = 0$

$$\begin{aligned}\widetilde{Q}^{(0,0)}_{0,0} &= \int d\tilde{c}^*_{0,0} d\tilde{c}_{0,0}\; e^{\tilde{c}_{0,0}\tilde{c}^*_{0,0}[\alpha_0 - \alpha_1 - \alpha_2 - \alpha_3]} \qquad (2.78)\\ &= \alpha_0 - \alpha_1 - \alpha_2 - \alpha_3, \qquad (2.79)\end{aligned}$$

where in the first step $\tilde{c}_{0,0}\tilde{c}_{N_1,N_2} = \tilde{c}^2_{0,0} = 0$ was used and similarly for the term containing only conjugate variables; additionally, in the second step (2.27) was employed. As will be shown later in (2.99), the above expression is equal to $-2\bar{\alpha}_0$, which can be shown to change sign, when crossing the critical point. However, this property is lost when introducing the squared auxiliary integral in (2.73), even though the final expression calls for the non-squared, original expression Q_{Δ_x,Δ_y}; to correct this, the sign factor in front of the last term is introduced [35, 45].

The free energy density is thus given by

$$\begin{aligned}f^{\text{trIs}} &= -\frac{1}{V}\ln Z^{\text{trIs}} \\ &= -\ln(2R) - \frac{1}{V}\ln\frac{1}{2}\left[Q_{0,\frac{1}{2}} + Q_{\frac{1}{2},\frac{1}{2}} + Q_{\frac{1}{2},0} - \operatorname{sgn}\left(\frac{T - T_c}{T_c}\right) Q_{0,0}\right] \qquad (2.80)\end{aligned}$$

[1] In the other phases, different modes with combinations of $p = 0, N_1$ and $q = 0, N_2$ may be responsible for the sign change, however, the same reasoning applies just with different critical conditions.

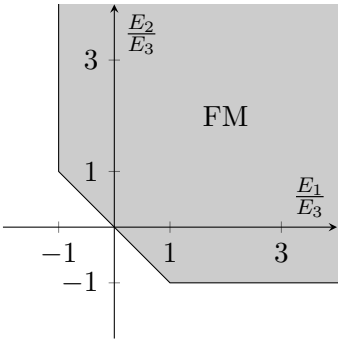

Figure 2.1: The ferromagnetic (FM) region as a function of the couplings E_i is the gray shaded part in this figure.

which converges in the limit of $V \to \infty$ to [37, 38]

$$v f_b^{\mathrm{trIs}} = -\ln(2R) - \frac{1}{2}\int_0^{2\pi}\frac{dp}{2\pi}\int_0^{2\pi}\frac{dq}{2\pi}\ln[(\alpha_0^2+\alpha_1^2+\alpha_2^2+\alpha_3^2) - 2(\alpha_0\alpha_1-\alpha_2\alpha_3)\cos(p) - 2(\alpha_0\alpha_2-\alpha_1\alpha_3)\cos(q) - 2(\alpha_0\alpha_3-\alpha_1\alpha_2)\cos(p+q)] \quad (2.81)$$

2.3 The ferromagnetic regime

Up until now, the results presented here have been applicable to all couplings E_i. However, from this point forward, attention will be restricted to the ferromagnetic region, which is defined by the simultaneous conditions [44]

$$E_1 + E_2 > 0, \quad E_1 + E_3 > 0, \quad E_2 + E_3 > 0, \quad (2.82)$$

illustrated in fig. 2.1. After the left side of (2.7) is expanded into exponential form,

$$\frac{1}{4}e^{-2\beta_c(E_1+E_2)}\left(e^{2\beta_c(E_1+E_2)} + e^{2\beta_c(E_1+E_3)} + e^{2\beta_c(E_2+E_3)} - 1\right) \times \left(e^{2\beta_c(E_1+E_2)} - e^{2\beta_c(E_1-E_3)} - e^{2\beta_c(E_2-E_3)} - 1\right), \quad (2.83)$$

it is apparent that the expression between the first parentheses can never lead to the total expression being zero, since it is always greater or equal to two. The term in the second parentheses, on the other hand, may be zero and thus the expression

$$e^{2\beta_c(E_1+E_2)} - e^{2\beta_c(E_1-E_3)} - e^{2\beta_c(E_2-E_3)} - 1 = 0 \quad (2.84)$$

can be used as a simplified critical condition in the ferromagnetic regime.

2.4 Correlation function at criticality

As discussed in the introduction, the correlation function of the ferromagnetic, triangular Ising model on a square lattice with orthonormal lattice vectors ($a_1 = a_2 = 1$, $\vartheta = \pi/2$) was obtained in [32] and was later put into the context of multi-parameter universality for

the case $E_1 = E_2$, $E_3 = 0$ and E_1 unequal E_2, $E_3 = 0$ as well as for $E_1 = E_2 = E_3$ in [28], furthermore the mean correlation length was discussed in [30] for general E_i as a function of the couplings on a square lattice. The general case of arbitrary E_i and a parallelogram lattice is discussed in [1]. There it was shown, that the asymptotic correlation function $C^{\mathrm{trIs}}(\boldsymbol{x}_i - \boldsymbol{x}_j) = \langle \sigma_i \sigma_j \rangle - \mathcal{M}^2$ is given by

$$C^{\mathrm{trIs}}(\boldsymbol{x}) = \frac{C^{\mathrm{trIs}}_{0+} \, (\bar{\xi}^{\mathrm{trIs}}_{0+})^{-7/4}}{[\boldsymbol{x} \cdot (\bar{\boldsymbol{A}}^{\mathrm{trIs}})^{-1} \boldsymbol{x}]^{1/8}} \Psi_{\pm} \left(\frac{[\boldsymbol{x} \cdot (\bar{\boldsymbol{A}}^{\mathrm{trIs}})^{-1} \boldsymbol{x}]^{1/2}}{\bar{\xi}^{\mathrm{trIs}}_{\pm}(t)} \right), \tag{2.85}$$

where $\mathcal{M}$ is the spontaneous magnetization, and $\Psi_{\pm}$ the universal scaling function above (+) and below (–) the critical point. The mean correlation length on the triangular lattice $\bar{\xi}^{\mathrm{trIs}}_{\pm}(t) = \bar{\xi}^{\mathrm{trIs}}_{0\pm} |t|^{-1}$ is given in terms of its amplitude

$$\bar{\xi}^{\mathrm{trIs}}_{0\pm} = \frac{\sqrt{v}}{2\beta_c (E_1 [\hat{S}^c_2 + \hat{S}^c_3]^{\frac{1}{2}} + E_2 [\hat{S}^c_1 + \hat{S}^c_3]^{\frac{1}{2}} + E_3 [\hat{S}^c_1 + \hat{S}^c_2]^{\frac{1}{2}})} \tag{2.86}$$

and the reduced temperature $t = (T - T_c)/T_c$. The structure of (2.85) agrees with the general proof for weakly ansiotropic Ising models on Bravais lattices (including parallelogram lattices) and with short-range pair interactions presented in [30]. The reduced anisotropy matrix $\bar{\boldsymbol{A}}^{\mathrm{trIs}}$ describes the angular dependency of the correlation function on an anisotropic parallelogram lattice, which can be decomposed into contributions from lattice anisotropy through a shear transform

$$\boldsymbol{S} = \begin{pmatrix} a_1 & a_2 \cos\vartheta \\ 0 & a_2 \sin\vartheta \end{pmatrix}, \tag{2.87}$$

that maps the rectangular lattice onto a parallelogram lattice with angle ϑ, spanned by the two lattice vectors

$$\mathbf{a}_1 = a_1 \begin{pmatrix} 1 \\ 0 \end{pmatrix}, \quad \mathbf{a}_2 = a_2 \begin{pmatrix} \cos(\vartheta) \\ \sin(\vartheta) \end{pmatrix}, \tag{2.88}$$

and a contribution from the different coupling strengths in the various lattice directions, through the reduced anisotropy matrix on a rectangular geometry with orthonormal lattice vectors [28],

$$\bar{\boldsymbol{A}}^{\mathrm{trIs,rec}} = \begin{pmatrix} \hat{S}^c_1 + \hat{S}^c_3 & \hat{S}^c_3 \\ \hat{S}^c_3 & \hat{S}^c_2 + \hat{S}^c_3 \end{pmatrix}. \tag{2.89}$$

Combining both contributions yields the anisotropy matrix on a parallelogram geometry through

$$\boldsymbol{A}^{\mathrm{trIs}} = \boldsymbol{S} \bar{\boldsymbol{A}}^{\mathrm{trIs,rec}} \boldsymbol{S}^T. \tag{2.90}$$

Note, that this is not a reduced anisotropy matrix, since it has not been normalized. However, since $\bar{\boldsymbol{A}} = \boldsymbol{A}/\sqrt{\det \boldsymbol{A}}$, one finds that

$$\bar{\boldsymbol{A}}^{\mathrm{trIs}} = \frac{1}{|\det \boldsymbol{S}|} \, \boldsymbol{A}^{\mathrm{trIs}}, \tag{2.91}$$

where $\det \boldsymbol{S} = a_1 a_2 \sin\vartheta$ is the area of a parallelogram lattice unit cell v. Additionally, as will be shown in the next section, the correlation length amplitudes are also related

through v, namely $\bar{\xi}_{0\pm}^{\mathrm{trIs}} = \sqrt{v}\,\bar{\xi}_{0\pm}^{\mathrm{trIs,rec}}$. This implies for the correlation function (2.85), that

$$C^{\mathrm{trIs}}(\boldsymbol{x}) \sim \Psi_{\pm}\left(\frac{[\boldsymbol{x}\cdot(\bar{\boldsymbol{A}}^{\mathrm{trIs}})^{-1}\boldsymbol{x}]^{1/2}}{\bar{\xi}_{\pm}^{\mathrm{trIs}}(t)}\right) \tag{2.92}$$

$$= \Psi_{\pm}\left(\frac{[(\boldsymbol{S}^{-1}\boldsymbol{x})^{T}(\bar{\boldsymbol{A}}^{\mathrm{trIs,rec}})^{-1}(\boldsymbol{S}^{-1}\boldsymbol{x})]^{1/2}}{\bar{\xi}_{\pm}^{\mathrm{trIs,rec}}(t)}\right) \tag{2.93}$$

$$\sim C^{\mathrm{trIs,rec}}(\boldsymbol{S}^{-1}\boldsymbol{x}), \tag{2.94}$$

it is related to the one on the rectangular lattice $C^{\mathrm{trIs,rec}}$ with the same coupling parameters through the shear transform $\boldsymbol{S}$. The amplitude of $C^{\mathrm{trIs}}(\boldsymbol{x})$ can also be related to the one on the rectangular lattice by using the above relations together with the fact that the susceptibility amplitude transforms as follows $C_{0+}^{\mathrm{trIs}} = v\,C_{0+}^{\mathrm{trIs,rec}}$, since the sum rule for the susceptibility yields:

$$\chi_{\pm}^{\mathrm{trIs,rec}} = \int \mathrm{d}\boldsymbol{x}\; C^{\mathrm{trIs,rec}}(\boldsymbol{x}) \tag{2.95}$$

$$= \frac{1}{v}\int \mathrm{d}\boldsymbol{x}\; C^{\mathrm{trIs,rec}}(\boldsymbol{S}^{-1}\boldsymbol{x}) \tag{2.96}$$

To illustrate these relations, in figure 2.2 a few examples with lattices, couplings and their associated correlations ellipsis are shown. Furthermore, in figure 2.3 the transformation relations between isotropic and anisotropic lattices are visualized; this flow chart also highlights the two different parallelograms that show up in multi-parameter universality – one isotropic and one anisotropic.

In the next sections, both the mean correlation length, through the amplitude of the singular free energy, as well as the reduced anisotropy matrix from the free energy scaling function, will be recovered. The correlation function is only mentioned here briefly, since it is not the main subject of this work, but it is still important to interpret the different quantities that will arise in the following sections.

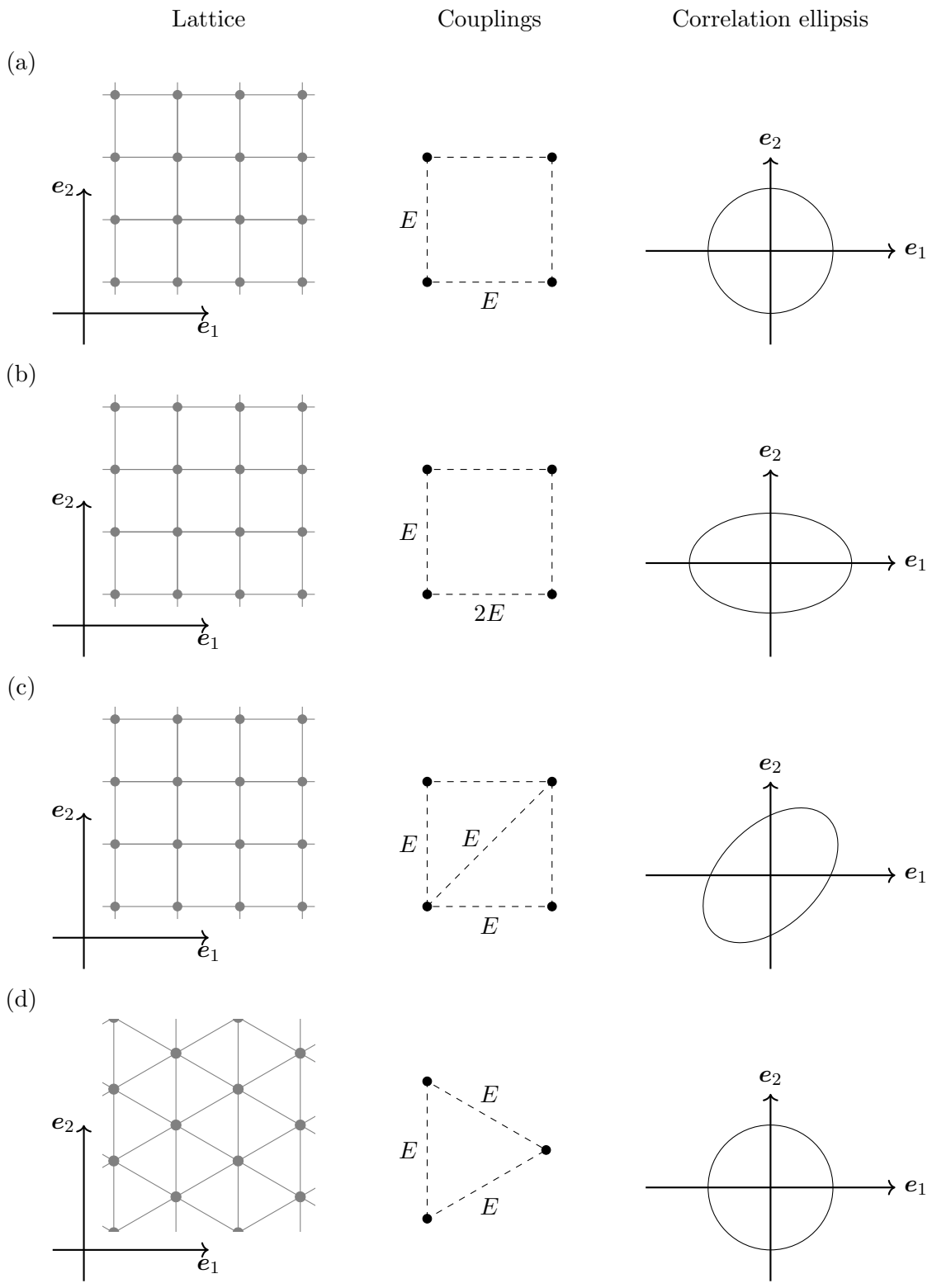

Figure 2.2: A range of different lattices and couplings with their associated correlation ellipsis. (a) showing the typical isotropic case, while (b) demonstrates rectangular anisotropy; i.e. the principle axis of the correlation ellipsis and the lattice vectors are aligned. (c) shows a square lattice with next nearest neighbor couplings while (d) shows the related triangular lattice; which visualizes how lattice deformation influences the correlation function.

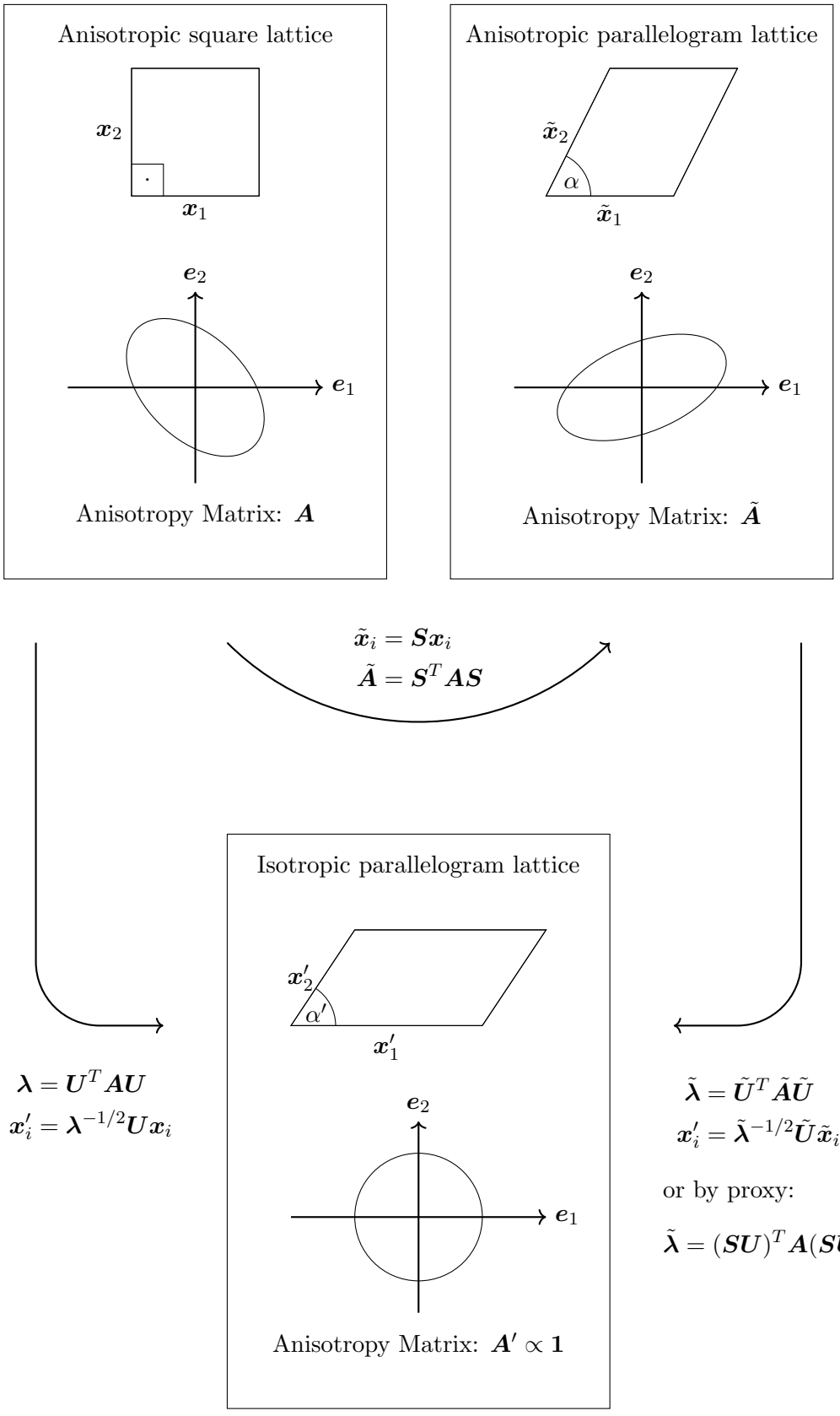

Figure 2.3: Flow chart of how different lattice geometries and the angular dependence of correlation functions are related. The shown formulas are explicitly given for a ϕ^4 model, while for more general models generalized shear transformations as presented in Ref. [30] apply.

2.5 Singular bulk free energy

To extract the singular contribution $f_{b,s}^{\mathrm{Is}}$ from the bulk free energy f_b^{Is}, it is first shown that the integrand of (2.81) diverges at the critical point for $(p,q)=(0,0)$. To this end, $\cos(x)$ is approximated as $1-x^2/2$ in (2.81):

$$\begin{aligned}-\frac{1}{2}\int_0^{2\pi}\frac{\mathrm{d}p_1}{2\pi}\int_0^{2\pi}\frac{\mathrm{d}p_2}{2\pi}\ln[&R^2(\alpha_1+\alpha_2+\alpha_3-\alpha_0)^2\\&+R^2(\alpha_0\alpha_1-\alpha_2\alpha_3)p_1^2\\&+R^2(\alpha_0\alpha_2-\alpha_1\alpha_3)p_2^2\\&+R^2(\alpha_0\alpha_3-\alpha_1\alpha_2)(p_1+p_2)^2].\end{aligned}\tag{2.97}$$

Here R was moved into the integral, the logarithms combined and used that

$$\begin{aligned}&(\alpha_0^2+\alpha_1^2+\alpha_2^2+\alpha_3^2)-\ 2(\alpha_0\alpha_1-\alpha_2\alpha_3)-\ 2(\alpha_0\alpha_2-\alpha_1\alpha_3)-\ 2(\alpha_0\alpha_3-\alpha_1\alpha_2)\\&=(\alpha_1+\alpha_2+\alpha_3-\alpha_0)^2\qquad(2.98)\\&\equiv(2\bar{\alpha}_0)^2,\qquad(2.99)\end{aligned}$$

where $\bar{\alpha}_0$ was defined. After many laborious steps or with the help of computer algebra software, one can show that

$$2\bar{\alpha}_0=\frac{e^{\beta(E_3-E_1-E_2)}\left(e^{2\beta(E_1+E_2)}-e^{2\beta(E_1-E_3)}-e^{2\beta(E_2-E_3)}-1\right)}{2R},\tag{2.100}$$

where for $\beta=\beta_c$ the left side of the critical condition (2.84) can be identified and thus one can see that at the critical point the integrand of (2.97) diverges at $(p,q)=(0,0)$. Additionally one finds, that

$$R^2(\alpha_2\alpha_3-\alpha_0\alpha_1)=R^2\frac{-\tanh(\beta E_1)}{\cosh^2(\beta E_2)\cosh^2(\beta E_3)}=-\frac{1}{2}\sinh 2\beta E_1,\tag{2.101}$$

and similarly for the other coefficients. Limiting the integration domain to a small circle section $S(\epsilon)$ of radius ϵ around the origin to only calculate the singular part, the bulk free energy density can be approximated as:

$$vf_b^{\mathrm{trIs}}\simeq-\ln 2-\frac{1}{2}\int_{\boldsymbol{p}\in S(\epsilon)}\frac{\mathrm{d}\boldsymbol{p}}{(2\pi)^2}\ln\left[(2R\bar{\alpha}_0)^2+\hat{S}_1\frac{p_1^2}{2}+\hat{S}_2\frac{p_2^2}{2}+\hat{S}_3\frac{(p_1+p_2)^2}{2}\right].\tag{2.102}$$

2.5.1 Identifying the reduced anisotropy matrix

In equation (2.102), a quadratic form can be identified

$$vf_b^{\mathrm{Is}}\simeq-\ln 2-\frac{1}{(2\pi)^2}\int_{\boldsymbol{p}\in S(\epsilon)}\mathrm{d}^2\boldsymbol{p}\ln\left[(2R\bar{\alpha}_0)^2+\frac{1}{2}\,\boldsymbol{p}^T\begin{pmatrix}\hat{S}_1+\hat{S}_3 & \hat{S}_3\\ \hat{S}_3 & \hat{S}_2+\hat{S}_3\end{pmatrix}\boldsymbol{p}\right],\tag{2.103}$$

where $\boldsymbol{p}=(p_1,p_2)^T$ was introduced. In anticipation of recovering the reduced anisotropy matrix (2.89), the matrix

$$\mathcal{A}^{\mathrm{trIs,rec}}=\begin{pmatrix}\hat{S}_1+\hat{S}_3 & \hat{S}_3\\ \hat{S}_3 & \hat{S}_2+\hat{S}_3\end{pmatrix}\tag{2.104}$$

is defined. However, note that here the $\hat{S}_i$ are not at β_c. The eigenvalue problem associated with $\mathcal{A}^{\mathrm{trIs,rec}}$ is given by

$$\boldsymbol{U}^T \mathcal{A}^{\mathrm{trIs,rec}} \boldsymbol{U} = \boldsymbol{\lambda} \tag{2.105}$$

where $\boldsymbol{U}$ is a unitary transformation matrix and $\boldsymbol{\lambda}$ the diagonal eigenvalue matrix. By defining $\boldsymbol{p} = \boldsymbol{U}\boldsymbol{\lambda}^{-1/2}\boldsymbol{p'}$, the integral simplifies to

$$v f_b^{\mathrm{Is}} \simeq -\ln 2 - \frac{1}{(2\pi)^2} \frac{1}{\sqrt{\det \mathcal{A}^{\mathrm{trIs,rec}}}} \int_{\boldsymbol{p'} \in S(\epsilon)} \mathrm{d}^2 \boldsymbol{p'} \ln \left[(2R\bar{\alpha}_0)^2 + \frac{|\boldsymbol{p'}|^2}{2} \right] \tag{2.106}$$

where it was assumed, that the above transformation has no influence of the infinitesimal integration domain $S(\epsilon)$.

2.5.2 Solving the integral

After introducing polar coordinates $p_1' = r\cos\phi$, $p_2' = r\sin\phi$, the integral is transformed to

$$v f_b^{\mathrm{trIs}} \simeq -\ln 2 - \frac{1}{4\pi} \frac{1}{\sqrt{\det \mathcal{A}^{\mathrm{trIs,rec}}}} \int_0^\epsilon r \ \mathrm{d}r \ln \left[(2R\bar{\alpha}_0)^2 + \frac{r^2}{2} \right], \tag{2.107}$$

where the integral over ϕ has already been evaluated. The integral over r can be done as well, and reads

$$\begin{aligned} v f_b^{\mathrm{trIs}} \simeq -\ln 2 - \frac{1}{8\pi} \frac{1}{\sqrt{\det \mathcal{A}^{\mathrm{trIs,rec}}}} \Bigg[& \epsilon^2 \ln \left((2R\bar{\alpha}_0)^2 + \frac{\epsilon^2}{2} \right) - \epsilon^2 \\ & - (2R\bar{\alpha}_0)^2 \ln 4 + 2(2R\bar{\alpha}_0)^2 \ln \frac{1}{(2R\bar{\alpha}_0)^2} \\ & - 2(2R\bar{\alpha}_0)^2 \ln \frac{1}{2(2R\bar{\alpha}_0)^2 + \epsilon^2} \Bigg]. \end{aligned} \tag{2.108}$$

As discussed above, for $T \to T_c$ it was found that $\bar{\alpha}_0 \to 0$, and thus for an $\epsilon > 0$ the singular part of f_b is found to be

$$v f_{b,s}^{\mathrm{trIs}} = -\frac{1}{4\pi} \frac{(2R\bar{\alpha}_0)^2}{\sqrt{\det \mathcal{A}^{\mathrm{trIs,rec}}}} \ln \frac{1}{(2R\bar{\alpha}_0)^2}, \tag{2.109}$$

since all other terms are either regularized by ϵ or vanish when one takes the second derivative with respect to t.

2.5.3 Scaling behavior near T_c

To find the scaling near T_c, $f_{b,s}^{\mathrm{trIs}}$ is expanded into a Taylor series around T_c; to this end $g(T) := 2R\bar{\alpha}_0$ and $h(T) := \det \mathcal{A}^{\mathrm{trIs,rec}}$ is defined for clarity, such that the amplitude of $f_{b,s}$ is given by $g(T)^2/\sqrt{h(T)}$, with the expansion

$$\begin{aligned} \frac{g(T)^2}{\sqrt{h(T)}} = & \frac{g(T_c)^2}{\sqrt{h(T_c)}} - \frac{g(T_c)^2 h'(T_c) - 4g(T_c)g'(T_c)h(T_c)}{2h(T_c)^{3/2}} (T - T_c) \\ & + \frac{1}{8} \Bigg(\frac{8h(T_c)^2 (g(T_c)g''(T_c) + g'(T_c)^2) + 3g(T_c)^2 h'(T_c)^2}{h(T_c)^{5/2}} \\ & - \frac{2g(T_c)h(T_c)(4g'(T_c)h'(T_c) + g(T_c)h''(T_c))}{h(T_c)^{5/2}} \Bigg) (T - T_c)^2 + \mathcal{O}\left(T - T_c\right)^3, \end{aligned} \tag{2.110}$$

but since $g(T_c) = 0$, only

$$\frac{g(T)^2}{\sqrt{h(T)}} = \frac{g'(T_c)^2}{\sqrt{h(T_c)}}(T - T_c)^2 + \mathcal{O}\left(T - T_c\right)^3 \tag{2.111}$$

$$= \frac{1}{\sqrt{\det \mathcal{A}^{\mathrm{trIs,rec}}(T = T_c)}} \left[\frac{\partial}{\partial T}(2R\bar{\alpha}_0)\Big|_{T=T_c}\right]^2 (T - T_c)^2 + \mathcal{O}\left(T - T_c\right)^3 \tag{2.112}$$

$$= \frac{1}{T_c^4} \left[\frac{\partial}{\partial \beta}(2R\bar{\alpha}_0)\Big|_{\beta=\beta_c}\right]^2 (T - T_c)^2 + \mathcal{O}\left(T - T_c\right)^3 \tag{2.113}$$

$$= \beta_c^2 \left[\frac{\partial}{\partial \beta}(2R\bar{\alpha}_0)\Big|_{\beta=\beta_c}\right]^2 t^2 + \mathcal{O}\left(t^3\right) \tag{2.114}$$

remains, and in the second step it was used that $\mathcal{A}^{\mathrm{trIs,rec}}(T = T_c)$ can be identified as the reduced anisotropy matrix $\bar{\boldsymbol{A}}^{\mathrm{trIs,rec}}$, which fulfills $\det \bar{\boldsymbol{A}}^{\mathrm{trIs,rec}} = 1$, as introduced in (2.89). Now only a first derivative has to be evaluated, which can be done by using (2.100), taking the derivative with respect to β,

$$\begin{aligned}
&\frac{\partial}{\partial \beta}(2R\bar{\alpha}_0) \\
&= -\frac{1}{2}(E_1 + E_2 + E_3)e^{-\beta(E_1+E_2+E_3)}\left(e^{2\beta E_1} + e^{2\beta E_2} + e^{2\beta E_3} - e^{2\beta(E_1+E_2+E_3)}\right) \\
&\quad + e^{-\beta(E_1+E_2+E_3)}\Big(E_1 e^{2\beta E_1} + E_2 e^{2\beta E_2} + E_3 e^{2\beta E_3} - (E_1 + E_2 + E_3)e^{2\beta(E_1+E_2+E_3)}\Big),
\end{aligned} \tag{2.115}$$

and using the critical condition (2.84), one finds that

$$\begin{aligned}
&\frac{\partial}{\partial \beta}(2R\bar{\alpha}_0)\Big|_{\beta=\beta_c} \\
&= e^{-\beta_c(E_1+E_2+E_3)}\Big(E_1 e^{2\beta_c E_1} + E_2 e^{2\beta_c E_2} + E_3 e^{2\beta_c E_3} - (E_1 + E_2 + E_3)e^{2\beta_c(E_1+E_2+E_3)}\Big).
\end{aligned} \tag{2.116}$$

Furthermore, E_3 can be replaced while defining ζ through rearranging (2.84),

$$E_3 = \frac{1}{2\beta_c} \ln\left[\frac{e^{2\beta_c E_1} + e^{2\beta_c E_2}}{e^{2\beta_c(E_1+E_2)} - 1}\right] \equiv \frac{1}{2\beta_c} \ln \zeta^2 \tag{2.117}$$

which leads to

$$\begin{aligned}
&\frac{\partial}{\partial \beta}(2R\bar{\alpha}_0)\Big|_{\beta=\beta_c} \\
&= E_1(\zeta^{-1}\ e^{\beta_c(E_1-E_2)} - \zeta\ e^{\beta_c(E_1+E_2)}) \\
&+ E_2(\zeta^{-1}\ e^{\beta_c(E_2-E_1)} - \zeta\ e^{\beta_c(E_1+E_2)}) \\
&+ \frac{1}{\sqrt{2}\beta_c}\sqrt{\sinh 2\beta_c E_1 + \sinh 2\beta_c E_2}\ \ln\left[\frac{e^{2\beta_c E_1} + e^{2\beta_c E_2}}{e^{2\beta_c(E_1+E_2)} - 1}\right].
\end{aligned} \tag{2.118, 2.119}$$

Once again plugging in the critical condition with the property

$$\hat{S}_3^c = \sinh \ln \zeta^2 = \frac{1}{2}(\zeta^2 - \zeta^{-2}), \tag{2.120}$$

one can show that for the first term

$$\sqrt{\hat{S}_2^c + \hat{S}_3^c} = \frac{1}{\sqrt{2}}(\zeta^{-1}\ e^{\beta_c(E_1-E_2)} - \zeta\ e^{\beta_c(E_1+E_2)}) \tag{2.121}$$

holds and similarly for the second term. In the third term, the critical condition for E_3 (2.117) can be used. This leads to

$$\begin{aligned}\frac{\partial}{\partial\beta}(2R\bar{\alpha}_0)\Big|_{\beta=\beta_c} =& \frac{1}{\sqrt{2}}\left[E_1\sqrt{\hat{S}_2^c+\hat{S}_3^c}+E_2\sqrt{\hat{S}_1^c+\hat{S}_3^c}+E_3\sqrt{\hat{S}_1^c+\hat{S}_2^c}\right]\\ =& \frac{1}{\sqrt{2}\beta_c\bar{\xi}_{0+}^{\mathrm{sqIs}}},\end{aligned} \tag{2.122}$$

upon comparing this to the inverse mean correlation length amplitude of the square lattice with $\vartheta=\pi/2$ and $a_1=a_2=1$ [1]

$$(\bar{\xi}_{0+}^{\mathrm{sqIs}})^{-1}=2\beta_cE_1\sqrt{\hat{S}_2^c+\hat{S}_3^c}+2\beta_cE_2\sqrt{\hat{S}_1^c+\hat{S}_3^c}+2\beta_cE_3\sqrt{\hat{S}_1^c+\hat{S}_2^c}. \tag{2.123}$$

Plugging the final result into the expansion (2.114), one gets

$$\frac{g(T)^2}{\sqrt{h(T)}}=\frac{1}{2}\frac{1}{(\bar{\xi}_{0+}^{\mathrm{sqIs}})^2}\,t^2+\mathcal{O}\left(t^3\right), \tag{2.124}$$

and thus for $|t|\ll 1$,

$$f_{b,s}^{\mathrm{trIs}}=-\frac{1}{8\pi}\frac{t^2}{v(\bar{\xi}_{0+}^{\mathrm{sqIs}})^2}\ln\frac{2(\bar{\xi}_{0+}^{\mathrm{sqIs}})^2}{t^2} \tag{2.125}$$

$$=\frac{1}{4\pi}\frac{t^2}{(\bar{\xi}_{0+}^{\mathrm{trIs}})^2}\ln|t|+\text{regular contributions}. \tag{2.126}$$

In the last line, the mean correlation length amplitude on the parallelogram lattice $\bar{\xi}_{0+}^{\mathrm{trIs}}=v^{1/2}\bar{\xi}_{0+}^{\mathrm{sqIs}}$ was identified. This scaling form had been predicted in [28] for general, anisotropic ϕ^4-theories and was previously conjectured [46] to hold for the anisotropic Ising model on the triangular lattice as well; a proposition that has now been proven. A general proof of (2.126) was given in [30] for arbitrary weakly anisotropic two-dimensional Ising models. For the case of the Ising model with rectangular anisotropy a similar result was shown in [47, see footnote 19].

2.6 Scaling function of the excess free energy

In the critical regime, it is understood that the free energy can be expressed, based on scaling theory, in terms of a universal function. This function, aside from non-universal prefactors, is independent of the microscopic details of the model and characteristic of the underlying universality class. The scaling function for the Ising model is derived in this chapter, starting from (2.80). More precisely, the expression for $(\widetilde{Q}^{(p,q)}_{\Delta_x,\Delta_y})^2$, as given in (2.76), is rewritten in terms of $\bar{\alpha}_0$ and $\hat{S}_i$, following the steps outlined up to (2.102).

Initially, the reduced partition function for the sector (Δ_x, Δ_y) is written as:

$$(2R)^{2N_1N_2}\, Q^2_{\Delta_x,\Delta_y} = \prod_{p=0}^{N_1-1}\prod_{q=0}^{N_2-1} (2R)^2 (\widetilde{Q}^{(p,q)}_{\Delta_x,\Delta_y})^2$$

$$= \exp\left(\sum_{p=0}^{N_1-1}\sum_{q=0}^{N_2-1} \ln[(2R)^2(\widetilde{Q}^{(p,q)}_{\Delta_x,\Delta_y})^2]\right) \tag{2.127}$$

$$= \exp\left(\sum_{\boldsymbol{k}} \ln \mathcal{Q}^2_{\Delta_x,\Delta_y}(\boldsymbol{k})\right), \tag{2.128}$$

where

$$\mathcal{Q}^2_{\Delta_x,\Delta_y}(\boldsymbol{k}) = [(2R)^2(\widetilde{Q}^{(p,q)}_{\Delta_x,\Delta_y})^2], \tag{2.129}$$

was defined with $\sum_{\boldsymbol{k}_{p,q}} = \sum_{p=0}^{N_1-1}\sum_{q=0}^{N_2-1}$. The total partition function then takes the form

$$Z^{\mathrm{trIs}} = \frac{1}{2}\Big[e^{\frac{1}{2}\sum_{\boldsymbol{k}} \ln \mathcal{Q}^2_{0,1/2}(\boldsymbol{k})} + e^{\frac{1}{2}\sum_{\boldsymbol{k}} \ln \mathcal{Q}^2_{1/2,0}(\boldsymbol{k})} + e^{\frac{1}{2}\sum_{\boldsymbol{k}} \ln \mathcal{Q}^2_{1/2,1/2}(\boldsymbol{k})} - \mathrm{sgn}(t)\, e^{\frac{1}{2}\sum_{\boldsymbol{k}} \ln \mathcal{Q}^2_{0,0}(\boldsymbol{k})}\Big]. \tag{2.130}$$

Now using the same approach as in the previous chapter to approximate $\cos x \simeq 1 - x^2/2$ and simplifying the constants yields

$$\mathcal{Q}^2_{\Delta_x,\Delta_y}(\boldsymbol{k}) \simeq (2R\bar{\alpha}_0)^2 + \hat{S}_1\frac{[\frac{2\pi}{N_1}(p+\Delta_x)]^2}{2} + \hat{S}_2\frac{[\frac{2\pi}{N_2}(q+\Delta_y)]^2}{2} + \hat{S}_3\frac{[\frac{2\pi}{N_1}(p+\Delta_x)+\frac{2\pi}{N_2}(q+\Delta_y)]^2}{2}, \tag{2.131}$$

with $\hat{S}_i = \sinh 2\beta E_i$. Again, one can express the above in terms of a quadratic form

$$\mathcal{Q}^2_{\Delta_x,\Delta_y}(\boldsymbol{k}) \simeq (2R\bar{\alpha}_0)^2 + \frac{1}{2}(\boldsymbol{k}+\boldsymbol{u})^T \boldsymbol{S}\boldsymbol{\mathcal{A}}^{\mathrm{trIs,rec}}\boldsymbol{S}^T(\boldsymbol{k}+\boldsymbol{u}), \tag{2.132}$$

where $\boldsymbol{u} = 2\pi\Delta_x/N_1\boldsymbol{b}_1 + 2\pi\Delta_y/N_2\boldsymbol{b}_2$. Here, $\boldsymbol{S}$ is again the shear transformation that maps the lattice vectors $\boldsymbol{a}_i$ from a rectangular lattice with orthonormal basis vectors, and

$$\mathcal{A}^{\mathrm{trIs,rec}} = \begin{pmatrix} \hat{S}_1 + \hat{S}_3 & \hat{S}_3 \\ \hat{S}_3 & \hat{S}_2 + \hat{S}_3 \end{pmatrix}. \tag{2.133}$$

The shear matrix itself is given by

$$\boldsymbol{S} = \begin{pmatrix} a_1 & a_2\cos\vartheta \\ 0 & a_2\sin\vartheta \end{pmatrix} \tag{2.134}$$

with $\det \boldsymbol{S} = a_1a_2\sin\vartheta = v$. Note that at criticality $\mathcal{A}^{\mathrm{trIs,rec}}$ equals the reduced anisotropy matrix $\bar{\boldsymbol{A}}^{\mathrm{trIs,rec}}$, equivalent to what was presented in (2.87) and (2.89). Furthermore, the partition function of the near critical Ising model is expressed through a sum of four Gaussian models with different values of $\boldsymbol{u}$.

2.6.1 Derivation of the scaling function

Further progress can be made by considering the sector specific quantities

$$\Omega_{\Delta_x,\Delta_y} = \frac{1}{N_1 N_2} \ln[(2R)^{2N_1N_2} Q^2_{\Delta_x,\Delta_y}] - \lim_{V\to\infty} \frac{1}{N_1 N_2} \ln[(2R)^{2N_1N_2} Q^2_{\Delta_x,\Delta_y}] \tag{2.135}$$

$$= \frac{1}{V} \sum_{\boldsymbol{k}} \ln \mathcal{Q}^2_{\Delta_x,\Delta_y}(\boldsymbol{k}) - \int \mathrm{d}\boldsymbol{k}\ \ln \mathcal{Q}^2_{\Delta_x,\Delta_y}(\boldsymbol{k}) \tag{2.136}$$

$\int \mathrm{d}\boldsymbol{k} = \int_{\mathrm{BZ}} \mathrm{d}V/(2\pi)^2$ is the integral over the Brillouin zone. The limit $V \to \infty$ is to be taken with fixed L_2/L_1. Eq. (2.136) is similar in structure to the excess free energy of the anisotropic Gaussian model on a parallelogram lattice with periodic/antiperiodic boundary conditions. For the case of a square lattice with periodic boundary conditions the exact Gaussian excess free energy has been derived in [24, 27, 41] for orthogonal geometries for general d including $d = 2$, in particular for cubic and rectangular geometry in the anisotropic [24, 27] and isotropic [41] cases. The following proof is an extension of the work in [24, 27, 41]. The derivation begins by utilizing the identity

$$\ln w = \int_0^\infty \mathrm{d}y\, y^{-1} \left[\exp(-y) - \exp(-wy)\right] \tag{2.137}$$

to rewrite the above equation and the fact that $(V)^{-1} \sum_{\boldsymbol{k}} 1 = \int \mathrm{d}\boldsymbol{k}\, 1 = 1$ to

$$\Omega_{\Delta_x,\Delta_y} = \int_0^\infty \mathrm{d}y\, y^{-1} \left[\int \mathrm{d}\boldsymbol{k} \exp(-\mathcal{Q}^2_{\Delta_x,\Delta_y}(\boldsymbol{k})\, y) - \frac{1}{V} \sum_{\boldsymbol{k}} \exp(-\mathcal{Q}^2_{\Delta_x,\Delta_y}(\boldsymbol{k})\, y) \right] \tag{2.138}$$

Using the Poisson sum formula [16, 48]

$$\frac{1}{L} \sum_{p=0}^{L-1} G(2\pi p/L) = \sum_{n=-\infty}^{\infty} \int \frac{\mathrm{d}q}{2\pi} G(q) e^{iqnL}, \tag{2.139}$$

where $G(q) = G(q + 2\pi)$ is the a periodic function, the term containing the sum can be brought into a more convenient form

$$\frac{1}{V} \sum_{\boldsymbol{k}} \exp(-\mathcal{Q}^2_{\Delta_x,\Delta_y}(\boldsymbol{k})\, y)$$

$$= \sum_{m,n\in\mathbb{Z}} \int \mathrm{d}\boldsymbol{k} \exp\left[-\mathcal{Q}^2_{\Delta_x,\Delta_y}(\boldsymbol{k})\, y + i\boldsymbol{k}\cdot(m\boldsymbol{L}_1 + n\boldsymbol{L}_2)\right] \tag{2.140}$$

Taking the above equations together yields

$$\Omega_{\Delta_x,\Delta_y} = -\int_0^\infty \mathrm{d}y\, y^{-1} \sum_{m,n\in\mathbb{Z}\setminus 0} \int \mathrm{d}\boldsymbol{k} \exp\left[-\mathcal{Q}^2_{\Delta_x,\Delta_y}(\boldsymbol{k})\, y + i\boldsymbol{k}\cdot(m\boldsymbol{L}_1 + n\boldsymbol{L}_2)\right] \tag{2.141}$$

In the scaling limit, one can replace $\mathcal{Q}^2_{\Delta_x,\Delta_y}(\boldsymbol{k})$ with the expression (2.132) yielding

$$\Omega_{\Delta_x,\Delta_y} = -\int_0^\infty \mathrm{d}y\, y^{-1} e^{-(2R\bar{\alpha}_0)^2 y} \sum_{m,n\in\mathbb{Z}\setminus 0} \int \mathrm{d}\boldsymbol{k}$$

$$\exp\left[-(\boldsymbol{k}+\boldsymbol{u})^T \boldsymbol{S}\boldsymbol{\mathcal{A}}^{\mathrm{trIs,rec}} \boldsymbol{S}^T (\boldsymbol{k}+\boldsymbol{u}) y + i\boldsymbol{k}\cdot(m\boldsymbol{L}_1 + n\boldsymbol{L}_2)\right] \tag{2.142}$$

This is a $2d$ Gaussian integral with respect to $\boldsymbol{k}$, which can be evaluated to

$$\begin{aligned}
&\int \mathrm{d}\boldsymbol{k} \exp\left[-(\boldsymbol{k}+\boldsymbol{u})^T(\boldsymbol{S}\mathcal{A}^{\mathrm{trIs,rec}}\boldsymbol{S}^T)(\boldsymbol{k}+\boldsymbol{u})\, y + i\boldsymbol{k}\cdot(m\boldsymbol{L}_1+n\boldsymbol{L}_2)\right] \\
&= \frac{1}{(2\pi)^2 y v}\frac{\pi}{\sqrt{\det \mathcal{A}^{\mathrm{trIs,rec}}}} \\
&\quad \exp\left[-\frac{1}{4y}(m\boldsymbol{L}_1+n\boldsymbol{L}_2)^T(\boldsymbol{S}\mathcal{A}^{\mathrm{trIs,rec}}\boldsymbol{S}^T)^{-1}(m\boldsymbol{L}_1+n\boldsymbol{L}_2) - i\,\boldsymbol{u}\cdot(m\boldsymbol{L}_1+n\boldsymbol{L}_2)\right] \quad (2.143)
\end{aligned}$$

Combining the above results gives

$$\begin{aligned}
&\Omega_{\Delta_x,\Delta_y} = \frac{1}{4\pi^2 v}\frac{\pi}{\sqrt{\det \mathcal{A}^{\mathrm{trIs,rec}}}}\int_0^\infty \mathrm{d}y\, y^{-2} e^{-(2R\bar{\alpha}_0)^2 y} \\
&\cdot\left\{1 - \sum_{m,n\in\mathbb{Z}} \exp\left[-\frac{(m\boldsymbol{L}_1+n\boldsymbol{L}_2)^T(\boldsymbol{S}\mathcal{A}^{\mathrm{trIs,rec}}\boldsymbol{S}^T)^{-1}(m\boldsymbol{L}_1+n\boldsymbol{L}_2)}{4y} - i\,\boldsymbol{u}\cdot(m\boldsymbol{L}_1+n\boldsymbol{L}_2)\right]\right\} \quad (2.144)
\end{aligned}$$

here the sum was extended to include the zero modes and thus a term was subtracted accordingly.

To proceed further, a set of orthogonal unit vectors $\tilde{\boldsymbol{a}}_i$, with $\tilde{\boldsymbol{a}}_i\cdot\tilde{\boldsymbol{a}}_j = \delta_{ij}$, is again considered, from which the lattice vectors $\boldsymbol{a}_i = \boldsymbol{S}\tilde{\boldsymbol{a}}_i$ are obtained via the shear transformation $\boldsymbol{S}$. The reciprocal lattice vectors $\boldsymbol{b}_i$ transform as $\boldsymbol{b}_i = \boldsymbol{S}^{-T}\tilde{\boldsymbol{b}}_i$, since $\boldsymbol{a}_i\cdot\boldsymbol{b}_j = \boldsymbol{a}_i^T\boldsymbol{b}_j = \delta_{ij}$, and the $\tilde{\boldsymbol{b}}_i$ are orthogonal as well, $\tilde{\boldsymbol{b}}_i\cdot\tilde{\boldsymbol{b}}_j = \delta_{ij}$. With the above it follows that $\boldsymbol{L}_i = N_i\boldsymbol{S}\tilde{\boldsymbol{a}}_i$ and thus

$$\begin{aligned}
&-\frac{(m\boldsymbol{L}_1+n\boldsymbol{L}_2)^T(\boldsymbol{S}\mathcal{A}^{\mathrm{trIs,rec}}\boldsymbol{S}^T)^{-1}(m\boldsymbol{L}_1+n\boldsymbol{L}_2)}{4y} - i\,\boldsymbol{u}\cdot(m\boldsymbol{L}_1+n\boldsymbol{L}_2) \\
&= -\frac{(mN_1\tilde{\boldsymbol{a}}_1+nN_2\tilde{\boldsymbol{a}}_2)^T(\mathcal{A}^{\mathrm{trIs,rec}})^{-1}(mN_1\tilde{\boldsymbol{a}}_1+nN_2\tilde{\boldsymbol{a}}_2)}{4y} - 2\pi i(m\Delta_x+n\Delta_y) \quad (2.145) \\
&= -\frac{N_2^2}{4y}\boldsymbol{m}^T(\mathcal{A}^{\mathrm{trIs,rec}})^{-1}\boldsymbol{m} - 2\pi i(m\Delta_x+n\Delta_y) \quad (2.146)
\end{aligned}$$

Where in the last line $\boldsymbol{m} = (m/\rho, n)^T$ with $\rho = N_2/N_1$ was defined; plugging the above in yields

$$\begin{aligned}
&\Omega_{\Delta_x,\Delta_y} = \frac{1}{4\pi^2 v}\frac{\pi}{\sqrt{\det \mathcal{A}^{\mathrm{trIs,rec}}}}\int_0^\infty \mathrm{d}y\, y^{-2} e^{-(2R\bar{\alpha}_0)^2 y} \\
&\left\{1 - \sum_{m,n\in\mathbb{Z}} \exp\left[-\frac{N_2^2}{4y}\boldsymbol{m}^T(\mathcal{A}^{\mathrm{trIs,rec}})^{-1}\boldsymbol{m} - 2\pi i(m\Delta_x+n\Delta_y)\right]\right\} \quad (2.147)
\end{aligned}$$

In the following, $\mathcal{A}^{\mathrm{trIs,rec}}$ needs to be expressed through a different matrix $\mathcal{C}^{\mathrm{rec}}$ introduced in [27], which will remove the explicit dependence of $\boldsymbol{m}$ on ρ; it is defined via (see eq. (6.9) of [27])

$$\mathcal{C}^{\mathrm{rec}}_{\alpha,\beta} = \rho_\alpha\rho_\beta\mathcal{A}^{\mathrm{trIs,rec}}_{\alpha,\beta} \quad (2.148)$$

with $\rho_1 = \rho = N_2/N_1$ and $\rho_2 = 1$. For its inverse one finds

$$(\mathcal{C}^{\mathrm{rec}})^{-1}_{\alpha,\beta} = \frac{1}{\rho_\alpha\rho_\beta}(\mathcal{A}^{\mathrm{trIs,rec}})^{-1}_{\alpha,\beta} \quad (2.149)$$

Now the quadratic form reads:

$$\boldsymbol{m}^T(\mathcal{A}^{\text{trIs, rec}})^{-1}\boldsymbol{m} = \boldsymbol{n}^T(\mathcal{C}^{\text{rec}})^{-1}\boldsymbol{n} \tag{2.150}$$

where $\boldsymbol{n} = (m,n)^T$. Next $z = 4\pi^2 y/N_2^2$ is substituted, which yields

$$\Omega_{\Delta_x,\Delta_y} = \frac{\pi}{N_2^2 v}\int_0^\infty \mathrm{d}z\, z^{-2} e^{-(2R\bar{\alpha}_0)^2 z N_2^2/(4\pi^2)} \left\{1 - \sum_{m,n\in\mathbb{Z}} \exp\left[-\frac{\pi^2}{z}\boldsymbol{n}^T(\mathcal{C}^{\text{rec}})^{-1}\boldsymbol{n} - 2\pi i(m\Delta_x + n\Delta_y)\right]\right\} \tag{2.151}$$

Now $\mathcal{A}^{\text{trIs, rec}}$ is also approximated by its value at the critical point, which corresponds to replacing it with the reduced anisotropy matrix $\bar{\boldsymbol{A}}^{\text{trIs, rec}}$ and thus also $\mathcal{C}^{\text{rec}}$ with $\hat{\boldsymbol{C}}^{\text{rec}}_{\alpha,\beta} = \rho_\alpha\rho_\beta\bar{\boldsymbol{A}}^{\text{trIs,rec}}_{\alpha,\beta}$. Furthermore, equations (7)-(8) of [29] are used to express $\bar{\boldsymbol{A}}^{\text{trIs,rec}}$ in terms of the modular parameter $\tau = \tau_0 + i\tau_1$ with $\tau_1 > 0$,

$$\bar{\boldsymbol{A}}^{\text{trIs,rec}} = \rho\begin{pmatrix} \frac{1}{\rho^2}\frac{|\tau|^2}{\tau_1} & -\frac{1}{\rho}\frac{\tau_0}{\tau_1} \\ -\frac{1}{\rho}\frac{\tau_0}{\tau_1} & \frac{1}{\tau_1}\end{pmatrix}, \tag{2.152}$$

In turn, τ can be expressed as

$$\tau = \rho\left[-\frac{\bar{\boldsymbol{A}}^{\text{trIs,rec}}_{21}}{\bar{\boldsymbol{A}}^{\text{trIs,rec}}_{22}} + i\frac{1}{\bar{\boldsymbol{A}}^{\text{trIs,rec}}_{22}}\right], \tag{2.153}$$

or, in terms of the couplings,

$$\tau = \frac{N_2}{N_1}\left[\frac{\hat{S}_3^c}{\hat{S}_2^c + \hat{S}_3^c} + i\frac{1}{\hat{S}_2^c + \hat{S}_3^c}\right]. \tag{2.154}$$

This yields

$$\hat{\boldsymbol{C}}^{\text{rec}} = \rho\begin{pmatrix} \frac{|\tau|^2}{\tau_1} & -\frac{\tau_0}{\tau_1} \\ -\frac{\tau_0}{\tau_1} & \frac{1}{\tau_1}\end{pmatrix} \equiv \rho\,\hat{\boldsymbol{D}}^{\text{rec}}, \tag{2.155}$$

where the matrix

$$(\hat{\boldsymbol{D}}^{\text{rec}})^{-1} = \begin{pmatrix} \frac{1}{\tau_1} & \frac{\tau_0}{\tau_1} \\ \frac{\tau_0}{\tau_1} & \frac{|\tau|^2}{\tau_1}\end{pmatrix}. \tag{2.156}$$

was defined; thus finally, the initial expression in the exponential of (2.151) simplifies to

$$\boldsymbol{n}^T(\boldsymbol{C}^{\text{rec}})^{-1}\boldsymbol{n} = \rho\,\boldsymbol{n}^T(\hat{\boldsymbol{D}}^{\text{rec}})^{-1}\boldsymbol{n} = \frac{1}{\tau_1}|m + n\tau|^2. \tag{2.157}$$

More over, the modular parameter τ can be expressed through its complex exponential form $\tau = \rho_p \exp(i\alpha)$ with

$$\cot\alpha = \hat{S}_3^c \tag{2.158}$$

$$(\rho_p)^2 = \left(\frac{N_2}{N_1}\right)^2 \frac{1+(\hat{S}_1^c)^2}{1+(\hat{S}_2^c)^2} \tag{2.159}$$

where α and ρ_p are the angle and aspect ratio describing the isotropic parallelogram as given in (1.37) and (1.38).

Furthermore, as shown in the previous section, the constants in the first exponential in (2.144) are related to the mean correlation length $\bar{\xi}_+^{\mathrm{sq}}(t)$ on the square lattice with orthonormal lattice vectors. More precisely, it was found, that

$$(2R\bar{\alpha}_0)^2 = \frac{1}{2}\frac{1}{[\bar{\xi}_+^{\mathrm{sq}}(t)]^2} + \mathcal{O}(t^3) \tag{2.160}$$

$$= \frac{1}{2}\frac{|t|^2}{[\bar{\xi}_{0+}^{\mathrm{sq}}]^2} + \mathcal{O}(t^3). \tag{2.161}$$

However, it was also shown that one can express the mean correlation length on a square lattice through the one on a general parallelogram lattice with unit cell area $v = a_1 a_2 \sin\vartheta$ and total system area $V = N_1 N_2 v$, which results in

$$x^2 \equiv \frac{N_1 N_2}{[\bar{\xi}_+^{\mathrm{sq}}(t)]^2} = \frac{V}{\bar{\xi}_+^2(t)} \tag{2.162}$$

with the mean correlation length $\bar{\xi}_+(t)$ on the parallelogram lattice. For later convenience, the scaling parameter x is chosen to be linear in t

$$x = \frac{V^{1/2}}{\bar{\xi}_{0+}}\, t. \tag{2.163}$$

Additionally, identity [49, Eq. 10.32.10] is used

$$K_\nu(t) = \frac{1}{2}\left(\frac{t}{2}\right)^\nu \int_0^\infty \frac{\mathrm{d}z}{z^{\nu+1}} \exp\left(-z - \frac{t^2}{4z}\right) \tag{2.164}$$

to express the integral through the modified Bessel function of the second kind $K_\nu(x)$ and find

$$\Omega_{\Delta_x,\Delta_y} = -\frac{1}{V}\,\mathcal{G}_0, \tag{2.165}$$

where

$$\mathcal{G}_0\left(x^2 \,\middle|\, \tau, \Delta_x, \Delta_y\right) = \left(\frac{x^2\tau_1}{2\pi^2}\right)^{1/2} \sum_{\substack{(m,n)\\ \in\mathbb{Z}^2\setminus(0,0)}} e^{-2\pi i\,(m\Delta_x + n\Delta_y)}\, \frac{K_1\left(\left[\frac{x^2}{2\tau_1}\right]^{1/2}|m+n\tau|\right)}{|m+n\tau|}. \tag{2.166}$$

With this expression at hand, attention is returned to the partition function of the Ising model. Recall from (2.135) that

$$\sum_{\boldsymbol{k}} \ln \mathcal{Q}^2_{\Delta_x,\Delta_y}(\boldsymbol{k}) = N_1 N_2\, \Omega_{\Delta_x,\Delta_y} + N_1 N_2 \int \mathrm{d}\boldsymbol{k}\ \ln \mathcal{Q}^2_{\Delta_x,\Delta_y}(\boldsymbol{k}) \tag{2.167}$$

$$= -\mathcal{G}_0\left(x^2 \,\middle|\, \tau, \Delta_x, \Delta_y\right) + N_1 N_2 \int \mathrm{d}\boldsymbol{k}\ \ln \mathcal{Q}^2_{\Delta_x,\Delta_y}(\boldsymbol{k}), \tag{2.168}$$

where the results from (2.165) were used and note that the second term on the right hand side is related to the bulk free energy density (2.81) and is independent of Δ_x, Δ_y. So for the total free energy density one finds:

$$f = -\frac{\ln Z}{A} = f_b^{\text{trIs}} - \frac{1}{A}\ln\frac{1}{2}\Big[e^{-\frac{1}{2}\mathcal{G}_0\left(x^2\middle|\tau,\frac{1}{2},\frac{1}{2}\right)} + e^{-\frac{1}{2}\mathcal{G}_0\left(x^2\middle|\tau,0,\frac{1}{2}\right)} + e^{-\frac{1}{2}\mathcal{G}_0\left(x^2\middle|\tau,\frac{1}{2},0\right)} - \operatorname{sgn}(x)\, e^{-\frac{1}{2}\mathcal{G}_0\left(x^2|\tau,0,0\right)}\Big] \tag{2.169}$$

From which the finite size scaling function of the excess free energy

$$\mathcal{F}_{\text{ex}}^{\text{trIs}}(x|\tau) = -\ln\frac{1}{2}\Big[e^{-\frac{1}{2}\mathcal{G}_0\left(x^2\middle|\tau,\frac{1}{2},\frac{1}{2}\right)} + e^{-\frac{1}{2}\mathcal{G}_0\left(x^2\middle|\tau,0,\frac{1}{2}\right)} + e^{-\frac{1}{2}\mathcal{G}_0\left(x^2\middle|\tau,\frac{1}{2},0\right)} - \operatorname{sgn}(x)\, e^{-\frac{1}{2}\mathcal{G}_0\left(x^2|\tau,0,0\right)}\Big], \tag{2.170}$$

can be extracted; here, as mentioned above, the square of the scaling parameter $x^2 = V/\bar{\xi}_+^2(t)$ is related to the mean correlation length and the total system volume with $\mathcal{G}_0(x^2|\tau,\Delta_x,\Delta_y)$ given in (2.166). Now it is also clear why x was chosen to be linear in t; this allows x to change sign, when the reduced temperature changes sign and instead of $\operatorname{sgn}(t)$, $\operatorname{sgn}(x)$ can be used in the above expression. In section 2.8 the relation to the results found in [50] are discussed .

2.6.2 Modular invariance of $\mathcal{F}_{\text{ex}}^{\text{trIs}}$

In general, a modular form is a bounded holomorphic function f from the upper half plane onto the complex numbers, which satisfies the modular condition

$$f\left(\frac{a\tau+b}{c\tau+d}\right) = (c\tau+d)^{-k} f(\tau) \tag{2.171}$$

with k the weight of the modular form and the matrix

$$\begin{pmatrix} a & b \\ c & d \end{pmatrix} \in \mathrm{SL}_2(\mathbb{Z}) \quad \text{and} \quad \det\begin{pmatrix} a & b \\ c & d \end{pmatrix} = +1 \tag{2.172}$$

where SL_2 is the special linear group in $2d$. In case of $k = 0$, f is called a modular function [51]. Intuitively, this can be thought of as a unit cell of a lattice spanned by the two linearly independent complex numbers ω_1 and ω_2. However, there are infinitely many lattice vector pairs that generate the same geometry, since taking any linear combination of ω_1 and ω_2 with integer factors yields the same lattice, where the new lattice vectors ω_1' and ω_2' point to different points of the original lattice. These constraints are exactly represented as the action of SL_2 on the ω_i, with

$$\begin{pmatrix} a & b \\ c & d \end{pmatrix}\begin{pmatrix} \omega_1 \\ \omega_2 \end{pmatrix} = \begin{pmatrix} \omega_1' \\ \omega_2' \end{pmatrix}. \tag{2.173}$$

Additionally, it is enough to only consider the ratio $\tau \equiv \omega_1/\omega_2$, which just corresponds to a rotation and rescaling of the original lattice such that $\omega_2 = 1$. Moreover, the special linear group is generated by the matrices

$$\mathcal{T} = \begin{pmatrix} 1 & 1 \\ 0 & 1 \end{pmatrix}, \quad \mathcal{S} = \begin{pmatrix} 0 & -1 \\ 1 & 0 \end{pmatrix} \tag{2.174}$$

and their respective inverses. They correspond to translation $\mathcal{T}$ and inversion $\mathcal{S}$, since they act on the modular parameter τ like

$$\mathcal{T}: \quad \tau \to \tau + 1 \qquad \text{(translation)}, \tag{2.175}$$

$$\mathcal{S}: \quad \tau \to -1/\tau \qquad \text{(inversion)}. \tag{2.176}$$

Function that are unchanged under theses transformations are called modular invariant [33, 51]. With regards to $\mathcal{G}_0\left(x^2\middle|\tau, \Delta_x, \Delta_y\right)$, one finds that under translation

$$\begin{aligned}
&\mathcal{G}_0\left(x^2 \,\middle|\, \tau+1, \Delta_x, \Delta_y\right) \\
&= \left(\frac{x^2\tau_1}{2\pi^2}\right)^{1/2} \sum_{\substack{(m,n)\\ \in\mathbb{Z}^2\setminus(0,0)}} e^{-2\pi i\,(m\Delta_x+n\Delta_y)}\, \frac{K_1\left(\left[\frac{x^2}{2\tau_1}\right]^{1/2}|(m+n)+n\tau|\right)}{|(m+n)+n\tau|} \\
&= \left(\frac{x^2\tau_1}{2\pi^2}\right)^{1/2} \sum_{\substack{(m',n)\\ \in\mathbb{Z}^2\setminus(0,0)}} e^{-2\pi i\,(m'\Delta_x+n(\Delta_y-\Delta_x))}\, \frac{K_1\left(\left[\frac{x^2}{2\tau_1}\right]^{1/2}|m'+n\tau|\right)}{|m'+n\tau|} \\
&= \mathcal{G}_0\left(x^2 \,\middle|\, \tau, \Delta_x, \Delta_y-\Delta_x\right),
\end{aligned} \tag{2.177}$$

where $m' = m + n$ was used. For behavior under inversion, it is first noted that

$$\mathrm{Re}(-1/\tau) = -\frac{\tau_0}{|\tau|^2}, \quad \text{and} \quad \mathrm{Im}(-1/\tau) = \frac{\tau_1}{|\tau|^2}, \tag{2.178}$$

from which follows for $\mathcal{G}_0$:

$$\begin{aligned}
&\mathcal{G}_0\left(x^2 \,\middle|\, -1/\tau, \Delta_x, \Delta_y\right) \\
&= \left(\frac{x^2\tau_1}{2\pi^2}\right)^{1/2} \frac{1}{|\tau|} \sum_{\substack{(m,n)\\ \in\mathbb{Z}^2\setminus(0,0)}} e^{-2\pi i\,(m\Delta_x+n\Delta_y)}\, \frac{K_1\left(\left[\frac{x^2}{2\tau_1}\right]^{1/2}|\tau||m-n/\tau|\right)}{|m-n/\tau|} \\
&= \left(\frac{x^2\tau_1}{2\pi^2}\right)^{1/2} \sum_{\substack{(m,n)\\ \in\mathbb{Z}^2\setminus(0,0)}} e^{-2\pi i\,(-m\Delta_y+n\Delta_x)}\, \frac{K_1\left(\left[\frac{x^2}{2\tau_1}\right]^{1/2}|m+n\tau|\right)}{|m+n\tau|} \\
&= \mathcal{G}_0\left(x^2 \,\middle|\, \tau, -\Delta_y, \Delta_x\right),
\end{aligned} \tag{2.179}$$

where in the second step $m \to n$ and $n \to -m$ were substituted. From the above discussion one concludes that $\mathcal{G}_0$ itself is in general not modular invariant. Before we continue, two further properties of the function in question are stated: First, since $\Delta_x, \Delta_y \in \{0, \frac{1}{2}\}$, $\mathcal{G}_0$ is real-valued, such that $\mathcal{G}_0\left(x^2|\tau, \Delta_x, \Delta_y\right) = \mathcal{G}_0^*\left(x^2|\tau, \Delta_x, \Delta_y\right) = \mathcal{G}_0\left(x^2|\tau, -\Delta_x, -\Delta_y\right)$ and secondly $\mathcal{G}_0\left(x^2|\tau, \Delta_x + r, \Delta_y + s\right) = \mathcal{G}_0\left(x^2|\tau, \Delta_x, \Delta_y\right)$ for $r, s \in \mathbb{Z}$. From these properties, it follows that on the one hand, $\mathcal{G}_0$ itself is only modular invariant if both $\Delta_x = \Delta_y = 0$, and on the other hand under translation

$$\begin{aligned}
&\mathcal{G}_0\left(x^2|\tau+1, \tfrac{1}{2}, \tfrac{1}{2}\right) = \mathcal{G}_0\left(x^2|\tau, \tfrac{1}{2}, 0\right) \\
&\mathcal{G}_0\left(x^2|\tau+1, 0, \tfrac{1}{2}\right) = \mathcal{G}_0\left(x^2|\tau, 0, \tfrac{1}{2}\right) \\
&\mathcal{G}_0\left(x^2|\tau+1, \tfrac{1}{2}, 0\right) = \mathcal{G}_0\left(x^2|\tau, \tfrac{1}{2}, -\tfrac{1}{2}\right) = \mathcal{G}_0\left(x^2|\tau, \tfrac{1}{2}, \tfrac{1}{2}\right),
\end{aligned}$$

and under inversion

$$\begin{aligned}
\mathcal{G}_0\left(x^2|-1/\tau,\tfrac{1}{2},\tfrac{1}{2}\right) &= \mathcal{G}_0\left(x^2|\tau,-\tfrac{1}{2},\tfrac{1}{2}\right) = \mathcal{G}_0\left(x^2|\tau,\tfrac{1}{2},\tfrac{1}{2}\right) \\
\mathcal{G}_0\left(x^2|-1/\tau,0,\tfrac{1}{2}\right) &= \mathcal{G}_0\left(x^2|\tau,-\tfrac{1}{2},0\right) = \mathcal{G}_0\left(x^2|\tau,\tfrac{1}{2},0\right) \\
\mathcal{G}_0\left(x^2|-1/\tau,\tfrac{1}{2},0\right) &= \mathcal{G}_0\left(x^2|\tau,0,\tfrac{1}{2}\right).
\end{aligned}$$

Thus, the other permissible combinations of Δ_i that comprise $\mathcal{F}_{\text{ex}}^{\text{trIs}}$ are just shuffled around when a modular transform is applied to the full expression.

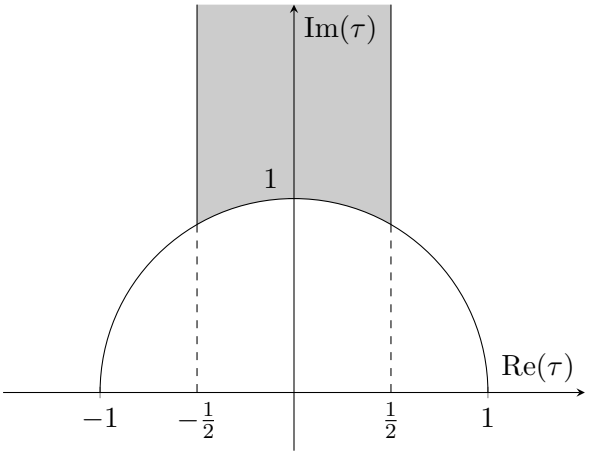

Figure 2.4: The fundamental domain shaded in gray in the complex upper half-plane. It extends between $|\text{Re}(\tau)| < 1/2$ and $|\tau| > 1$.

The implications of modular invariance of the near critical scaling function are far reaching. Since τ is related to the couplings of the system through (2.154) and modular invariance constrains all unique values of the excess free energy to the set of τ within the fundamental domain (cf. Fig. 2.4),

$$\{\tau \in \mathbb{C} : \text{Im}(\tau) > 0 \wedge |\text{Re}(\tau)| > 1/2 \wedge |\tau| > 1\}, \tag{2.180}$$

this implies that the set of all possible couplings E_i is highly symmetric and all possible (near) critical Ising models on this lattice are represented by a limited set in the space of all couplings.

2.6.3 Behavior at criticality

Finally, the previously derived expression for the excess free energy (2.170) is considered at the critical point, where the correlation length diverges and thus $x \to 0$. In this limit, the property [49]

$$K_\nu(z) \sim \frac{\Gamma(\nu)}{2}\left(\frac{2}{z}\right)^\nu \tag{2.181}$$

for $z \to 0$ and $\nu > 0$ and where Γ is the Gamma function, is used. This results in

$$\mathcal{G}_{0,c}\left(\tau,\Delta_x,\Delta_y\right) = \frac{1}{\pi}\sum_{(m,n)\in\mathbb{Z}^2\setminus(0,0)} e^{2\pi i\,(m\Delta_x+n\Delta_y)}\,\frac{\tau_1}{|m\tau+n|^2}, \tag{2.182}$$

where the $m = 0$ term is split off, which leads to

$$\mathcal{G}_{0,c}(\tau, \Delta_x, \Delta_y) = \frac{2}{\pi} \sum_{n=1}^{\infty} \frac{\tau_1}{n^2} \cos(2\pi n \Delta_x) + \frac{1}{\pi} \sum_{(m,n)\in\mathbb{Z}^2, m\neq 0} e^{2\pi i (m\Delta_x + n\Delta_y)} \frac{\tau_1}{|m\tau + n|^2}. \tag{2.183}$$

Comparing this to Eq. (4.2) and Theorem 4.1 of [52] one finds that

$$\mathcal{G}_{0,c}(\tau, \Delta_x, \Delta_y) = -\ln \left| e^{i\pi\Delta_x^2 \tau} \frac{\theta_1(\Delta_y - \tau\Delta_x|\tau)}{\eta(\tau)} \right|^2. \tag{2.184}$$

Here, $\theta_1(z|\tau)$ is the first Jacobi theta function and $\eta(\tau)$ the Dedekind eta function. Inserted into the free energy density, at the critical point this simplifies to

$$f = f_b^{\mathrm{trIs}} - \frac{1}{N_1 N_2} \ln \frac{1}{2} \left[\left| \frac{\theta_2(0|\tau)}{\eta(\tau)} \right| + \left| \frac{\theta_3(0|\tau)}{\eta(\tau)} \right| + \left| \frac{\theta_4(0|\tau)}{\eta(\tau)} \right| \right] \tag{2.185}$$

where the following properties of the Jacobi theta function [33] were used:

$$\ln \left| \frac{\theta_1(\frac{1}{2}|\tau)}{\eta(\tau)} \right|^2 = \ln \left| \frac{\theta_2(0|\tau)}{\eta(\tau)} \right|^2, \tag{2.186}$$

$$\text{since } \theta_1(z + \tfrac{1}{2}|\tau) = \theta_2(z|\tau), \tag{2.187}$$

$$\ln \left| e^{i\pi\tau/4} \frac{\theta_1(-\frac{1}{2}\tau|\tau)}{\eta(\tau)} \right|^2 = \ln \left| \frac{\theta_4(0|\tau)}{\eta(\tau)} \right|^2, \tag{2.188}$$

$$\text{since } \theta_1(-\tfrac{1}{2}\tau|\tau) = -i\, e^{-i\pi\tau/4} \theta_4(0|\tau), \tag{2.189}$$

$$\ln \left| e^{i\pi\tau/4} \frac{\theta_1(\frac{1}{2} - \frac{1}{2}\tau|\tau)}{\eta(\tau)} \right|^2 = \ln \left| \frac{\theta_3(0|\tau)}{\eta(\tau)} \right|^2, \tag{2.190}$$

$$\begin{aligned} \text{since } \theta_1(\tfrac{1}{2} - \tfrac{1}{2}\tau|\tau) &= -i\, e^{i\pi\tau/4} \theta_4(\tfrac{1}{2}|\tau) \\ &= \theta_3(1|\tau) = \theta_3(0|\tau), \end{aligned} \tag{2.191}$$

as well as $\theta_1(0|\tau) = 0$. Correspondingly, one obtains

$$\lim_{x\to 0} \mathcal{F}_{\mathrm{ex}}^{\mathrm{trIs}}(x|\tau) = -\ln \frac{1}{2} \left[\left| \frac{\theta_2(0|\tau)}{\eta(\tau)} \right| + \left| \frac{\theta_3(0|\tau)}{\eta(\tau)} \right| + \left| \frac{\theta_4(0|\tau)}{\eta(\tau)} \right| \right], \tag{2.192}$$

which in agreement with the results obtained in [33] through the methods of conformal field theory and are discussed for the anisotropic Ising model in [29].

2.7 Visualizations

In this section some visualizations of the excess free energy $\mathcal{F}_{\mathrm{ex}}^{\mathrm{trIs}}(x|\tau)$ and the associated excess heat capacity

$$C_{\mathrm{ex}}(x|\tau) = -T \frac{\partial^2 \mathcal{F}_{\mathrm{ex}}^{\mathrm{trIs}}}{\partial T^2}(x|\tau) = -\frac{2V}{\xi_{0+}^2} \frac{T}{T_c^2} \left[\frac{\partial \mathcal{F}_{\mathrm{ex}}^{\mathrm{trIs}}}{\partial x}(x|\tau) + 2x \frac{\partial^2 \mathcal{F}_{\mathrm{ex}}^{\mathrm{trIs}}}{\partial x^2}(x|\tau) \right] \tag{2.193}$$

are shown. However, there are a range of possible representations that could be chosen. $\mathcal{F}_{\mathrm{ex}}^{\mathrm{trIs}}(x|\tau)$ has two parameters, the scaling parameter x and modular parameter τ; x itself

indicates the distance from the critical point, with $x = 0$ being at the critical point and the sign communicates whether the system is currently in the ordered or disordered phase. This may not be very intuitive and one could chose the reduced temperature t and use $x^2(t) = V/\bar{\xi}^2_{0+}|t|^2$ as the first parameter, but now the ratio of system volume V and correlation volume $\bar{\xi}^2_{0+}$ needs to be specified. On the other hand, if one is interested in the excess free energy as a function of temperature T or β, now in addition the critical temperature is needed – all of which a non universal quantities. Similarly, from looking at (2.166) one is easily convinced, that τ is the natural choice as the parameter describing the anisotropy and indeed, if one is interested in modular invariance and related properties, this might be the correct choice. However, if one comes from a microscopic perspective, expressing τ through the couplings E_i as in (2.154) might be preferred; on the other hand, from the perspective of universality and theory of phase transitions, expressing τ through the parameters of the correlation ellipsis q and Ω like in (1.30) may be advantageous, since it retains the physical interpretation of the quantities, while abstracting away the model dependence into determining the correlation ellipsis and thus emphasizing the universal character.

All that said, since the main concern of this work is universality and to limit the number of plots, a range of different visualizations for the anisotropy will be shown, however, for the first variable, only the scaling parameter x will be used. To this end, the excess heat capacity will not be plotted directly, but rather

$$\zeta_{\mathrm{ex}}(x|\tau) \equiv \frac{\xi^2_{0+}}{2V}\frac{T_c^2}{T}C_{\mathrm{ex}}(x|\tau) = -\left[\frac{\partial \mathcal{F}^{\mathrm{trIs}}_{\mathrm{ex}}}{\partial x}(x|\tau) + 2x\frac{\partial^2 \mathcal{F}^{\mathrm{trIs}}_{\mathrm{ex}}}{\partial x^2}(x|\tau)\right] \tag{2.194}$$

to again emphasis the universal behavior.

One key takeaway from these visualizations is that, for both the excess free energy density and heat capacity, the modular invariant structure is preserved both above, at and below the critical temperature.

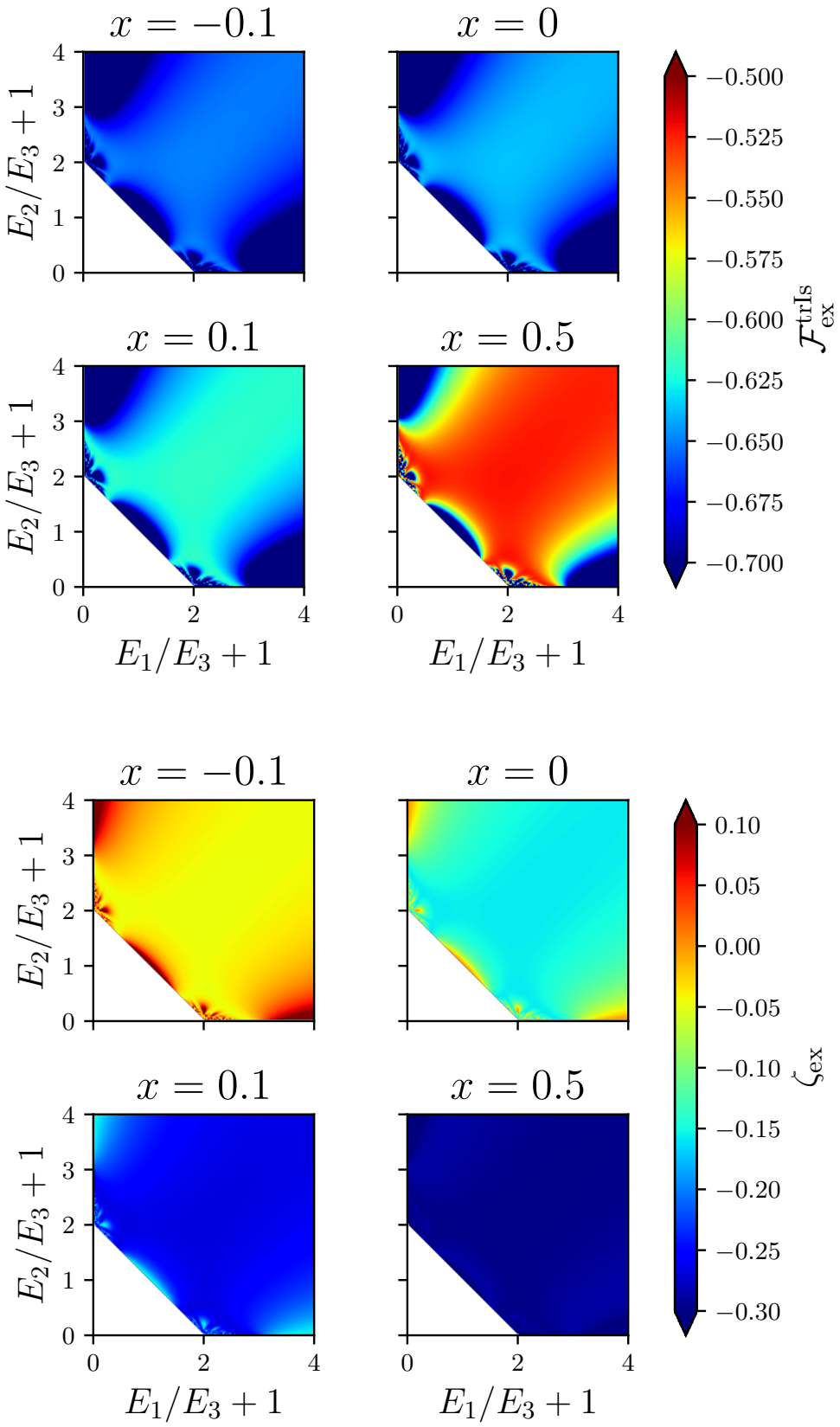

Figure 2.5: Excess free energy (top) and heat capacity (bottom) as a function of the microscopic couplings and for a range of scaling parameters both in the ordered and disordered phase.

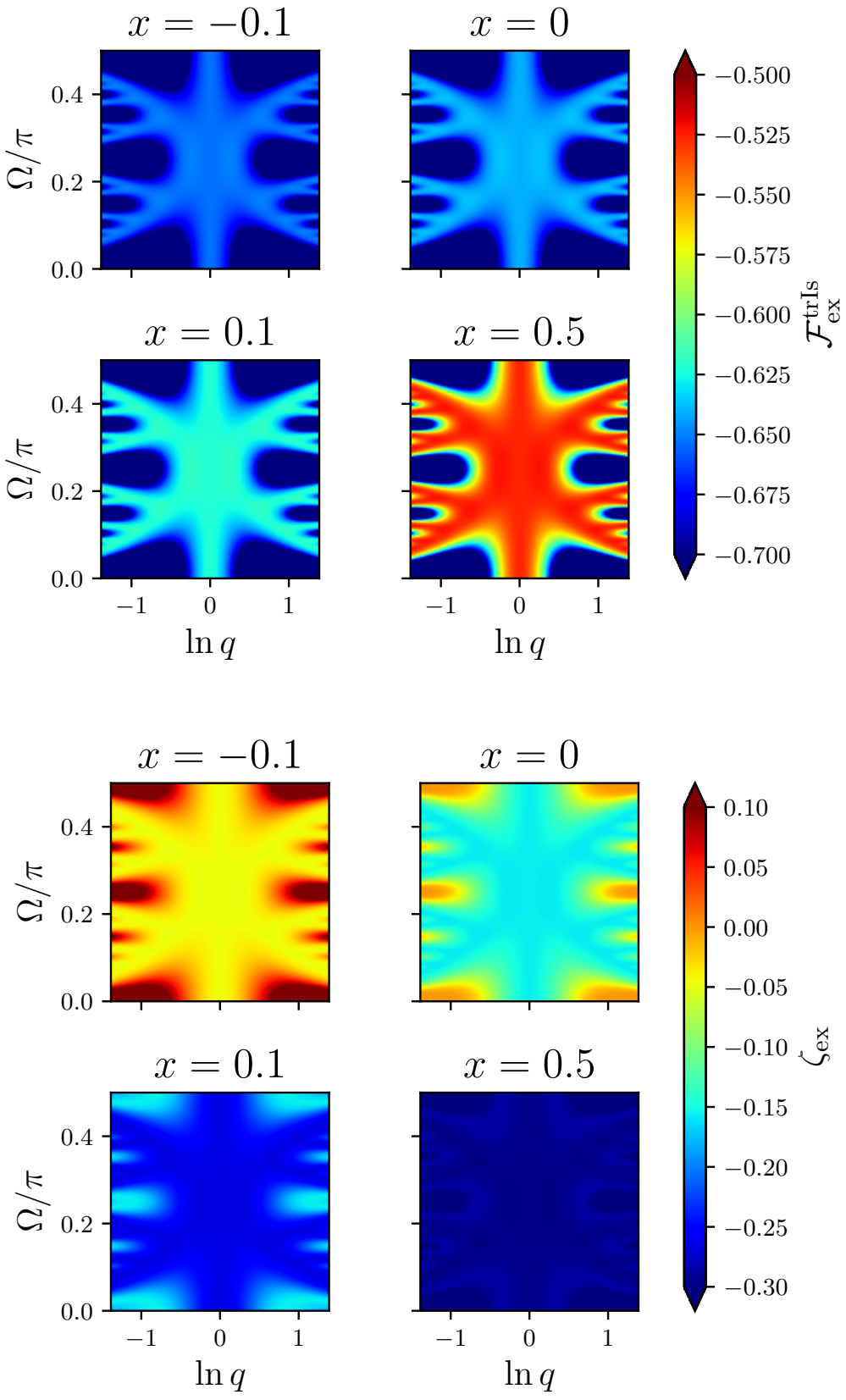

Figure 2.6: Again, on the upper plot shows the excess free energy and lower one the heat capacity, this time as a function of the correlation ellipsis parameters q and Ω; both for different scaling parameters x in the para- and ferromagnetic phase.

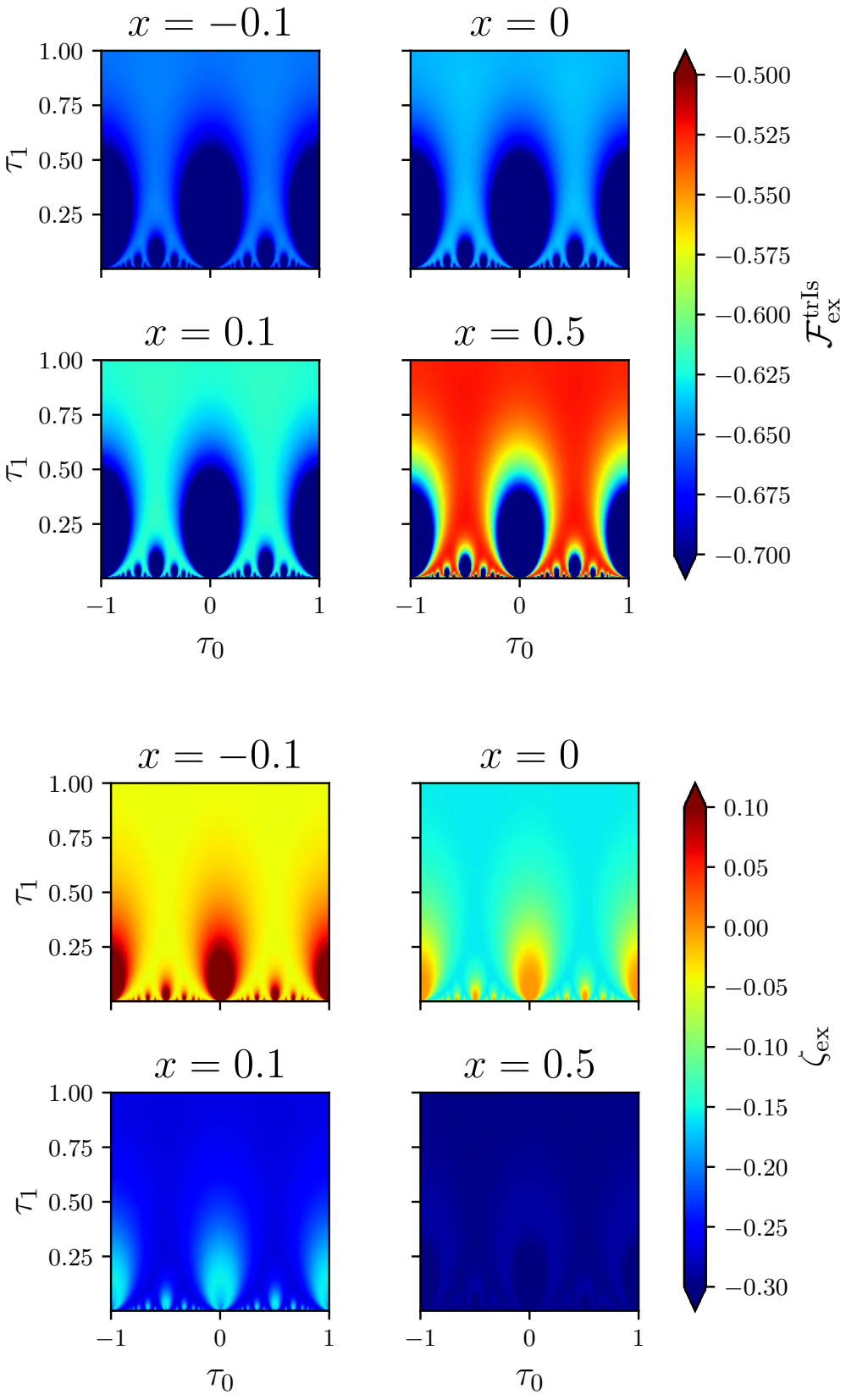

Figure 2.7: The Ising excess free energy (top) and heat capacity (bottom) as a function of the modular parameter τ.

2.8 Comparison with [50]

In this section, it is shown that the free energy scaling function derived here is equivalent to the one found by Nash and O'Connor [50] for the isotropic system. The identity in question is

$$\begin{aligned}
&-\sqrt{\frac{x\tau_1}{\pi^2}} \sum_{(m,n)\in\mathbb{Z}^2\setminus(0,0)} e^{-2\pi i\,(m\Delta_x+n\Delta_y)}\ \frac{K_1\left(\sqrt{\frac{x}{\tau_1}}\ |m+n\tau|\right)}{|m+n\tau|} \\
&\quad = \tau_1 \int_{-\infty}^{\infty} \frac{\mathrm{d}p}{2\pi} \ln\left|1-e^{-\sqrt{p^2+x/\tau_1}+2\pi i\Delta_x}\right|^2 \\
&\quad + \sum_{m=-\infty}^{\infty} \ln\left|1-e^{-2\pi\tau_1\sqrt{(m+\Delta_x)^2+x/(4\pi^2\tau_1)}-2\pi i[\Delta_y-\tau_0(m+\Delta_x)]}\right|^2
\end{aligned} \tag{2.195}$$

where $K_\nu(x)$ is again the modified Bessel function of the second kind, $\tau = \tau_0 + i\tau_1$ and $x > 0$. Note that here x is not the scaling variable as defined before, but actually its square; however, since the manipulations in this section are purely mathematical and do not reveal any new physics, this should not be of any concern.

As a first step, the sum on the left hand side of (2.195) is split into two parts, with $n = 0$ and $n \neq 0$, respectively. In the following, it will be shown that for the contribution with $n = 0$ one finds

$$-\sqrt{\frac{x\tau_1}{\pi^2}} \sum_{\substack{m=-\infty \\ m\neq 0}}^{\infty} e^{-2\pi i\, m\Delta_x}\ \frac{K_1\left(\sqrt{\frac{x}{\tau_1}}\ |m|\right)}{|m|} = \tau_1 \int_{-\infty}^{\infty} \frac{\mathrm{d}p}{2\pi} \ln\left|1-e^{-\sqrt{p^2+x/\tau_1}+2\pi i\Delta_x}\right|^2 \tag{2.196}$$

and for $n \neq 0$

$$\begin{aligned}
&-\sqrt{\frac{x\tau_1}{\pi^2}} \sum_{\substack{(m,n)\in\mathbb{Z}^2 \\ n\neq 0}} e^{-2\pi i\,(m\Delta_x+n\Delta_y)}\ \frac{K_1\left(\sqrt{\frac{x}{\tau_1}}\ |m+n\tau|\right)}{|m+n\tau|} \\
&\quad = \sum_{m=-\infty}^{\infty} \ln\left|1-e^{-2\pi\tau_1\sqrt{(m+\Delta_x)^2+x/(4\pi^2\tau_1)}-2\pi i[\Delta_y-\tau_0(m+\Delta_x)]}\right|^2
\end{aligned} \tag{2.197}$$

2.8.1 Proof for $n = 0$

First, the Fourier transform of the modified Bessel function [53, 4.2:29] is used

$$K_1(x) = \frac{1}{2i} \lim_{\epsilon\to 0} \int_{-\infty}^{\infty} e^{itx} \frac{te^{-\epsilon|t|}}{\sqrt{t^2+1}} dt, \tag{2.198}$$

which can also be seen from the fact that, after exchanging the limit with the integration in the second step,

$$\frac{1}{2i}\lim_{\epsilon\to 0}\int_{-\infty}^{\infty} e^{itx}\frac{te^{-\epsilon|t|}}{\sqrt{t^2+1}}dt = -\frac{1}{2}\lim_{\epsilon\to 0}\frac{\partial}{\partial x}\int_{-\infty}^{\infty} e^{itx}\frac{e^{-\epsilon|t|}}{\sqrt{t^2+1}}dt \tag{2.199}$$

$$= -\frac{1}{2}\frac{\partial}{\partial x}\int_{-\infty}^{\infty}\frac{e^{itx}}{\sqrt{t^2+1}}dt \tag{2.200}$$

$$= -\frac{\partial}{\partial x}\int_{0}^{\infty}\frac{\cos(tx)}{\sqrt{t^2+1}}dt \tag{2.201}$$

$$= -\frac{\partial}{\partial x}K_0(x) = K_1(x). \tag{2.202}$$

the same identity for the modified Bessel function can be recovered. Inserting this into (2.196) one arrives at

$$-\sqrt{\frac{x\tau_1}{\pi^2}}\sum_{\substack{m=-\infty\\ m\neq 0}}^{\infty} e^{-2\pi i\, m\Delta_x}\,\frac{K_1\left(\sqrt{\frac{x}{\tau_1}}\,|m|\right)}{|m|}$$

$$= -\frac{1}{2i}\sqrt{\frac{x\tau_1}{\pi^2}}\sum_{\substack{m=-\infty\\ m\neq 0}}^{\infty}\lim_{\epsilon\to 0}\int_{-\infty}^{\infty}\mathrm{d}t\,\frac{e^{it\sqrt{x/\tau_1}|m|-2\pi i\, m\Delta_x}}{|m|}\frac{te^{-\epsilon|t|}}{\sqrt{t^2+1}} \tag{2.203}$$

Now the sum over m can be evaluated by considering that

$$\ln(1-x) = -\sum_{n=1}^{\infty}\frac{x^n}{n} \tag{2.204}$$

and noting that the sum is of the following structure

$$\sum_{\substack{m=-\infty\\ n\neq 0}}^{\infty} a_m = \sum_{m=1}^{\infty} a_m + \sum_{m=-1}^{-\infty} a_m = \sum_{m=1}^{\infty}(a_m + a_m^*) \tag{2.205}$$

where $a_{-m} = a_m^*$ was used. With the property $\ln z + \ln z^* = \ln|z|^2$ it remains to be shown, that

$$\frac{\sqrt{x\tau_1}}{2i\pi}\lim_{\epsilon\to 0}\int_{-\infty}^{\infty}\mathrm{d}t\,\ln\left|1-e^{it\sqrt{x/\tau_1}+2\pi i\Delta_x}\right|^2\frac{t\,e^{-\epsilon|t|}}{\sqrt{t^2+1}}$$

$$= \tau_1\int_{-\infty}^{\infty}\frac{\mathrm{d}p}{2\pi}\ln\left|1-e^{-\sqrt{p^2+x/\tau_1}+2\pi i\Delta_x}\right|^2 \tag{2.206}$$

To this end, the above equations can be rewritten using $a = \sqrt{x/\tau_1}$

$$\frac{a}{i}\lim_{\epsilon\to 0}\int_{-\infty}^{\infty}\mathrm{d}t\,\ln\left|1-e^{ita+2\pi i\Delta_x}\right|\frac{t\,e^{-\epsilon|t|}}{\sqrt{t^2+1}}$$

$$= \int_{-\infty}^{\infty}\mathrm{d}p\ln\left|1-e^{-\sqrt{p^2+a^2}+2\pi i\Delta_x}\right| \tag{2.207}$$

and an analytic continuation with $z\in\mathbb{C}$ of the integrand on the left hand side is made:

$$f(z) = \ln\left|1-e^{iza+2\pi i\Delta_x}\right|\frac{z\,e^{-\epsilon|z|}}{\sqrt{z^2+1}} \tag{2.208}$$

Now it is convenient to introduce a complex contour integral of the above expression

$$\oint_\Gamma f(z)\mathrm{d}z = 0 \tag{2.209}$$

with

$$\Gamma = L_{[-R,R]} \cup \gamma_R(\delta) \cup L_{[iR+\delta,i+\delta]} \cup \gamma_\delta(i) \cup L_{[i-\delta,iR-\delta]} \cup \gamma_R(\delta) \tag{2.210}$$

where $L_{[a,b]}$ is a line connecting the two points a, b and $\gamma_r(p)$ is a circle segment centered at p with radius r. Γ is also shown in figure 2.8. In the limit $R \to \infty$ the contribution from the segment $L_{[-R,R]}$ is equal to the original integral; in the same limit, the contributions from the $\gamma_R(\delta)$ vanish exponentially for an $\epsilon > 0$. The contribution from the semicircle centered around i is

$$i\int_{2\pi}^{\pi} \mathrm{d}\phi \ln\left|1 - \exp\left(ia(i+\delta e^{i\phi}) + 2\pi i\Delta_x\right)\right| \frac{(i+\delta e^{i\phi})e^{-\epsilon|(i+\delta e^{i\phi})|}}{\sqrt{(i+\delta e^{i\phi})^2+1}}\,\delta e^{i\phi} \tag{2.211}$$

$$\simeq i\int_{2\pi}^{\pi} \mathrm{d}\phi \ln\left|1 - \exp\left(ia(i+\delta e^{i\phi}) + 2\pi i\Delta_x\right)\right| \frac{1}{\sqrt{2i}}(i\delta^{1/2} + \delta^{3/4}e^{i\phi})\, e^{-\epsilon+i\phi/2} \tag{2.212}$$

which vanishes as $\delta \to 0$. Note that the logarithm does not contribute to the convergence behavior since the semicircle contour always has a positive imaginary part. The final contribution is from the contours along the imaginary axis; where for the right section one finds

$$\oint_{L_{[i\infty+\delta,i+\delta]}} f(z)\,\mathrm{d}z$$

$$= i\int_{\infty}^{1} \mathrm{d}t\, \ln\left|1 - e^{-ta+i\delta a+2\pi i\Delta_x}\right| \frac{(it+\delta)}{\sqrt{(it+\delta)^2+1}} \tag{2.213}$$

$$\simeq i\int_{\infty}^{1} \mathrm{d}t\, \ln\left|1 - e^{-ta+i\delta a+2\pi i\Delta_x}\right| \frac{(it+\delta)}{\sqrt{-t^2+2it\delta+1}} \tag{2.214}$$

where ϵ was set to zero already, since it is not needed for convergence. Next $ta \to \sqrt{t^2+a^2}$ is substituted, which yields

$$\frac{i}{a}\int_{\infty}^{0} \mathrm{d}t\, \ln\left|1 - e^{-\sqrt{t^2+a^2}+i\delta a+2\pi i\Delta_x}\right| \cdot \frac{(i\sqrt{t^2+a^2}+a\delta)}{\sqrt{-t^2+2i\sqrt{t^2+a^2}\delta a}} \frac{t}{\sqrt{t^2+a^2}} \tag{2.215}$$

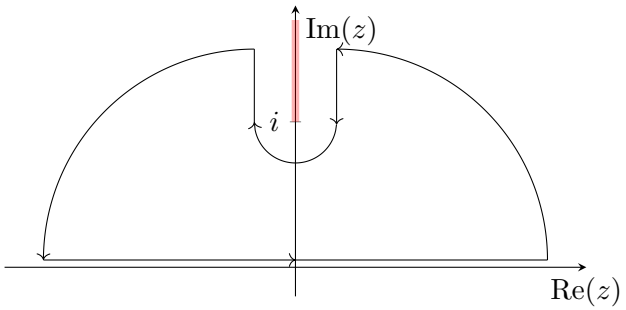

Figure 2.8: The contour shown in the upper half plane is used to rewrite the integral; the red line indicates the branch cut. The contour along the real axis is equal to the original integral, whereas the contours to the left and right of the branch cut are the only remaining, non vanishing contributions.

For $\delta \to 0$ one finds that $1/\sqrt{-t^2 + 2i\sqrt{t^2+a^2}\delta a} \simeq -i/t$, which results in

$$\lim_{\delta\to 0} \oint_{L_{[i\infty+\delta, i+\delta]}} f(z)\,\mathrm{d}z = \frac{i}{a}\int_{\infty}^{0} \mathrm{d}t\, \ln\left|1 - e^{-\sqrt{t^2+a^2}+2\pi i\Delta_x}\right| \tag{2.216}$$

Similarly one finds for the left contour along the imaginary axis

$$\lim_{\delta\to 0} \oint_{L_{[i-\delta, i\infty-\delta]}} f(z)\,\mathrm{d}z = -\frac{i}{a}\int_{0}^{\infty} \mathrm{d}t\, \ln\left|1 - e^{-\sqrt{t^2+a^2}+2\pi i\Delta_x}\right| \tag{2.217}$$

where the main difference is that $1/\sqrt{-t^2 - 2i\sqrt{t^2+a^2}\delta a} \simeq i/t$ which is a different sign than previously. With the above, one arrives at

$$\begin{aligned} &\lim_{\delta\to 0}\left[\oint_{L_{[i\infty+\delta, i+\delta]}} f(z)\,\mathrm{d}z + \oint_{L_{[i-\delta, i\infty-\delta]}} f(z)\,\mathrm{d}z\right] \\ &= -\frac{i}{a}\int_{-\infty}^{\infty} \mathrm{d}t\, \ln\left|1 - e^{-\sqrt{t^2+a^2}+2\pi i\Delta_x}\right| \end{aligned} \tag{2.218}$$

and so finally

$$\lim_{\epsilon\to 0}\int_{-\infty}^{\infty} \mathrm{d}t\, \ln\left|1 - e^{ita+2\pi i\Delta_x}\right| \frac{t\, e^{-\epsilon|t|}}{\sqrt{t^2+1}} = \frac{i}{a}\int_{-\infty}^{\infty} \mathrm{d}t\, \ln\left|1 - e^{-\sqrt{t^2+a^2}+2\pi i\Delta_x}\right| \tag{2.219}$$

which completes the proof.

2.8.2 Proof for $n \neq 0$

First, the integral representation of the modified Bessel function of the second kind [49, Eq. 10.32.10] is used

$$\sqrt{\frac{a}{b}}\, K_1(\sqrt{ab}) = \int_0^{\infty} \frac{\mathrm{d}t}{t^2}\, e^{-at/4 - b/t} \tag{2.220}$$

with $a = x$ and $b = |m + n\tau|^2/\tau_1$. It then follows from (2.197) that

$$-\sqrt{\frac{x\tau_1}{\pi^2}} \sum_{\substack{(m,n)\in\mathbb{Z}^2 \\ n\neq 0}} e^{-2\pi i\,(m\Delta_x + n\Delta_y)}\, \frac{K_1\left(\sqrt{\frac{x}{\tau_1}}\,|m+n\tau|\right)}{|m+n\tau|} \tag{2.221}$$

$$= -\frac{1}{\pi} \sum_{\substack{(m,n)\in\mathbb{Z}^2 \\ n\neq 0}} \int_0^{\infty} \frac{\mathrm{d}t}{t^2}\, \exp\left(-\frac{xt}{4} - \frac{|m+n\tau|^2}{t\tau_1} - 2\pi i\,[m\Delta_x + n\Delta_y]\right) \tag{2.222}$$

expanding the absolute value on the right hand side yields

$$-\frac{1}{\pi} \sum_{\substack{(m,n)\in\mathbb{Z}^2 \\ n\neq 0}} \int_0^{\infty} \frac{\mathrm{d}t}{t^2}\, \exp\left(-\frac{xt}{4} - \frac{(m+n\tau_0)^2}{t\tau_1} + \frac{n^2\tau_1}{t} - 2\pi i\,[m\Delta_x + n\Delta_y]\right) \tag{2.223}$$

Now the Poisson summation is made use of, which states

$$\sum_{n=-\infty}^{\infty} f(n) = \sum_{n=-\infty}^{\infty} \hat{f}(n) \tag{2.224}$$

for a function f with its Fourier transform $\hat{f}$. In the above case the sum over m is considered with

$$f(m) = \exp\left(-\frac{(m+n\tau_0)^2}{t\tau_1} - 2\pi i m\Delta_x\right) \tag{2.225}$$

which is a Gaussian. It follows that

$$\hat{f}(m) = \sqrt{\pi\tau_1 t}\ \exp\left(2\pi i n\tau_0(-m+\Delta_x) - \pi^2(-m+\Delta_x)^2\tau_1 t\right), \tag{2.226}$$

with the usual rules for the Fourier transform of a Gaussian; this can be plugged in above

$$-\sqrt{\frac{\tau_1}{\pi}} \sum_{\substack{(m,n)\in\mathbb{Z}^2\\ n\neq 0}} \int_0^\infty \frac{\mathrm{d}t}{t^{3/2}}\ \exp\Bigg(-\Big[\frac{x}{4} + \pi^2(m+\Delta_x)^2\tau_1\Big]t \\ - \frac{n^2\tau_1}{t} - 2\pi i n\Big[\Delta_y - \tau_0(m+\Delta_x)\Big]\Bigg) \tag{2.227}$$

Here $m \to -m$ was substituted since the sum runs over all m. This integral can be evaluated; more specifically one has

$$\int_0^\infty \frac{\mathrm{d}t}{t^{3/2}}\ e^{-ut-v/t} = \sqrt{\frac{\pi}{v}} e^{-2\sqrt{uv}} \tag{2.228}$$

with

$$u = \frac{x}{4} + \pi^2(m+\Delta_x)^2\tau_1 \quad \text{and} \quad v = n^2\tau_1 \tag{2.229}$$

which results in the expression

$$-\sqrt{\frac{\tau_1}{\pi}} \sum_{\substack{(m,n)\in\mathbb{Z}^2\\ n\neq 0}} \int_0^\infty \frac{\mathrm{d}t}{t^{3/2}}\ \exp\Bigg(-\Big[\frac{x}{4} + \pi^2(m+\Delta_x)^2\tau_1\Big]t \\ - \frac{n^2\tau_1}{t} - 2\pi i n\left[\Delta_y - \tau_0(m+\Delta_x)\right]\Bigg) \tag{2.230}$$

$$= -\sum_{\substack{(m,n)\in\mathbb{Z}^2\\ n\neq 0}} \frac{1}{|n|} \exp\Bigg(-2\pi\tau_1\sqrt{(m+\Delta_x)^2 + \frac{x}{4\pi^2\tau_1}}\,|n| \\ - 2\pi i n\left[\Delta_y - \tau_0(m+\Delta_x)\right]\Bigg) \tag{2.231}$$

Here again the sum over n was evaluated using (2.204) which yields the final result

$$-\sum_{\substack{(m,n)\in\mathbb{Z}^2\\ n\neq 0}} \frac{1}{|n|} \exp\left(-2\pi\tau_1\sqrt{(m+\Delta_x)^2 + \frac{x}{4\pi^2\tau_1}}\,|n| - 2\pi i n\left[\Delta_y - \tau_0(m+\Delta_x)\right]\right) \tag{2.232}$$

$$= \sum_{m=-\infty}^{\infty} \ln\left|1 - \exp\left(-2\pi\tau_1\sqrt{(m+\Delta_x)^2 + \frac{x}{4\pi^2\tau_1}} + 2\pi i\left[\Delta_y - \tau_0(m+\Delta_x)\right]\right)\right|^2 \tag{2.233}$$

and thus completes the proof.

2.9 Strip limit

To evaluate the strip limit as the aspect ratio ρ_p goes to either zero or infinity, consider

$$\mathcal{F}_{\rm ex}^{\rm trIs}(x|\tau) = -\ln\frac{1}{2}\Big[e^{-\frac{1}{2}\mathcal{G}_0\left(x^2\middle|\tau,\frac{1}{2},\frac{1}{2}\right)} + e^{-\frac{1}{2}\mathcal{G}_0\left(x^2\middle|\tau,0,\frac{1}{2}\right)} + e^{-\frac{1}{2}\mathcal{G}_0\left(x^2\middle|\tau,\frac{1}{2},0\right)} - \mathrm{sgn}\,(x)\, e^{-\frac{1}{2}\mathcal{G}_0\left(x^2|\tau,0,0\right)}\Big], \tag{2.234}$$

with now the alternative expression for $\mathcal{G}_0$

$$\mathcal{G}_0\left(x^2|\tau,\Delta_x,\Delta_y\right) = -\tau_1\int_{-\infty}^{\infty}\frac{\mathrm{d}p}{2\pi}\ln\left|1-e^{-\sqrt{p^2+x^2/\tau_1}+2\pi i\Delta_x}\right|^2 - \sum_{m=-\infty}^{\infty}\ln\left|1-e^{-2\pi\tau_1\sqrt{(m+\Delta_x)^2+x^2/(4\pi^2\tau_1)}-2\pi i[\Delta_y-\tau_0(m+\Delta_x)]}\right|^2 \tag{2.235}$$

where $x = t\sqrt{V}/\bar{\xi}_{0+}$ is the scaling variable with the system volume $V = L_1L_2\sin(\vartheta)$ and mean correlation length amplitude $\bar{\xi}_{0+}$; $\tau = \rho_p\exp(i\,\alpha) = \tau_0 + i\,\tau_1 = \rho_p\cos\alpha + i\,\rho_p\sin\alpha$ is the modular parameter, see (2.159).

2.9.1 Limit $\rho_p \to \infty$

Note that the ratio x^2/τ_1 in the above expressions becomes independent of ρ_p, when using that $L_2 = \rho_p L_1$, namely

$$\frac{x^2}{\tau_1} = \frac{L_1^2\sin\vartheta}{\bar{\xi}_{0+}^2\sin\alpha}\,t^2. \tag{2.236}$$

To further simplify the calculations, the ρ_p dependence is made explicit by introducing:

$$c_1(\Delta_x) = \sin(\alpha)\int_{-\infty}^{\infty}\frac{\mathrm{d}p}{2\pi}\ln\left|1-e^{-\sqrt{p^2+x^2/\tau_1}+2\pi i\Delta_x}\right|^2 \tag{2.237}$$

$$c_2(m,\Delta_x) = 2\pi\sin(\alpha)\sqrt{(m+\Delta_x)^2+x^2/(4\pi^2\tau_1)} \tag{2.238}$$

$$c_3 = \cos(\alpha) \tag{2.239}$$

With these, the terms can be simplified by using the (complex) exponential representation of the (hyperbolic) cosine,

$$e^{-\frac{1}{2}\mathcal{G}_0(x^2|\tau,\Delta_1,\Delta_2)} = \exp\left(\rho_p c_1(\Delta_x) + \sum_{m=-\infty}^{\infty}\ln\left|1-e^{-\rho_p c_2(m,\Delta_x)-2\pi i[\Delta_y+\rho_p c_3(m+\Delta_x)]}\right|^2\right) \tag{2.240}$$

$$= \begin{cases} e^{\rho_p c_1(\Delta_x)}\displaystyle\prod_{m=-\infty}^{\infty} 2e^{-\rho_p c_2(m,\Delta_x)}\left(\cosh[\rho_p c_2(m,\Delta_x)] - \cos[2\pi m\rho_p c_3]\right), & \Delta_y = 0 \\ e^{\rho_p c_1(\Delta_x)}\displaystyle\prod_{m=-\infty}^{\infty} 2e^{-\rho_p c_2(m,\Delta_x)}\left(\cosh[\rho_p c_2(m,\Delta_x)] + \cos[2\pi(m+\frac{1}{2})\rho_p c_3]\right), & \Delta_y = 1/2 \end{cases} \tag{2.241}$$

In this form it is easier to understand the functions behavior as a lot of the unnecessary terms for the limiting behavior are hidden away in the c_i. Next, note that the factors in the above product converge to unity as ρ_p approaches infinity,

$$\lim_{\rho_p\to\infty} 2e^{-\rho_p c_2(m,\Delta_x)}\left(\cosh[\rho_p c_2(m,\Delta_x)] - \cos[2\pi m\rho_p c_3]\right) = 1 \tag{2.242}$$

$$\lim_{\rho_p\to\infty} 2e^{-\rho_p c_2(m,\Delta_x)}\left(\cosh[\rho_p c_2(m,\Delta_x)] + \cos[2\pi (m+1/2)\rho_p c_3]\right) = 1 \tag{2.243}$$

The overall limit of the excess free energy density

$$\lim_{\rho_p\to\infty}\frac{1}{V}\mathcal{F}_{\text{ex}}^{\text{trIs}}(x|\tau) = -\frac{1}{L_1^2\sin\vartheta}\lim_{\rho_p\to\infty}\frac{1}{\rho_p}\mathcal{F}_{\text{ex}}^{\text{trIs}}(x|\tau) \tag{2.244}$$

can then be evaluated exactly:

$$\lim_{\rho_p\to\infty}\frac{1}{V}\mathcal{F}_{\text{ex}}^{\text{trIs}}(x|\tau) = -\frac{\sin\alpha}{L_1^2\sin\vartheta}\int_0^\infty\frac{\mathrm{d}p}{\pi}\ln\left|1+e^{-\sqrt{p^2+x^2/\tau_1}}\right| \tag{2.245}$$

To show the above, equations (2.242) and (2.243) are made use of, which imply that as ρ_p approaches infinity the relevant term in $\mathcal{G}(x^2,\tau,\Delta_1,\Delta_2)$ is only $\rho_p c_1(\Delta_x)$, such that the free energy density can be written as

$$\lim_{\rho_p\to\infty}\frac{1}{V}\mathcal{F}_{\text{ex}}^{\text{trIs}}(x|\tau) = -\frac{1}{L_1^2\sin\vartheta}\lim_{\rho_p\to\infty}\ln\left[e^{\rho_p c_1(1/2)}+\frac{1}{2}\left(1-\frac{x}{|x|}\right)e^{\rho_p c_1(0)}\right]^{1/\rho_p} \tag{2.246}$$

$$= -\frac{c_1(1/2)}{L_1^2\sin\vartheta} \tag{2.247}$$

The above result holds for both $x>0$ and $x<0$ (the case of $x=0$ is commented on further below). In the first case one has $1-x/|x|=0$, which makes the expression in the logarithm independent of ρ_p and the limit trivial. In the second case, the term $\exp(\rho_p c_1(0))$ approaches zero as $\rho_p\to\infty$ since $c_1(0)<0$ and $c_1(1/2)>0$, leaving only $\exp(\rho_p c_1(1/2))$, where again the ρ_p dependence is canceled with the power of $1/\rho_p$. At $x=0$ the sector represented by $\exp(\mathcal{G}(x^2,\tau,0,0))$ vanishes, as can be seen from the discussion in section 2.6.3 on the behavior at criticality, leaving only the expression:

$$\lim_{\rho_p\to\infty}\frac{1}{V}\mathcal{F}_{\text{ex}}^{\text{trIs}}(x|\tau) = -\frac{1}{L_1^2\sin\vartheta}\lim_{\rho_p\to\infty}\ln\left[e^{\rho_p c_1(1/2)}+\frac{1}{2}e^{\rho_p c_1(0)}\right]^{1/\rho_p} \tag{2.248}$$

$$= -\frac{c_1(1/2)}{L_1^2\sin\vartheta} \tag{2.249}$$

In the second step $c_1(0)<0$ and $c_1(1/2)>0$ were used again. For the special case where both $\vartheta=\alpha=\pi/2$ in (2.245), one gets

$$\lim_{\rho_p\to\infty}\frac{1}{V}\mathcal{F}_{\text{ex}}^{\text{trIs}}(x|\tau) = -\frac{1}{L_1^2}\int_0^\infty\frac{\mathrm{d}p}{\pi}\ln\left|1+e^{-\sqrt{p^2+x^2/\tau_1}}\right| \tag{2.250}$$

Furthermore, in this special case,

$$\frac{x^2}{\tau_1} = \frac{L_1^2\sin\vartheta}{\bar{\xi}_{0+}^2\sin\alpha}\,t^2 \quad \overset{\vartheta=\alpha=\pi/2}{=} \quad \frac{L_1^2}{\bar{\xi}_{0+}^2}\,t^2. \tag{2.251}$$

In this form, one can directly compare to the results in Ref. [54], where the result for the scaling function of the excess free energy density in case $\vartheta = \alpha = \pi/2$ is given by (see eq. (23), (57) and (59) of Ref. [54]):

$$f_{\text{ex}} = \frac{1}{L_\parallel^2}\,\Theta_\parallel(x_\parallel, \rho = \infty) \tag{2.252}$$

with

$$\Theta_\parallel(x_\parallel, \rho = \infty) = -\frac{1}{\pi}\int_0^\infty \mathrm{d}\omega \ln\left(1 + e^{-\sqrt{x_\parallel^2+\omega^2}}\right), \tag{2.253}$$

where $x_\parallel^2 = t^2(L_\parallel^2/\xi_+^2)$, with the reduced temperature t and the correlation length amplitude ξ_+. Note that $L_\parallel$ in Ref. [54] corresponds to L_1 as defined in this work, such that both results agree.

2.9.2 Limit $\rho_p \to 0$

As discussed previously, the Ising partition function near the scaling limit is modular invariant, the inversion of the modular parameter $\tau \to \tau' = -1/\tau$ can thus be used to treat this limit. Specifically, this means that $\tau_0 \to \tau_0' = -\tau_0/\rho_p^2 = -\cos\alpha/\rho_p$ and $\tau_1 \to \tau_1' = \tau_1/\rho_p^2 = \sin\alpha/\rho_p$. To keep the ratio x^2/τ_1 independent of ρ_p in this case, $L_1 = L_2/\rho_p$ is substituted. For the limit of the excess free energy, this means

$$\lim_{\rho_p\to 0}\frac{1}{V}\mathcal{F}_{\text{ex}}^{\text{trIs}}(x|\tau) = \lim_{\rho_p\to 0}\frac{1}{V}\mathcal{F}_{\text{ex}}^{\text{trIs}}(x|-1/\tau) = -\frac{1}{L_2^2\sin\vartheta}\lim_{\rho_p\to 0}\rho_p\mathcal{F}_{\text{ex}}^{\text{trIs}}(x|-1/\tau) \tag{2.254}$$

For the different sectors of the Ising partition function, one thus gets

$$\begin{aligned} &e^{-\frac{1}{2}\mathcal{G}_0(x^2|-1/\tau,\Delta_1,\Delta_2)} \\ &= \exp\left(c_1(\Delta_x)/\rho_p + \sum_{m=-\infty}^{\infty}\ln\left|1 - e^{-c_2(m,\Delta_x)/\rho_p - 2\pi i[\Delta_y - c_3(m+\Delta_x)/\rho_p]}\right|^2\right) \end{aligned} \tag{2.255}$$

By substituting $\rho_p \to 1/\rho_p'$, the mathematical problem as in the limit of $\rho_p \to \infty$ is recovered, since after substitution the limit in (2.254) of $\rho_p \to 0$ is replaced by $\rho_p' \to \infty$:

$$\lim_{\rho_p\to 0}\frac{1}{V}\mathcal{F}_{\text{ex}}^{\text{trIs}}(x|-1/\tau) = -\frac{1}{L_2^2\sin\vartheta}\lim_{\rho_p'\to\infty}\frac{1}{\rho_p'}\mathcal{F}_{\text{ex}}^{\text{trIs}}(x|-1/\tau) \tag{2.256}$$

and

$$e^{-\frac{1}{2}\mathcal{G}_0(x^2|-1/\tau,\Delta_1,\Delta_2)} = \exp\left(\rho_p' c_1(\Delta_x) + \sum_{m=-\infty}^{\infty}\ln\left|1 - e^{-\rho_p' c_2(m,\Delta_x) - 2\pi i[\Delta_y - \rho_p' c_3(m+\Delta_x)]}\right|^2\right) \tag{2.257}$$

Note the change in sign in front of c_3 that appears in the above expression since, as discussed in section 2.6.2, only the full partition function is modular invariant, but not the individual sectors themselves. Now proceeding as above, one finally arrive at the result

$$\lim_{\rho_p\to 0}\frac{1}{V}\mathcal{F}_{\text{ex}}^{\text{trIs}}(x|\tau) = -\frac{\sin\alpha}{L_2^2\sin\vartheta}\int_0^\infty\frac{\mathrm{d}p}{\pi}\ln\left|1 + e^{-\sqrt{p^2+x^2/\tau_1'}}\right| \tag{2.258}$$

with

$$\frac{x^2}{\tau_1'} = \frac{L_2^2 \sin\vartheta}{\bar{\xi}_{0+}^2 \sin\alpha}\, t^2 \tag{2.259}$$

For the special case $\vartheta = \alpha = \pi/2$, one can again compare to Ref. [54] (eq. (10)–(13) and (57)), where the excess free energy is given by:

$$f_{\text{ex}} = \frac{1}{L_\perp^2}\, \Theta_\perp(x_\perp, \rho = 0) \tag{2.260}$$

with

$$\Theta_\perp(x_\perp, \rho = 0) = -\frac{1}{\pi} \int_0^\infty \mathrm{d}\omega \ln\left(1 + e^{-\sqrt{x_\perp^2 + \omega^2}}\right), \tag{2.261}$$

and the scaling variable $x_\perp^2 = t^2(L_\perp^2/\bar{\xi}_+^2)$. Both results were thus shown to be in agreement in both limits.

2.9.3 Limit $x \to 0$

Using that $\int_0^\infty \frac{\mathrm{d}p}{\pi} \ln|1 + e^{-p}| = \pi/12$, one obtains from the above

$$\lim_{x\to 0} \lim_{\rho_p \to 0} \frac{1}{V} \mathcal{F}_{\text{ex}}^{\text{trIs}}(x|\tau) = -\frac{\sin\alpha}{L_2^2 \sin\vartheta} \frac{\pi}{12}, \tag{2.262}$$

which agrees with a direct calculation at criticality, using the results of [55]. In a similar fashion,

$$\lim_{x\to 0} \lim_{\rho_p \to \infty} \frac{1}{V} \mathcal{F}_{\text{ex}}^{\text{trIs}}(x|\tau) = -\frac{\sin\alpha}{L_1^2 \sin\vartheta} \frac{\pi}{12}. \tag{2.263}$$

can be obtained.

2.10 Comparison to previous results

In the following, quite technical sections, it will be shown that it is possible to recover some previously known results for the scaling functions, specifically for the case of nearest-neighbor couplings with equal strength; as well as the case of rectangular anisotropy.

2.10.1 Isotropic couplings

In this chapter the equivalence between the finite size scaling functions $\Theta(x, \rho)$ of the nearest neighbor Ising model as defined in [56] and $\mathcal{F}_{\text{ex}}^{\text{trIs}}(x, \tau)$ for the case $E_1 = E_2$, $E_3 = 0$ on the rectangular lattice is shown. Under these conditions the lattice parameters are $a_1 = a_2 = a$, $\vartheta = \pi/2$ and thus $\rho_p = aN_2/(aN_1) \equiv \rho$. Here again, the previously derived expression for the excess free energy (2.170) with the integral expression for $\mathcal{G}_0$, is used:

$$\begin{aligned}\mathcal{G}_0\left(x^2|\tau, \Delta_x, \Delta_y\right) = &-\tau_1 \int_{-\infty}^{\infty} \frac{\mathrm{d}p}{2\pi} \ln\left|1 - e^{-\sqrt{p^2 + x^2/\tau_1} + 2\pi i \Delta_x}\right|^2 \\ &- \sum_{m=-\infty}^{\infty} \ln\left|1 - e^{-2\pi\tau_1\sqrt{(m+\Delta_x)^2 + x^2/(4\pi^2\tau_1)} - 2\pi i[\Delta_y - \tau_0(m+\Delta_x)]}\right|^2\end{aligned} \tag{2.264}$$

To show the equivalence in the case of a rectangular system, the modular invariance of the excess free energy is employed to set $\tau \to -1/\tilde{\tau}$, furthermore the modular parameter is given as a function of the couplings by (2.154) and simplifies to $\tau \to i/\rho$, with which $\tilde{\tau}_0 = 0$ and $\tilde{\tau}_1 = 1/\rho$ follows; simplifying the integral in the first term of $\mathcal{G}_0$ yields:

$$\begin{aligned}
&\int_{-\infty}^{\infty} \frac{\mathrm{d}p}{2\pi} \ln \left| 1 - e^{-\sqrt{p^2 + x^2/\tilde{\tau}_1} + 2\pi i u_0} \right|^2 \\
&= 2 \int_{-\infty}^{\infty} \mathrm{d}p \ln \left| 1 \pm e^{-\sqrt{4\pi^2 p^2 + \rho\, x^2}} \right| && (2.265) \\
&\equiv 2 I_{\pm}(\sqrt{\rho\, x^2}) && (2.266)
\end{aligned}$$

where variable substitution $p \to 2\pi p$ was made and the function

$$I_{\pm}(x) = \int_{-\infty}^{\infty} \mathrm{d}p \ln \left| 1 \pm e^{-\sqrt{4\pi^2 p^2 + x^2}} \right| \tag{2.267}$$

defined; here the $\pm$ is $+$ if $\Delta_x = 1/2$ and $-$ if $\Delta_x = 0$. The second term of $\mathcal{G}_0$ simplifies to

$$\begin{aligned}
&\sum_{n=-\infty}^{\infty} \ln \left| 1 - e^{-2\pi\tilde{\tau}_1 \sqrt{(n+\Delta_x)^2 + (x^2/4\pi^2\tilde{\tau}_1)} + 2\pi i [\Delta_y - \tilde{\tau}_0 (n+\Delta_x)]} \right|^2 && (2.268) \\
&= 2 \ln \left[\prod_{n=-\infty}^{\infty} 1 - e^{-2\pi\tau_1 \sqrt{(n+\Delta_x)^2 + (x^2/4\pi^2\tilde{\tau}_1)} + 2\pi i \Delta_y} \right] && (2.269) \\
&= 2 \ln \left[\prod_{n=-\infty}^{\infty} 1 \pm e^{-\sqrt{4\pi^2 (n-\Delta_x)^2 + \rho\, x^2}/\rho} \right] && (2.270) \\
&=: 2 \ln P^{\pm}_{\Delta_x}(\sqrt{\rho\, x^2}, \rho) && (2.271)
\end{aligned}$$

in the second to last line the index n was shifted and

$$P^{\pm}_{\Delta_x}(x, \rho) = \prod_{n=-\infty}^{\infty} 1 \pm e^{-\sqrt{4\pi^2 (n-\Delta_x)^2 + x^2}/\rho} \tag{2.272}$$

was defined, here the $\pm$ is $+$ if $\Delta_y = 1/2$ and $-$ if $\Delta_y = 0$. So in total one finds the expression

$$\mathcal{G}_0 \left(x^2 \middle| \tilde{\tau}, \Delta_x, \Delta_y \right) = -\frac{2}{\rho} I_{\pm}(\sqrt{\rho\, x^2}) - 2 \ln P^{\pm}_{u_0}(\sqrt{\rho\, x^2}, \rho) \tag{2.273}$$

and thus the scaling function on the rectangular lattice, denoted as Θ, is

$$\begin{aligned}
\mathcal{F}^{\mathrm{trIs}}_{\mathrm{ex}} \left(x \middle| -\tfrac{1}{i\rho} \right) &= \Theta(\sqrt{\rho\, x^2}, \rho) \\
&= -\ln \frac{1}{2} \left[\underbrace{P^{+}_{0} e^{I_-/\rho}}_{\Delta_x = 0, \Delta_y = 1/2} + \underbrace{P^{-}_{1/2} e^{I_+/\rho}}_{\Delta_x = 1/2, \Delta_y = 0} + \underbrace{P^{+}_{1/2} e^{I_+/\rho}}_{\Delta_x = 1/2, \Delta_y = 1/2} \mp \underbrace{P^{-}_{0} e^{I_-/\rho}}_{\Delta_x = 0, \Delta_y = 0} \right] && (2.274) \\
&= -\ln \left[\frac{P^{+}_{1/2} + P^{-}_{1/2}}{2 e^{-I_+/\rho}} + \frac{P^{+}_{0} \mp P^{-}_{0}}{2 e^{-I_-/\rho}} \right] && (2.275)
\end{aligned}$$

which is the same as in equation (49) together with equations (6) and (12) of [56]. As discussed in section 2.6, the scaling variable is given by

$$x^2 = \frac{V}{(\bar{\xi}_{0+})^2}|t|^2 \tag{2.276}$$

where $\bar{\xi}_{0+}$ is the dimensionless mean correlation length amplitude of the anisotropic on the parallelogram lattice and $V = N_1 N_2 a_1 a_2 \sin\vartheta$ the system volume; from this it follows that the scaling variable in the rectangular case has the form $\rho\, x^2 = (|t|N_2/\xi_{0+})^2$, which is the same as the one defined in the beginning of chapter III in [56]. This holds, since on the rectangular lattice $\rho V = N_2^2 a^2$ and $\bar{\xi}_{0+} = a\xi_{0+}$ with the dimensionless (or $a = 1$) correlation length amplitude ξ_{0+}.

2.10.2 Rectangular, anisotropic couplings

Similarly, in equation (3.13) and (4.37) of [57] an expression for the excess free energy scaling function for rectangular anisotropy with only $E_3 = 0$ on the rectangular lattice with $a_1 = a_2 = a$, $\vartheta = \pi/2$ was given as

$$F_{\infty,\mathrm{res}} = \rho'\, \Theta_{\parallel}(x_{\parallel}, \rho') \tag{2.277}$$

with

$$\Theta_{\parallel}(x_{\parallel}, \rho') = \Theta_b(x_{\parallel}) + \rho'^{-1}\Psi_o(x_{\parallel}, \rho') - \rho'^{-1} \ln\left[1 + e^{-\rho'\delta\Theta_b(x_{\parallel}) - \delta\Psi(x_{\parallel}, \rho')}\right] \tag{2.278}$$

where

$$\Theta_b(x) = -\frac{1}{2\pi}\int_{-\infty}^{\infty} \mathrm{d}\Phi \ln\left[1 + e^{-\sqrt{x^2+\Phi^2}}\right] \tag{2.279}$$

$$\delta\Theta_b(x) = -\frac{1}{2\pi}\int_{-\infty}^{\infty} \mathrm{d}\Phi \ln\frac{1 - e^{-\sqrt{x^2+\Phi^2}}}{1 + e^{-\sqrt{x^2+\Phi^2}}} \tag{2.280}$$

$$\Psi_e(x, \rho') = -\ln\frac{P_e^+(x, \rho') - \mathrm{sgn}(x) P_e^-(x, \rho')}{2} \tag{2.281}$$

$$\Psi_o(x, \rho') = -\ln\frac{P_e^+(x, \rho') + P_e^-(x, \rho')}{2} \tag{2.282}$$

$$\delta\Psi(x, \rho') = \Psi_e(x, \rho') - \Psi_o(x, \rho') \tag{2.283}$$

$$P_{e/o}^{\pm}(x, \rho') = \prod_{\substack{m=-\infty \\ \text{m even/odd}}}^{\infty} (1 \pm e^{-\rho'\sqrt{x^2+\pi^2 m^2}}) \tag{2.284}$$

First note the different definition of the aspect ratio in the original paper given in equation (3.10), where

$$\rho' = \frac{L/\hat{\xi}_{\perp}}{M/\hat{\xi}_{\parallel}} = \rho\,\frac{\hat{\xi}_{\parallel}}{\hat{\xi}_{\perp}} \tag{2.285}$$

with $\rho = L/M$ the usual definition; the $\hat{\xi}$ are the correlation length amplitudes in parallel and perpendicular direction. One can also rewrite the expression

$$\delta\Theta_b(x) = -\frac{1}{2\pi}\int_{-\infty}^{\infty} \mathrm{d}\Phi \ln\frac{1 - e^{-\sqrt{x^2+\Phi^2}}}{1 + e^{-\sqrt{x^2+\Phi^2}}} = \Theta_b^-(x) - \Theta_b^+(x) \tag{2.286}$$

where a generalization of $\Theta_b(x) = \Theta_b^+(x)$ was introduced, namely

$$\Theta_b^\pm(x) = -\frac{1}{2\pi}\int_{-\infty}^{\infty} \mathrm{d}\Phi \ln\left|1 \pm e^{-\sqrt{x^2+\Phi^2}}\right| \tag{2.287}$$

this makes it possible to write the scaling function as

$$\Theta_\parallel(x_\parallel, \rho') = -\frac{1}{\rho'} \ln e^{-\rho'\Theta_\parallel(x_\parallel,\rho')} \tag{2.288}$$

$$= -\frac{1}{\rho'} \ln\left[\frac{P_o^+ + P_o^-}{2e^{\rho'\Theta_b^+}}\left(1 + e^{-\rho'(\Theta_b^- - \Theta_b^+)}\frac{(P_e^+ - \mathrm{sgn}(x_\parallel)P_e^-}{P_o^+ + P_o^-}\right)\right] \tag{2.289}$$

$$= -\frac{1}{\rho'} \ln\left[\frac{P_o^+ + P_o^-}{2e^{\rho'\Theta_b^+}} + \frac{P_e^+ - \mathrm{sgn}(x_\parallel)P_e^-}{2e^{\rho'\Theta_b^-}}\right] \tag{2.290}$$

which is already of a similar form as the scaling function for the system with isotropic couplings. It is easy to see that $\Theta_b^\pm(x) = -I_\pm(x)$, where $I_\pm(x)$ was defined above in equation (2.266); furthermore, note that

$$4(n - \Delta_x)^2 = \begin{cases} (2n)^2, & \text{if } \Delta_x = 0 \\ (2n-1)^2, & \text{if } \Delta_x = \dfrac{1}{2} \end{cases} \tag{2.291}$$

with which the even/odd condition in $P_{e/o}^\pm(x,\rho)$ can be replaced by introducing a $\Delta_x = 0, 1/2$:

$$P_{e/o}^\pm(x,\rho') = \prod_{m=-\infty}^{\infty} (1 \pm e^{-\rho'\sqrt{x^2+4\pi^2(m-\Delta_x)^2}}) \tag{2.292}$$

which can be expressed as the function defined in equation (2.271) with the relation $P_{e/o}^\pm(x,\rho) = P_{\Delta_x}^\pm(x,\rho^{-1})$. Finally, the scaling variable x is discussed; to this end the two correlation length amplitudes $\hat{\xi}_\parallel$ and $\hat{\xi}_\perp$ are computed. The total correlation length are given in equations (3.23) of [57] as

$$\xi_\perp^{(\infty)} = (\ln\coth K^\parallel - 2K^\perp)^{-1}, \quad \xi_\parallel^{(\infty)} = (\ln\coth K^\perp - 2K^\parallel)^{-1} \tag{2.293}$$

the amplitudes can be found by Taylor approximation around the critical point (2.7) defined by $\hat{S}_\parallel^c \hat{S}_\perp^c = 1$, where $\hat{S}_i^c = \sinh(2K_i)$ with $K_i = \beta E_i$. This gives

$$(\hat{\xi}_\perp)^{-1} = 2K_\perp \frac{1}{\hat{S}_\perp^c} + 2K_\parallel, \quad (\hat{\xi}_\parallel)^{-1} = 2K_\perp + 2K_\parallel \frac{1}{\hat{S}_\parallel^c} \tag{2.294}$$

such that $\xi^{(\infty)} \approx \hat{\xi}\,|t|^{-1}$ for $|t| = |(T - T_c)/T_c| \ll 1$. Now the aspect ratio ρ' can be expressed as

$$\rho' = \rho\,\frac{\hat{\xi}_\parallel}{\hat{\xi}_\perp} = \rho\,\hat{S}_\parallel^c \tag{2.295}$$

furthermore, the square of the scaling variables $x_\parallel$, given in equation (3.9) of [57], can be written as

$$x_\parallel^2 = \frac{M^2 t^2}{\hat{\xi}_\parallel^2} = \frac{ML\,t^2}{\rho\,\hat{\xi}_\parallel^2} = \frac{ML\,t^2}{(\rho\hat{S}_\parallel^c)\,(\frac{1}{\hat{S}_\parallel^c}\hat{\xi}_\parallel^2)} \tag{2.296}$$

here we have once again $\rho' = \rho \hat{S}^c_{\parallel}$, as well as

$$\frac{\hat{\xi}^2_{\parallel}}{\hat{S}^c_{\parallel}} = \left(2K_{\perp} \sqrt{\hat{S}^c_{\parallel}} + 2K_{\parallel} \frac{1}{\sqrt{\hat{S}^c_{\parallel}}} \right)^{-2} \tag{2.297}$$

Comparing this to the results, as presented in section 2.4 for the Ising model on the triangular lattice, where it was found, that

$$\bar{\xi}^{-1}_{0+} = 2\beta_c E_1 \sqrt{\hat{S}^c_2 + \hat{S}^c_3} + 2\beta_c E_2 \sqrt{\hat{S}^c_1 + \hat{S}^c_3} + 2\beta_c E_3 \sqrt{\hat{S}^c_1 + \hat{S}^c_2} \tag{2.298}$$

which simplifies to

$$\tilde{\xi}^{-1}_{0+} = 2\beta_c E_1 \frac{1}{\sqrt{\hat{S}^c_1}} + 2\beta_c E_2 \sqrt{\hat{S}^c_1} \tag{2.299}$$

for $E_3 = 0$; implying the relation $\hat{\xi}^2_{\parallel}/\hat{S}^c_{\parallel} = \tilde{\xi}^2_{0+}$. It was also found in (2.159), that the modular parameter on the triangular lattice can be expressed in its complex exponential form via $\tau = \rho_p e^{i\alpha}$; by

$$\cot \alpha = \hat{S}^c_3 \tag{2.300}$$

$$(\rho_p)^2 = \rho^2 \frac{1 + (\hat{S}^c_1)^2}{1 + (\hat{S}^c_2)^2} \tag{2.301}$$

which again can be simplified using the critical condition $\hat{S}_1 \hat{S}_2 = 1$ for $E_3 = 0$ to

$$\tilde{\tau} = \tilde{\tau}_0 + i\tilde{\tau}_1 = i\rho \hat{S}^c_1 \tag{2.302}$$

with this one finds $\rho' = \tilde{\tau}_1$ and

$$x^2_{\parallel} = \frac{ML\,t^2}{\tilde{\tau}_1 \tilde{\xi}^2_{0+}} = \frac{x^2}{\tilde{\tau}_1}. \tag{2.303}$$

where x is the usual scaling variable. Comparing $\Theta^{\pm}_b(x_{\parallel}) = -I_{\pm}(x_{\parallel})$ to the first term of (2.264) and $P^{\pm}_{e/o}(x_{\parallel}, \rho')$ to equation (2.272), it is straight forward to see, that (2.290) and (2.275) are essentially the same expression. The pre factor $1/\rho'$ is canceled when taking the actual scaling function (2.277) into account. Moreover, one finds

$$\begin{aligned} &\mathcal{G}_0(x^2 | i\rho \hat{S}^c_1, \Delta_x, \Delta_y) \\ &= -2\rho' I_{\pm}(x_{\parallel}) - 2 \ln P^{\pm}_{u_0}(x_{\parallel}, \tfrac{1}{\rho'}) \qquad (2.304) \\ &= -\rho' \int_{-\infty}^{\infty} \frac{\mathrm{d}p}{2\pi} \ln \left| 1 \pm e^{-\sqrt{p^2 + x^2_{\parallel}}} \right|^2 - \sum_{n=-\infty}^{\infty} \ln \left| 1 \pm e^{-2\pi\rho' \sqrt{(n-\Delta_x)^2 + (x^2_{\parallel}/4\pi^2)}} \right|^2 \qquad (2.305) \end{aligned}$$

and see that the scaling function found in [58] is just a special case of (2.170) with $E_3 = 0$ and on a rectangular lattice with square unit cells.

2.11 Conclusions

In this chapter the partition function of the triangular Ising model in $2d$ on a finite parallelogram lattice was calculated, along with the associated singular bulk free energy and the scaling function near and at T_c in the ferromagnetic regime. The derivation of the prefactor of the singular part of the free energy enabled the recovery of the mean correlation length of the system, aligning with results from investigations on the correlation function. Furthermore, by deriving the scaling function and demonstrating its explicit dependence on microscopic details of the model through τ in (2.154), a contribution was made to the body of evidence supporting multi-parameter universality. Furthermore, the proof of modular invariance of the scaling function established that there exists only a finite domain of couplings in the near critical Ising model that encompasses all possible values of the free energy. Additionally, the strip limit for both extreme cases of zero and infinite aspect ratios was evaluated and connection to previous research was made, by explicitly deriving an integral expression of the scaling function, which was initially only thought to be valid in isotropic systems; finally, the Ising scaling function for a few special cases with more restricted couplings and lattices was recovered.

Chapter 3

Numerical study of non-universal critical behavior

To confirm the predictions made by multi-parameter universality additional models should be investigated; there are, however, only very few systems in $d \geq 2$ that are exactly solvable and exhibit non-rectangular anisotropy, i.e. allow for an arbitrary rotation of the correlation ellipsis. But it is of course possible to make use of numerical simulations to probe such systems. To this end, the method of corner transfer matrix renormalization group (CTMRG) [59, 60] is used to investigate the $2d$ q-state Potts model. The details of the model are explained later, but it has the advantage that one recovers the Ising model for $q = 2$ and thus allows easy comparisons with exactly known results. Furthermore, for $q \leq 4$ the Potts model is known to exhibit a continuous phase transition [61, 62], which allows testing if and how two-factor universality is violated.

More specifically, the following steps need to be taken to check multi-parameter universality:

(1) Setup and validate the CTMRG algorithm for the $2d$ Potts model

(2) Extract the correlation length in x and y direction with the CTMRG method

(3) Obtain theoretical predictions for the correlation ellipsis parameters $\tilde{q}$[1] and Ω

(4) Compare the correlations length ratio of the x and y directions with theory. These ought to only depend on $\tilde{q}$ and Ω.

(5) Alternatively: Calculate a universal property, like the excess free energy, for two sets of couplings with the same correlation ellipsis parameters and determine if they are equal or not. (Not part this work.)

At the end of this chapter additional predictions for the corner free energy of the Potts model are presented, which imply, if confirmed by simulation, that this contribution, which is usually considered to be universal, does depend on the microscopic couplings of the Hamiltonian. Chen and Dohm [22] previously predicted the nonuniversality of this quantity in anisotropic systems.

[1] In this chapter $\tilde{q}$ instead of q is used to denote the ellipsis parameter, to avoid conflict with the variable for the number of states in the Potts model.

3.1 Overview and notation

The CTMRG algorithm is a sophisticated numerical method developed to study $2d$ statistical and quantum systems. This technique, emerging from the broader framework of renormalization group methods, is particularly effective for analyzing systems with strong correlations where traditional methods have difficulty. The CTMRG method is a pivotal advancement in computational physics, enabling the accurate calculation of thermodynamic quantities and the analysis of phase transitions in complex systems.

The concept of the corner transfer matrix (CTM) was initially introduced in the context of exactly solvable models in statistical mechanics [63, 64]. As discussed in the introduction, the renormalization group (RG) is a fundamental concept in theoretical physics for addressing scale-invariant phenomena, which was later combined with the CTM concept to form the CTMRG method. This hybrid method was primarily developed in [59, 60], enhancing the ability to analyze $2d$ lattice models efficiently.

In the CTM approach, a $2d$ lattice model is divided into four quadrants, each represented by a corner transfer matrix that encapsulates the statistical sum of configurations within that quadrant. The total partition function of the system, a key quantity describing its statistical properties, can be represented as a product of these matrices. The RG aspect deals with the systematic thinning of degrees of freedom in a system to study its behavior at different scales. By integrating out short-range details, the RG method focuses on long-range, scale-invariant properties, crucial for understanding critical phenomena near phase transitions.

The CTMRG method combines these two approaches by applying the RG idea to the CTM. Specifically, it iteratively renormalizes the corner matrices and edge tensors to study the system at progressively larger scales. This process involves generally the following steps [65]:

(1) **Tensor representation**: Starting from the partition function expressed through the Hamiltonian, a transfer tensor/matrix representation for the bulk unit cells needs to be found and the environment consisting of the corner transfer matrices as well as the edge tensors setup.

(2) **Decomposition and truncation**: The CTM is decomposed using techniques such as the singular value decomposition (SVD), which separates the matrix into components ranked by their significance to the systems state. The components associated with the smallest singular values, which contribute minimally to the system's properties, are truncated to reduce the computational complexity and memory requirements.

(3) **Iteration and renormalization**: After truncation, the renormalized matrices are used to construct a new, effective CTM that represents the system at a larger scale. This iterative process is repeated, each time increasing the scale and refining the approximation to the system's true behavior.

(4) **Extraction of physical quantities**: Thermodynamic and statistical properties, such as free energy, correlation lengths, and order parameters, can be calculated from the renormalized matrices. These quantities provide insight into the system's phase behavior and critical phenomena.

This process is sketched in the figure below:

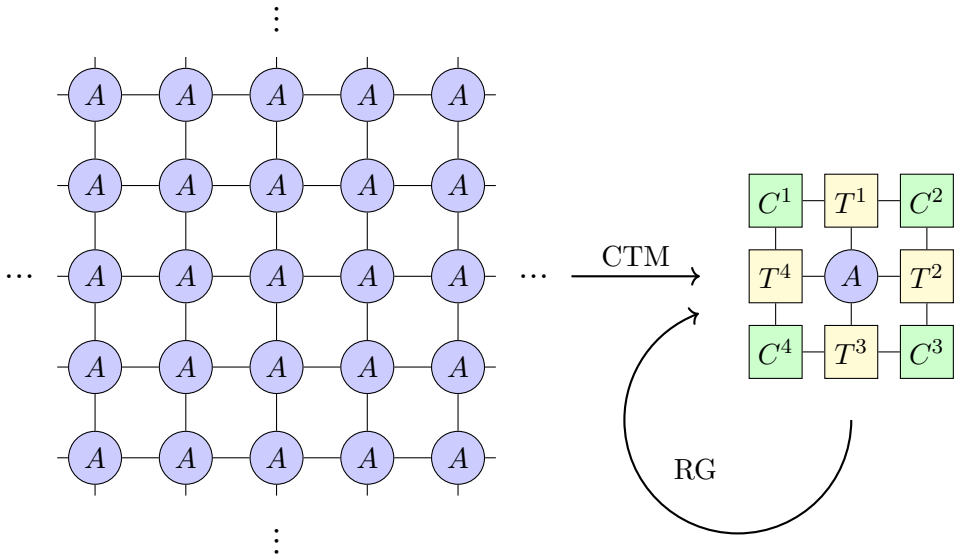

Figure 3.1: Visualization of the CTMRG method. Starting from an infinite system decomposed into tileable tensors (left), these get iteratively absorbed into the environment (right).

The diagrammatic notation used here to visualize the tensors and their contraction works as follows: A tensor of rank n is indicated by a circle with n legs, here demonstrated for $n = 4$:

$$T_{\alpha\beta\gamma\delta} = \qquad \delta,\ \gamma,\ T,\ \alpha,\ \beta \tag{3.1}$$

Every leg corresponds to an index of the tensor; the dimension of each rank depends on the context. Two tensors can be contracted, as long as they are compatible, by connecting at least one pair of legs together. The common index is then summed over:

$$\alpha,\ A,\ \beta,\ B,\ \gamma \quad = \quad \alpha,\ C,\ \gamma$$

$$\sum_{\beta} A_{\beta\alpha} B_{\gamma\beta} \quad = \quad C_{\alpha\gamma} \tag{3.2}$$

resulting here in a tensor C of rank 2 after the contraction of two other rank 2 tensors A and B. The advantage of this notation is, that it allows large contractions to be visualized

efficiently. E.g. the network

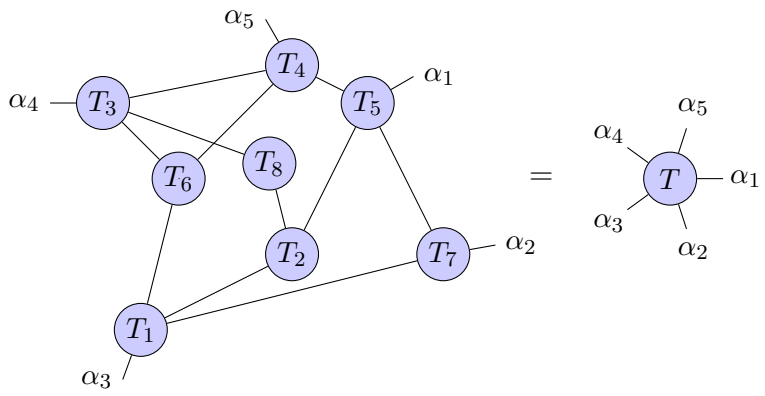

(3.3)

would be impossible to interpret if normal index and sum notation had been used. Since the above definition of tensor contraction is compatible with the commonly used matrix and vector operations, it is straight forward to identify

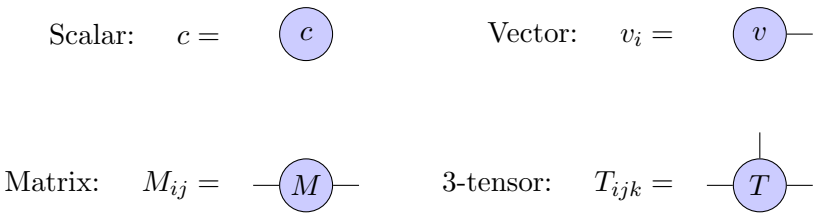

(3.4)

As in this example, legs may not always be labeled by their respective index, if the naming is either not important or is implicitly clear.

3.2 Bulk tensor of the q-state Potts model

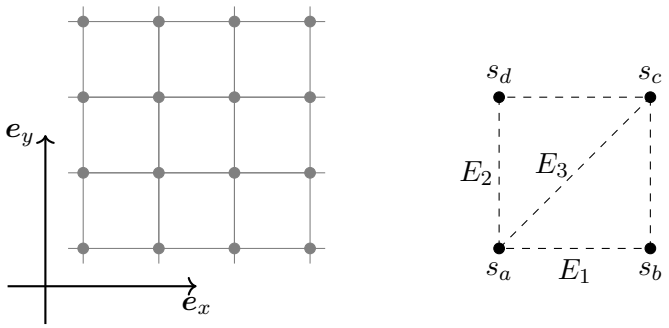

Figure 3.2: The square lattice with the principle directions x and y (left) and the couplings within a unit cell together with the naming convention for the degrees of freedom (right).

To apply the CTMRG algorithm, the partition function of the model of interest needs to be expressed in terms of tensors that are as compact as possible (i.e., contain the smallest amount of unit cells), to make the computations as efficient as possible. To this end, the results presented in [66, 67] for the Ising model are expanded upon. The Hamiltonian

of the $2d$ q-state Potts model on a square lattice with nearest and next-nearest neighbor couplings is given by

$$H^{\text{Potts}} = -\sum_{i,j} E_1\delta(s_{i,j} - s_{i+1,j}) + E_2\delta(s_{i+1,j} - s_{i+1,j+1}) + E_3\delta(s_{i+1,j+1} - s_{i,j}) \tag{3.5}$$

here $\delta(n)$ is delta function which is equal one if $n = 0$ and zero otherwise, the degrees of freedom can take the values $s_{i,j} = 0, 1, ..., q-1$. Similar to the Ising Hamiltonian presented previously, the couplings E_1 and E_2 are nearest neighbor and E_3 diagonally next-nearest neighbor in one direction. The partition function follows as

$$Z^{\text{Potts}} = \sum_{\{s_{i,j}\}} \exp(-\beta H_p) \tag{3.6}$$

$$= \sum_{\{s_{i,j}\}} \prod_{i,j} w(s_{i,j}, s_{i+1,j}, s_{i+1,j+1}, s_{i,j+1}), \tag{3.7}$$

where the Boltzmann weight was extended to a full square unit cell by including the missing spin. To avoid double counting, its square takes the explicit form:

$$\begin{aligned} w^2(s_{i,j}, s_{i+1,j}, s_{i+1,j+1}, s_{i,j+1}) = \; & \exp(\beta E_1\delta(s_{i,j} - s_{i+1,j}) + \beta E_1\delta(s_{i,j+1} - s_{i+1,j+1}) \\ & + \beta E_2\delta(s_{i,j} - s_{i,j+1}) + \beta E_2\delta(s_{i+1,j} - s_{i+1,j+1}) \\ & + 2\beta E_3\delta(s_{i,j} - s_{i+1,j+1}) \end{aligned} \tag{3.8}$$

To make the following expressions more readable, a notation for the variables in the unit cell at (i, j) is introduced

$$w_{i,j}(s_a, s_b, s_c, s_d) \equiv w(s_{i,j}, s_{i+1,j}, s_{i+1,j+1}, s_{i,j+1}), \tag{3.9}$$

which can also be seen in fig. 3.2. Expressing the total partition function through a tensor network requires to transition to a bond representation of the Boltzmann weight. To this end, the bond variables

$$x_1 = s_a - s_b \quad x_2 = s_b - s_c \tag{3.10}$$

$$x_3 = s_c - s_d \quad x_4 = s_d - s_a \tag{3.11}$$

are introduced. However, these variables are not independent, since some share some of the original degrees of freedom; to enforce the correct behavior, one should first note that

$$x_1 + x_2 + x_3 + x_4 = 0, \tag{3.12}$$

which can explicitly be enforced through a delta function. Moreover, there is no bond variable that specifically represents the diagonal connection given by $s_a - s_c$; this can be fixed by using

$$x_1 + x_2 = s_a - s_c \quad \text{or} \quad -(x_3 + x_4) = s_a - s_c. \tag{3.13}$$

The total Boltzmann weight as a function of the bonds is thus given by

$$\begin{aligned} A_{x_1x_2x_3x_4} \equiv \delta(x_1 + x_2 + x_3 + x_4) \exp\Big(\frac{\beta}{2}(& E_1\delta(x_1) + E_1\delta(x_3) \\ & + E_2\delta(x_2) + E_2\delta(x_4) \\ & + E_3\delta(x_1 + x_2) + E_3\delta(x_3 + x_4))\Big) \end{aligned} \tag{3.14}$$

where the notation for the bulk tensor $A_{x_1x_2x_3x_4}$ was introduced. The partition function can thus be written as

$$Z = \operatorname*{Tr}_{\{x\}} \prod_{i,j} (A_{x_1x_2x_3x_4})_{i,j}, \tag{3.15}$$

where the trace goes over all bond variables. In diagrammatic notation, the tensor can be expressed as follows:

$A_{x_1x_2x_3x_4} =$ 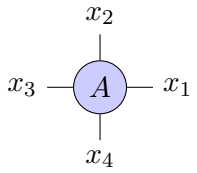

(3.16)

3.3 The CTMRG algorithm

As alluded to in the introduction, the CTMRG method can be used to compute the bulk properties of classical statistical systems and its associated physical observables. As shown in fig. 3.1 the algorithms works by continuously building the environment consisting of the corner tensors C^i and edge tensors T^i. In principle, this can be done exactly, since any part of the lattice can be contracted into one tensor. The problem, however, is that the bond dimension and with it the computation time would increase rapidly, since all degrees of freedom would need to be accounted for. The solution to this is to truncate the environment tensors at some bond dimension χ, which regulates the accuracy to which the details of the bulk system are retained. The difficulty now is to decide which information within these tensors is important and which are not. Different schemes have been devised over time, the details of which will be discussed below, but generally they are presented in terms of a projector (red triangles in fig. 3.3) which takes the corner or edge tensor together with additional bulk tensor, determines the important contributions and projects them down to a bond dimension of χ within the environment. If the bulk tensor has a bond dimension of (d, d, d, d) (in the case of the Potts model $d = q$), then the corner tensors C^i would start with bond dimension (d, d) and the edge tensors T^i with (d, d, d). Under the assumption of no projector or a naive projector that just combines additional indices from newly absorbed bulk tensors into super indices, the bond dimension in the environment tensors would increase exponentially after n steps as (d^n, d^n) and (d^n, d^n, d) for C^i and T^i, respectively. With a projector however, this will be limited to (χ, χ) and (χ, χ, d).

3.3.1 The original projector

In the original paper that proposed the CTMRG [59] the projector that is responsible for, e.g., the top left corner was chosen such that it would take into account the total system as shown in fig. 3.4. This is achieved by cutting open the system in the direction the projector is supposed to act in and decomposing the complete system via singular value decomposition (SVD).

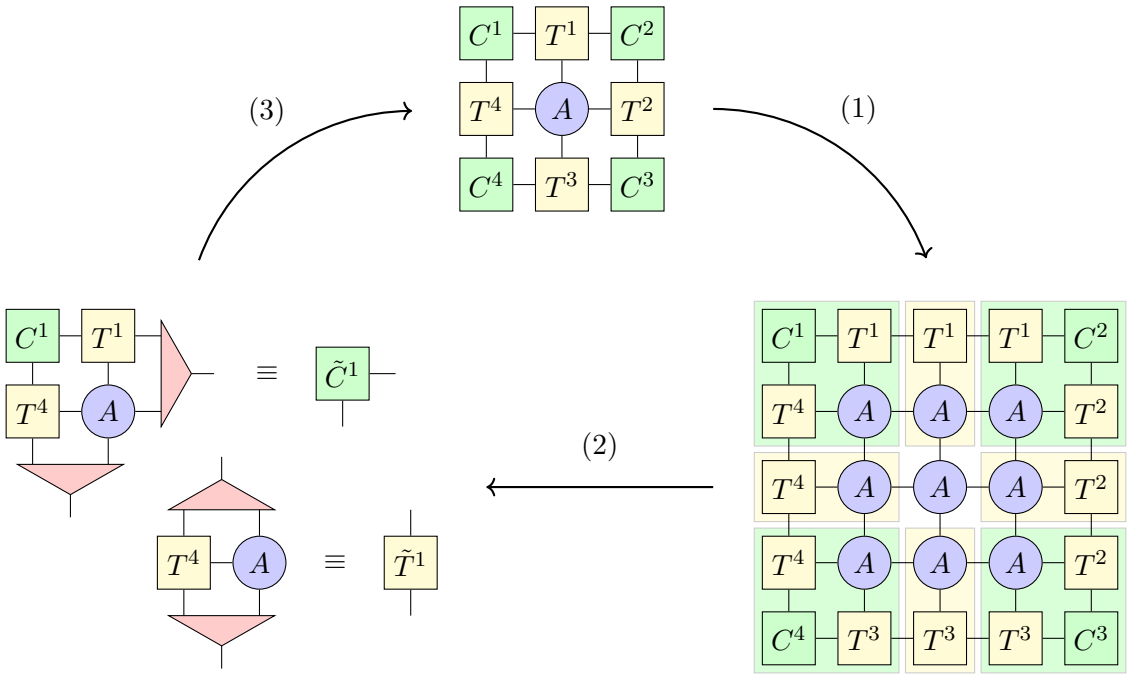

Figure 3.3: The current system surrounded by the environment tensors gets extend by adding additional bulk tensors (1), the environment tensors are combined with the newly added bulk tensors and projectors (red triangles) are formed to reduced the bond dimension (2); finally, a new system is created with the projected environment tensors (3). Between step (2) and (3) only the process for C^1 and T^4 is shown, but of course should be applied in a similar fashion to the other sides and corners as well.

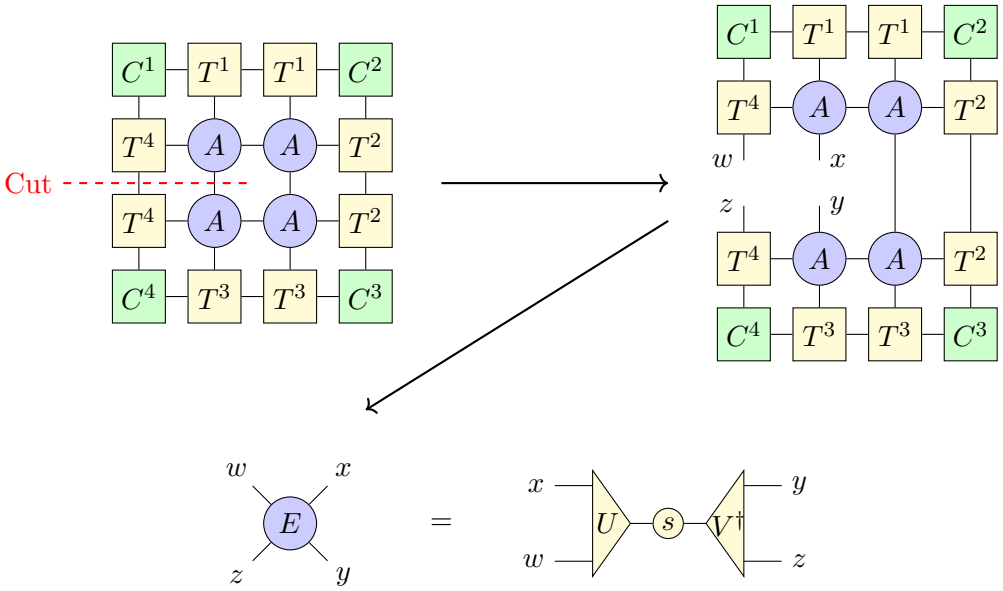

Figure 3.4: In the first step the system is cut between two column tensors T^4. This new rank 4 tensor E is the decomposed into the unitary matrix U, the adjoint of a unitary matrix $V^\dagger$ and the diagonal matrix of singular values s via the singular value decomposition (SVD).

Usually an SVD is only defined for an $m \times n$ complex matrix M which can than be expressed via an $m \times m$ unitary matrix U, adjoint of an $n \times n$ unitary matrix $V^\dagger$ and the $m \times n$ rectangular diagonal matrix s, such that $M = U\, s\, V^\dagger$. It is, however, possible to define a tensor SVD by combining two or more indices of a higher rank tensor into two multi-indices representing a matrix. The bond dimension of the multi index is than the product of the dimension of the combined indices. For example in fig. 3.4: $m = \dim w \times \dim x$ and $n = \dim y \times \dim z$; from this it is clear that the SVD of a tensor is not uniquely defined but depends on how one decides to combine the tensors legs.

The projector itself is then created by only considering the largest χ singular values and their associated directions:

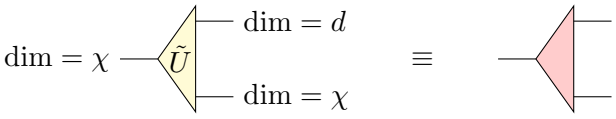

(3.17)

where $\tilde{U}$ denotes the truncated U. It is important to note that if both the lattice and its couplings were isotropic, it would be sufficient to keep only one projector, in the most general case, however, the steps described above in fig. 3.4 need to be repeated by cutting between the T^1, T^2 and T^3 as well. Even in the case of the Potts model with all couplings equal, this step would be required, due to the lattice anisotropy introduced by the diagonal bond.

As a last remark: It is possible to simplify the above procedure by just taking one corner of the system, consisting of a corner tensor with two adjacent edge tensors and one bulk tensor, to calculate the SVD and thus the projector.

3.3.2 A more advanced projector

Refs [68–72] established an improved projector, the construction of which is shown in fig. 3.5, with better convergence behavior for a given bond dimension χ. It can be useful to initially use the basic algorithm, which is observed to make faster progress at first but lacks precision later on, and then switch to the procedure presented in this section. To construct this projector, the system is first cut in halves, and each is decomposed into an orthonormal matrix Q and an upper triangular matrix R using the QR factorization scheme.

3.3.3 Initializing the environment

If one is only interested in bulk behavior, the edge and corner tensors T^i and C^i can be initialized randomly, since the initial state will become irrelevant after sufficient renormalization steps. However, to accelerate convergence or if one is interested in finite systems, the environment tensors may be initialized by omitting from (3.14) one bond for the edge tensor or two bonds for the corner tensors. Note that in case of finite systems, the linear system size starts at one unit cell and is increased by two in every iteration.

3.3.4 Convergence

Unfortunately, there is no guaranteed way to check if the algorithm has converged or if it is converging towards the correct value. However, one common way to test for convergence is by evaluating some observable A and check whether the change between two iterations is below a threshold[73]:

$$\left| \frac{A - \tilde{A}}{A} \right| < \epsilon, \tag{3.18}$$

where ϵ is, typically around 10^{-7}. Furthermore, it is not clear whether converged local observables imply a converged CTM. Therefore, one needs to be careful when evaluating, for example, correlation lengths or free energy derivatives, for which convergence was never tested. A different method is to check the singular value spectrum of the corner transfer matrices, such that

$$\frac{1}{\max_i s_i} \sum_i |s_i - \tilde{s}_i| < \epsilon \tag{3.19}$$

where s_i are the singular values and the tilde indicates the previous iteration.

3.4 Calculating the correlation length

The asymptotic properties of the system are stored in the environment tensors; more specifically, the correlations can be extracted from the row and column transfer matrices,

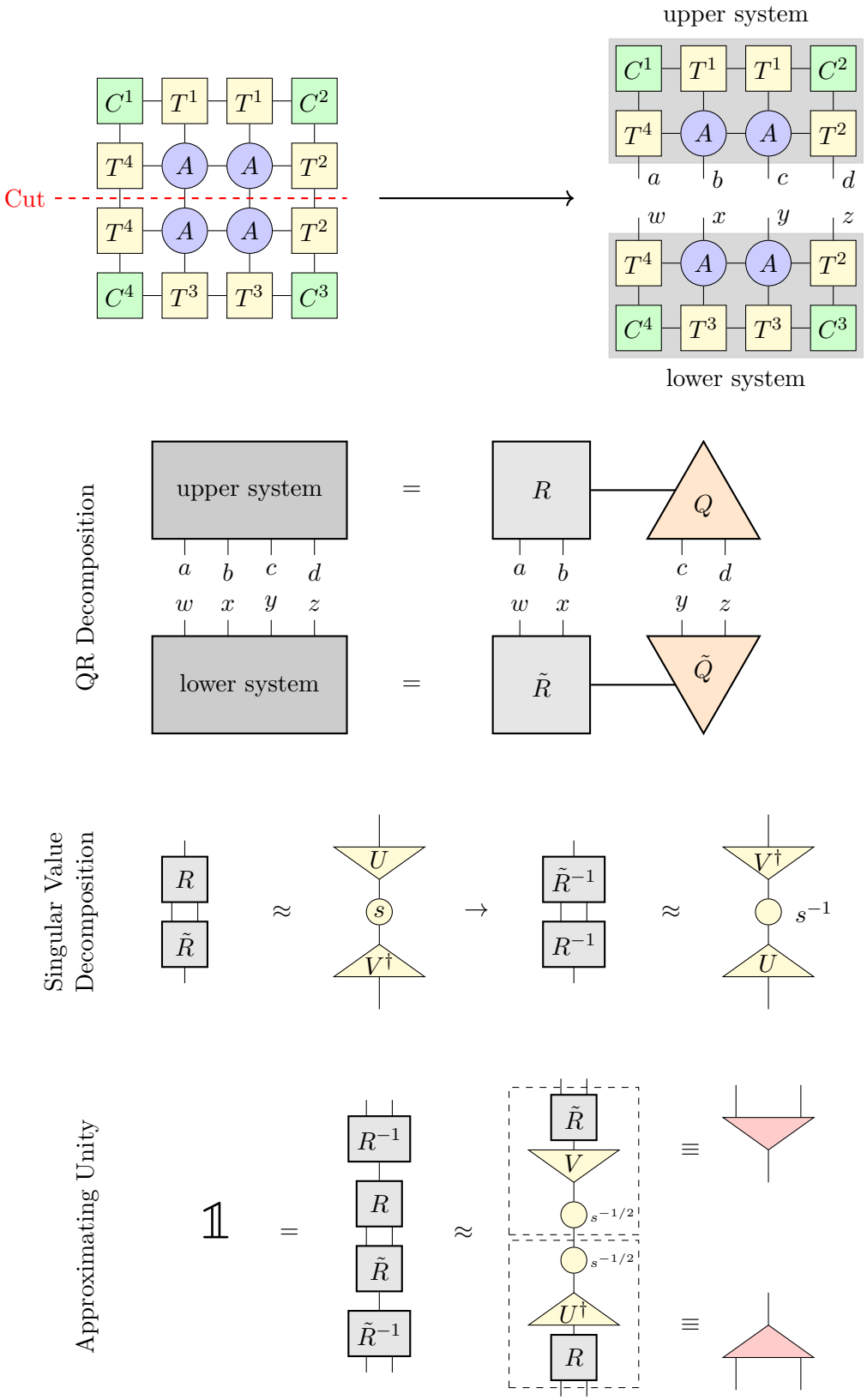

Figure 3.5: Construction of a different type of projector used in the CTMRG scheme. Here the system is cut in half and decomposed using the QR decomposition. Only after that the bond dimension is reduced, through limiting the number of singular values retained in the SVD.

which are defined as

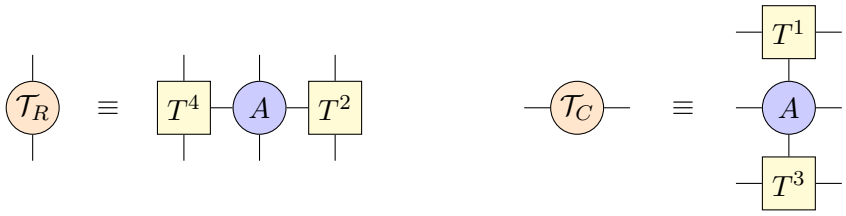

(3.20)

The usual approach to measure correlation lengths, is by taking the, possibly complex, eigenvalue spectrum of one of the row or column transfer matrices at bond dimension χ, where

$$\lambda_j = e^{-(\epsilon_j + i\phi_j)} \tag{3.21}$$

are the ordered eigenvalues with $|\lambda_0| > |\lambda_1| \geq |\lambda_2| \geq \ldots$; with $\epsilon_j \geq 0$ and phases $\phi_j \in (-\pi, \pi]$. The correlation length is then given by the ratios of the real exponents [65, 74]

$$\xi(\chi) = \frac{1}{\epsilon_1 - \epsilon_0}. \tag{3.22}$$

However, even away from the critical point, it is generally quite difficult to extract the bulk correlation length directly without going to prohibitively large bond dimensions. Though, it is often feasible to extrapolate to infinite bond dimension by a linear fit

$$\frac{1}{\xi(\chi)} = \frac{1}{\xi_\infty} + \frac{a}{\chi}. \tag{3.23}$$

Even though a quite straight forward approach, it has been shown [75], that there is no real justification to approach this problem by extrapolation of the bond dimension. One should instead use the difference between the fist and second eigenvalues $\delta = \epsilon_2 - \epsilon_1$, since, in the thermodynamic limit, the spectrum of the transfer matrix should be continuous, up to a gap between the zeroth and first eigenvalue, which is proportional to the inverse correlation length. In this picture, $\delta \equiv \delta(\chi)$ measures how close to continuous the system is and again, doing so for a range of bond dimensions χ allows for an extrapolation to $\delta = 0$. It should be noted, that the row and column transfer matrices are not equal and thus result in different correlation lengths.

To get more reliable results, it is also possible to not just use the difference $\epsilon_2 - \epsilon_1$ to estimate the distance from the thermodynamic limit, but more generally $\epsilon_m - \epsilon_n$ with $m > n$. This can be used to obtain multiple estimates for the same correlation length and makes it possible to estimate the error.

3.5 Comparison with exact results

To check the results obtained from CTMRG simulations, it is prudent to compare to exact results. However, there are no exact predictions for the correlation length in the anisotropic q state Potts model, but predictions for the critical free energy exist.

First, the critical temperature β_c is implicitly given by [61, 76]

$$\sqrt{q}\, x_1 x_2 x_3 + x_1 x_2 + x_2 x_3 + x_3 x_1 = 1 \tag{3.24}$$

where

$$x_i = \frac{1}{\sqrt{q}} \left(e^{\beta E_i} - 1 \right). \tag{3.25}$$

Furthermore, the critical bulk free energy density for $q \leq 4$ was found to be [61]

$$-f_{b,c}^{\text{Potts}} = \frac{1}{2}\ln q + \Psi(\alpha_1) + \Psi(\alpha_2) + \Psi(\alpha_3) \tag{3.26}$$

where

$$\Psi(\alpha_i) = \frac{1}{2}\int_{-\infty}^{\infty} \mathrm{d}x \; \frac{\sinh([\pi-\phi]x)\sinh(2[\phi-\nu]x)}{x\sinh(\pi x)\cosh(\phi x)} \tag{3.27}$$

with

$$\phi = -i\lambda, \quad \nu = -i\alpha_i \tag{3.28}$$

and λ, α_i are implicitly defined via

$$x_i = \frac{\sinh(\lambda-\alpha_i)}{\sinh\alpha_i}, \quad \sqrt{q} = 2\cosh\lambda. \tag{3.29}$$

Note, that solutions for other q are also available in the above reference, however, since only second order phase transitions are of interest here, the other solutions are omitted. A plot with some test results is presented in fig. 3.6, showing good agreement between theory and simulation for the free energy density for a generic anisotropic case.

Additionally, the critical exponents for the correlation length ν can be extracted, where $\xi_0(t) = \xi_{0+}|t|^{-\nu}$. To this end, the extraction of the bulk correlation length is shown in fig. 3.7, based on the method described in the section above with a maximum bond dimension of $\chi = 100$. Using the results for a range of temperatures, the correlation length amplitude and critical exponents can be obtained through a fit; an example of this procedure is shown in fig. 3.8 and fig. 3.9. The resulting parameters are given in table 3.1; the theoretical predicted value for the critical exponent is $\nu = 5/6 = 0.833\ldots$ [77–79].

dir.	E_1	E_2	E_3	ξ_{0+}	ν
x	1	1	1	0.245(7)	0.832(8)
y				0.245(1)	0.832(3)
x	1	2	3	0.210(4)	0.833(3)
y				0.241(6)	0.825(6)

Table 3.1: Results of the power law fit of the $q = 3$ Potts model with the extracted correlation lengths and amplitudes.

Note, that the ratios of correlation length amplitudes in the case of $E_1 = E_2 = E_3 = 1$ is approximately unity as is expected; even though the correlation function is not assumed to be isotropic, due to symmetry, the correlation lengths in x and y direction are (see (c) of fig. 2.2 for an illustration).

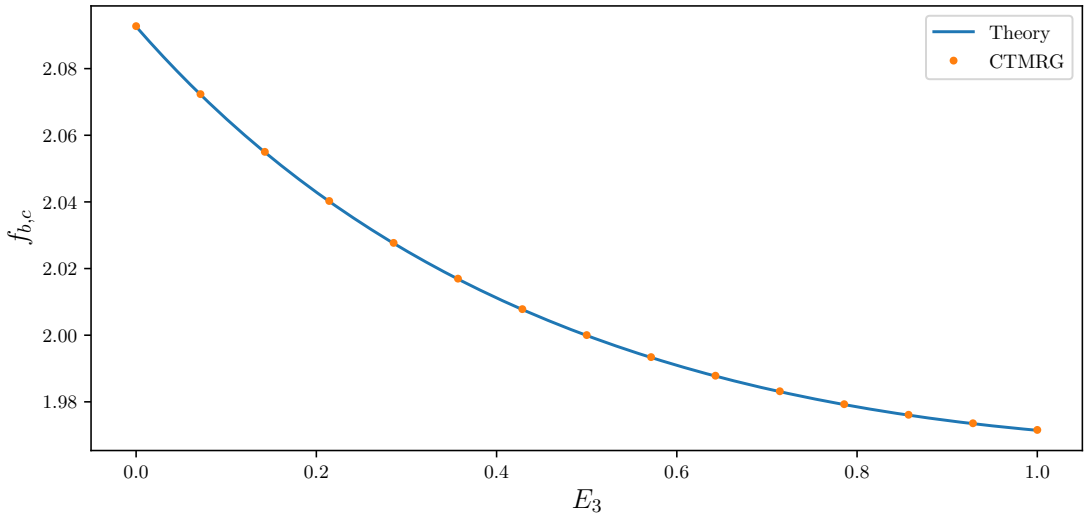

Figure 3.6: A comparison between the critical bulk free energy density $f_{b,c}^{\text{Potts}}$ with $E_1 = 1$, $E_2 = 1.5$ and $q = 3$ computed using the exact theory and CTMRG calculations.

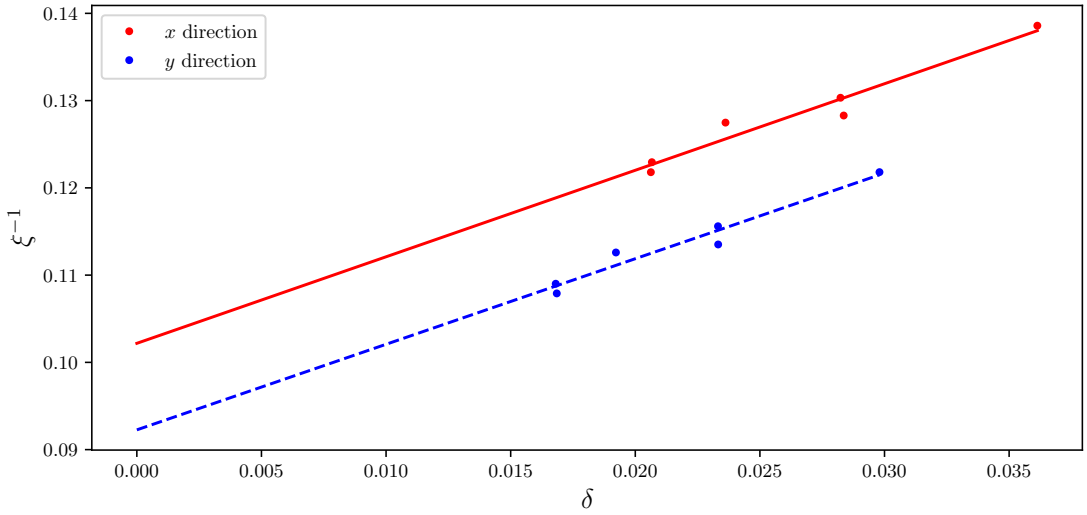

Figure 3.7: This plot shows the extrapolation of the correlation length to the thermodynamic limit with $E_1 = 1$, $E_2 = 2$, $E_3 = 3$, $q = 3$, at a reduced temperature of $t = 0.01$ and using $\delta = \epsilon_2 - \epsilon_1$. Every point belongs to a different bond dimension χ, the lines are linear fits which allow extrapolation to $\delta = 0$ which indicates a continuous spectrum expected in the bulk.

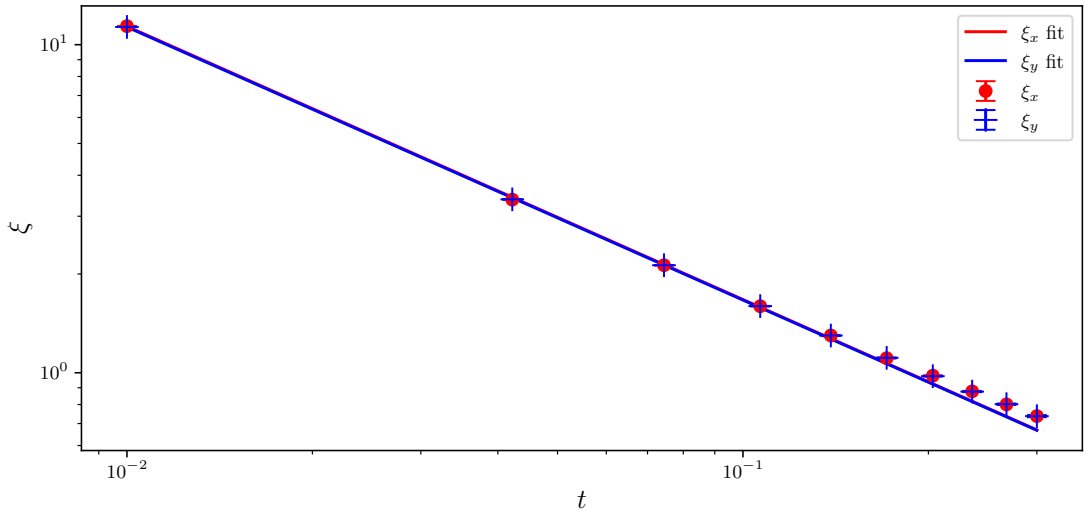

Figure 3.8: Fit of the correlation length near the critical temperature of the $q = 3$ Potts model with couplings $E_1 = E_2 = E_3 = 1$ on a log-log plot. Note the small deviations from scaling for larger temperatures.

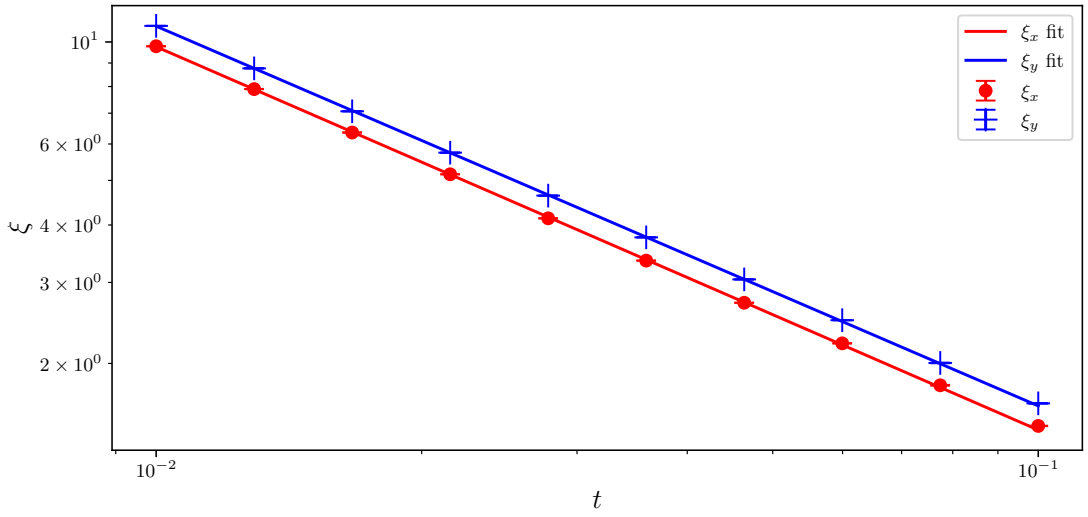

Figure 3.9: Fit of the correlation length near the critical temperature of the $q = 3$ Potts model with couplings $E_1 = 1, E_2 = 2, E_3 = 3$ on a log-log plot. The deviations for larger temperatures are smaller compared to the above plot, since the temperature range is closer to $|t| = 0$.

Furthermore, in [80, 81] the critical anisotropic $2d$ Potts model is discussed via correspondence to the random cluster model and results for the effective aspect ratio ρ_e and the boundary twist t_e are presented, with

$$\rho_e = \sin\left(\frac{\theta_3}{2}\right)\sin\left(\frac{\theta_2}{2}\right)/\sin\left(\frac{\theta_1}{2}\right) \tag{3.30}$$

$$t_e = \cos\left(\frac{\theta_3}{2}\right)\sin\left(\frac{\theta_2}{2}\right)/\sin\left(\frac{\theta_1}{2}\right) \tag{3.31}$$

and where the angles θ_i are given via the implicit equations [82]:

$$e^{\beta_c E_i} - 1 = \begin{cases} \sqrt{q}\,\dfrac{\sin(r(\pi-\theta_i))}{\sin(r\theta_i)}, & \text{if } q < 4 \\ \dfrac{2(\pi-\theta_i)}{\theta_i}, & \text{if } q = 4 \end{cases} \tag{3.32}$$

and

$$r = \frac{1}{\pi}\arccos\left(\frac{\sqrt{q}}{2}\right) \tag{3.33}$$

For $q = 2$ these quantities can be identified with the modular parameter of the Ising model $\tau = \tau_0 + i\tau_1$ with $\tau_0 \leftrightarrow t_e$ and $\tau_1 \leftrightarrow \rho_e$, since with $q = 2$ (3.32) yields

$$\theta_i = -8\arctan\left(e^{\beta_c E_i} \pm \sqrt{1 + e^{2\beta_c E_i}}\right) \tag{3.34}$$

and thus in turn

$$\rho_e = \frac{\cosh(\beta_c E_1)}{\cosh(\beta_c E_2)\cosh(\beta_c E_3)} \tag{3.35}$$

$$t_e = \frac{\cosh(\beta_c E_1)\sinh(\beta_c E_3)}{\cosh(\beta_c E_2)\cosh(\beta_c E_3)}. \tag{3.36}$$

If one now makes the identification as above, the absolute value of the modular parameter can be expressed as

$$|\tau|^2 = t_e^2 + \rho_e^2 = \frac{1 + \sinh^2(\beta_c E_1)}{1 + \sinh^2(\beta_c E_2)} \tag{3.37}$$

and the argument of τ is given by

$$\arg\tau = \operatorname{acot}(t_e/\rho_e) = \operatorname{acot}(\sinh(\beta_c E_3)). \tag{3.38}$$

Finally, note that the coupling constants between the $q = 2$ Potts model and the Ising model are related by a factor 2 and thus one can easily see that the above expressions agree with (2.159) for the Ising model. By extending this insight to other $q \leq 4$, one can take (1.30) and (2.153) to relate the modular parameter of the Potts model to the correlation ellipsis parameters $\tilde{q}$ and Ω. More precisely, one finds the system of equations for $\rho = 1$

$$t_e = -\frac{(\tilde{q} - \tilde{q}^{-1})\cos\Omega\sin\Omega}{\tilde{q}\sin^2\Omega + \tilde{q}^{-1}\cos^2\Omega} \tag{3.39}$$

$$\rho_e = \frac{1}{\tilde{q}\sin^2\Omega + \tilde{q}^{-1}\cos^2\Omega}, \tag{3.40}$$

which has to be solved numerically.

Under the assumption that multi-parameter universality holds, the asymptotic correlation function at distance $\boldsymbol{x} = (r\cos\theta, r\sin\theta)^T$ in the scaling limit should be of the form [1, 28]

$$C^{\text{Potts}}(\boldsymbol{x}) \sim \Psi_\pm\left(\frac{r}{\xi_\pm^{\text{Potts}}(t,\theta)}\right) \tag{3.41}$$

$$= \Psi_\pm\left(\frac{\left[\boldsymbol{x}\cdot(\bar{\boldsymbol{A}}^{\text{Potts}})^{-1}\boldsymbol{x}\right]^{1/2}}{\bar{\xi}_\pm^{\text{Potts}}(t)}\right) \tag{3.42}$$

where $\xi_\pm^{\text{Potts}}(t,\theta)$ is the angle dependent correlation length, $\bar{\boldsymbol{A}}^{\text{Potts}}$ the reduced anisotropy matrix and $\bar{\xi}_\pm^{\text{Potts}}(t)$ the mean correlation length of the Potts model. No explicit expressions of $\bar{\xi}_\pm^{\text{Potts}}(t)$ as functions of the couplings are known. However, the general form of the anisotropy matrix as a function of the correlation ellipsis parameters $\tilde{q}$ and Ω given in (1.30) should hold. Furthermore, the simulation provides the correlation length in x direction with $\boldsymbol{x} = (r,0)^T$ and y direction with $\boldsymbol{x} = (0,r)^T$; resulting in the prediction

$$\xi_{\pm,x}^{-1}(t) \equiv \frac{\sqrt{(\bar{\boldsymbol{A}}^{\text{Potts}})^{-1}_{1,1}}}{\bar{\xi}_\pm^{\text{Potts}}(t)} = \frac{f(\Omega,\tilde{q})}{\bar{\xi}_\pm^{\text{Potts}}(t)} \tag{3.43}$$

$$\xi_{\pm,y}^{-1}(t) \equiv \frac{\sqrt{(\bar{\boldsymbol{A}}^{\text{Potts}})^{-1}_{2,2}}}{\bar{\xi}_\pm^{\text{Potts}}(t)} = \frac{f(\pi/2-\Omega,\tilde{q})}{\bar{\xi}_\pm^{\text{Potts}}(t)} \tag{3.44}$$

where the correlation lengths in x and y directions were defined; the function f is given by [1, 28]

$$f(\theta-\Omega,\tilde{q}) = [\tilde{q}\sin^2(\theta-\Omega) + \tilde{q}^{-1}\cos^2(\theta-\Omega)]^{1/2}. \tag{3.45}$$

However, the mean correlation length is a non-universal quantity and multi-parameter universality makes no predictions in this regard. Thus only the temperature independent ratio

$$R \equiv \frac{\xi_{\pm,x}(t)}{\xi_{\pm,y}(t)} = \frac{f(\pi/2-\Omega,\tilde{q})}{f(\Omega,\tilde{q})} \tag{3.46}$$

can be compared to simulation, where theoretical predictions for $\tilde{q}$ and Ω were obtained through (3.39) and (3.40).

The results are presented in fig. 3.10 to 3.13 by showing a range of anisotropic couplings with the predicted value for the correlation length ratio. Two things are of note here: Firstly, the error bars do not account for the total error, since it is difficult to estimate the error of the transfer matrix eigenvalues, thus only the correlation length extrapolation error estimate is shown. And secondly, even though the error gets smaller the closer the temperature gets to the critical point, the simulation can not accurately take into account the strong correlation near the critical point with limited bond dimension, resulting in inaccurate values. In the fits the data for $|t| < 0.025$, indicated by the gray shaded region, was excluded. In general, however, the simulations are in good agreement with the predictions.

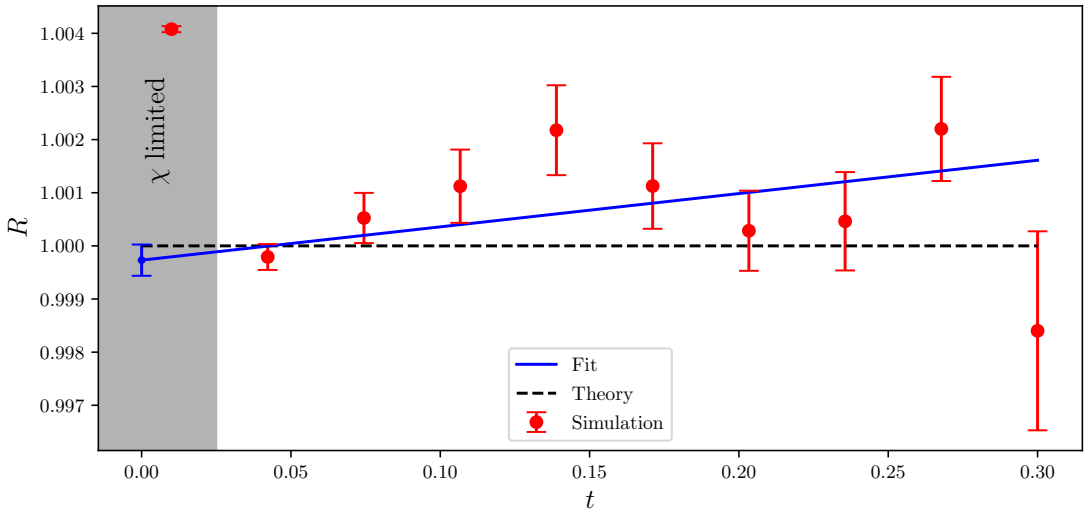

Figure 3.10: Correlation length ratio of the $q = 3$ Potts model with couplings $E_1 = E_2 = E_3 = 1$. The dashed line shows the predicted value.

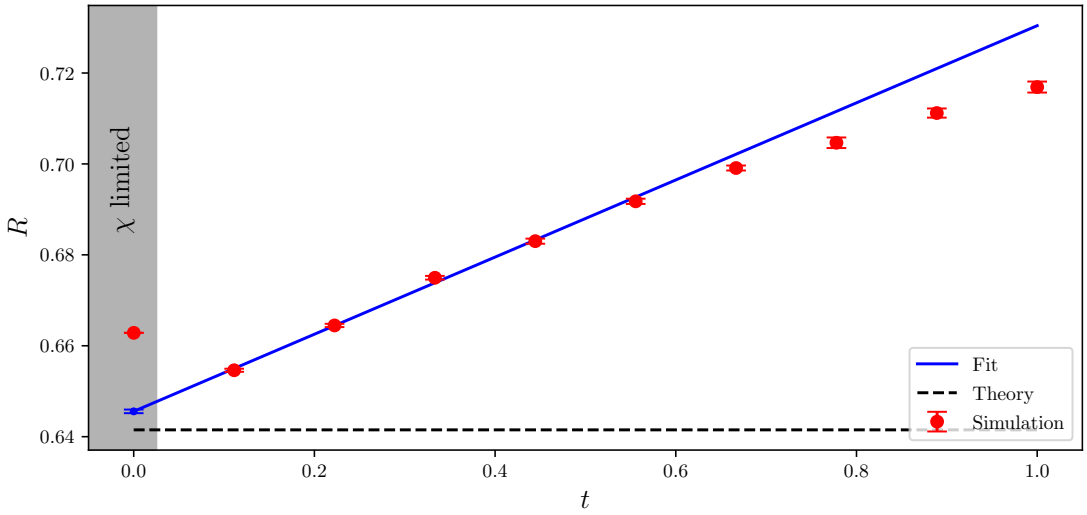

Figure 3.11: Correlation length ratio of the $q = 3$ Potts model with couplings $E_1 = 1, E_2 = 2, E_3 = 0$. The dashed line shows the predicted value. Note the large temperature range and how the simulation slowly converges towards the expected value. Additionally, the points with $|t| > 0.6$ were excluded from the fit, since they are outside of the scaling region.

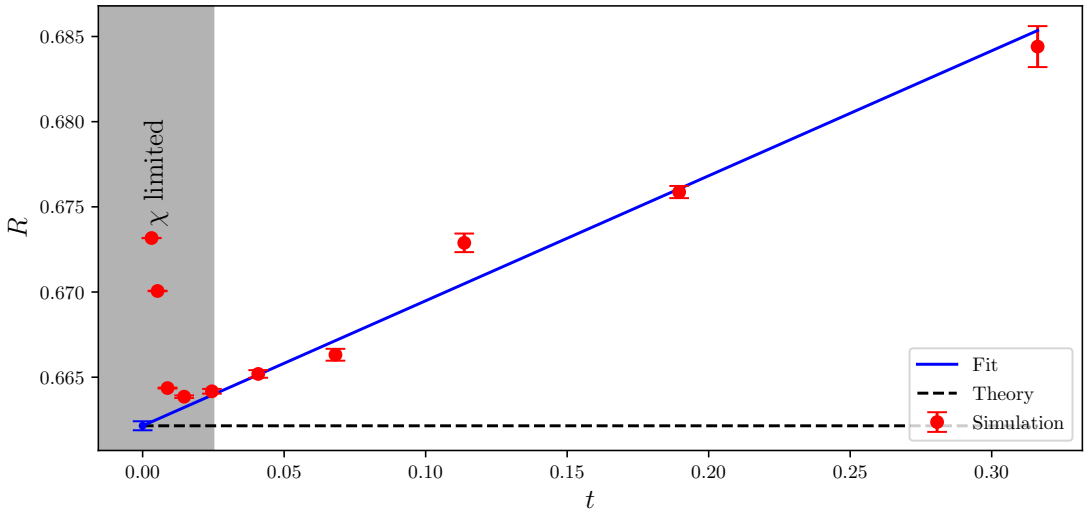

Figure 3.12: Correlation length ratio of the $q = 3$ Potts model with couplings $E_1 = 1, E_2 = 3, E_3 = 1$. The dashed line shows the predicted value. Here the temperature points are clustered closer to the critical point and the ratio converge generally towards the expected value as T_c is approached.

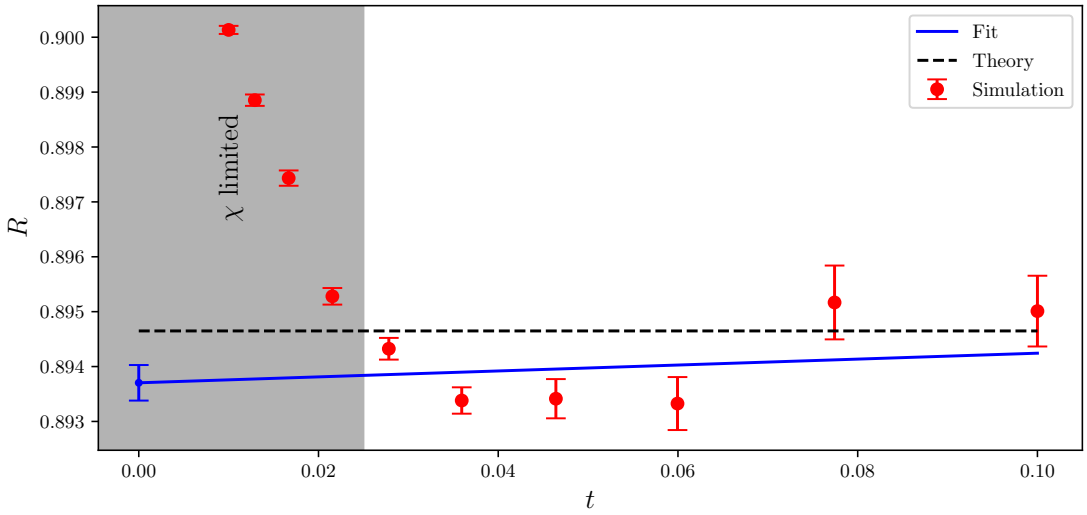

Figure 3.13: Correlation length ratio of the $q = 3$ Potts model with couplings $E_1 = 1, E_2 = 2, E_3 = 3$. The dashed line shows the predicted value. Note the much smaller temperature range and how the measurements near the critical points do not match the predictions well.

3.6 Predictions for the corner free energy

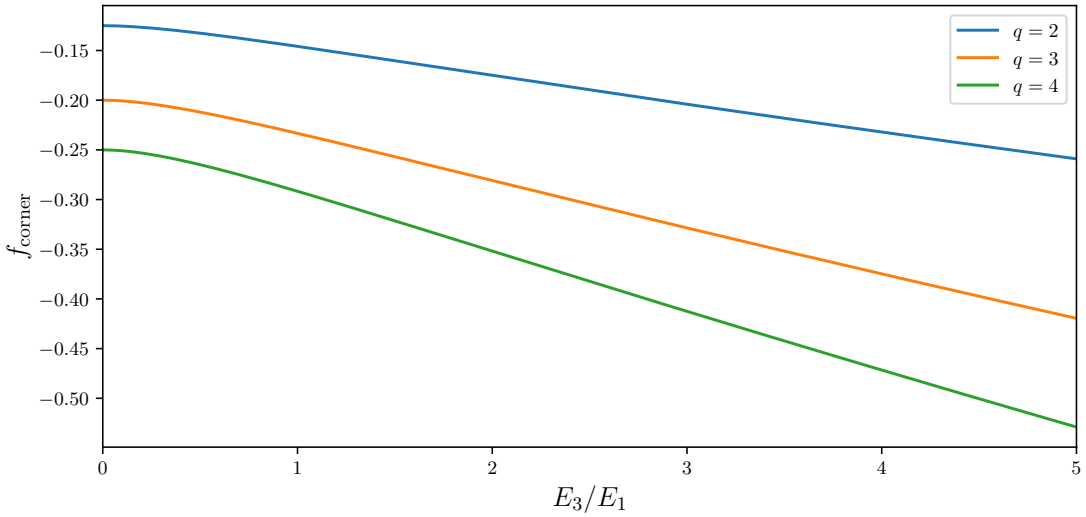

Figure 3.14: Predictions for the corner free energy f_{corner} for the critical q-state Potts model at $E_1 = E_2$.

The total free energy density, of $2d$ critical systems with open boundary conditions and linear system size L can be split into the following geometry-associated parts [83, 84]

$$f = f_{\text{bulk}} + f_{\text{surface}} \frac{1}{L} + f_{\text{corner}} \frac{\log L}{L^2} + \sum_{k=2}^{\infty} \frac{f_k}{L^k}, \tag{3.47}$$

of which only the contributions from the corners f_{corner} and the next contribution f_2 proportional to L^{-2} are thought to be universal [85, 86]. Specifically, the corner contribution has been predicted [85], in the context of conformal field theory (CFT), to be dependent on the angle α spanned by the boundaries meeting in the corner and the universal, model dependent central charge c. The contribution of one corner takes the form

$$f_{\angle} = \frac{c}{24} \left(\frac{\alpha}{\pi} - \frac{\pi}{\alpha} \right) \tag{3.48}$$

and in case of a parallelogram lattice with two corners of angle α and another two with $\pi - \alpha$ yield a total contribution to the corner term of

$$f_{\text{corner}} = -\frac{c}{12} \left(1 + \frac{\alpha}{\pi - \alpha} + \frac{\pi - \alpha}{\alpha} \right). \tag{3.49}$$

However, the limiting factor in CFT is that it requires the system to be conformal invariant which, among others, requires isotropy. But, as has been discusses in the introduction, the chapter on the Ising model and in [29], multi-parameter universality maps anisotropic systems to isotropic parallelograms, where the angle α is given via the modular parameter $\tau = \rho_p \exp(i\alpha)$, or more specifically in case of the Potts model by (3.30) and (3.31). This results in the identification of $\alpha = \theta_3/2$ with which the value of f_{corner} can be predicted. Furthermore, the central charge is given in [87] as

$$c = 1 - \frac{6}{p(p+1)} \quad \text{with} \quad q = 4\cos^2 \frac{\pi}{p+1} \tag{3.50}$$

which yields $c = 1/2, 4/5, 1$ for the cases of interest with $q = 2, 3, 4$, respectively. An examples for the predicted values are shown in fig. 3.14. Note that the corner contribution does not depend on the aspect ratio ρ_p and that the dependence of the angle α on the microscopic couplings E_i predicts the breakdown of universality. This has been shown through explicit simulation of the Ising model in [3].

3.7 Conclusions

Through the application of the CTMRG algorithm to the q-state Potts model and evaluation of the correlation lengths therein, strong evidence has been collected that the predictions made by multi-parameter universality for the dependence of the critical bulk correlation function on microscopic details, in the form of the correlation ellipsis parameters $\tilde{q}$ and Ω, hold. Furthermore, predictions were made for the corner free energy in the Potts model, which should show dependence on the microscopic details through the parallelogram angle α. This can be confirmed through additional tensor network or Monte Carlo simulations.

Chapter 4

Crossover in models with discrete and continuous variables

In this chapter the q-state clock model in $3d$ with an additional biquadratic term, a relative of the Potts model, is investigated in the limit of increasing q. More specifically, this model exhibits a first order phase transition for $q \geq 3$. At the transition temperature phase coexistence between a paramagnetic and dipole long range order (DPLRO) is observed. It was shown in [88], that the relative contribution to the statistical weight of the phases in a classical spin XXZ model with continuous degrees of freedom, which also exhibits a first order phase transition, turns out to be π. On the other hand, it is known that the Potts model, which is recovered from the model investigated here at $q = 3$, has, due to the degeneracy of the ordered phase, a relative weight q of its two phases at the transition point. Since the model under investigation here is well defined as $q \to \infty$ and thus approaches continuous degrees of freedom, it can be conjectured that the relative weight starts out with Potts like behavior (i.e. linear in q), transitions through a crossover region and, for large q, approaches a constant value of 2π. The general idea is illustrated in fig. 4.1. More details and the numerical findings of my investigation are presented in the following sections.

4.1 First order phase transitions

First-order phase transitions represent a fundamental class of collective behavior in many-body systems, characterized by abrupt changes in physical properties, such as density, magnetization, or order parameter. Unlike continuous transitions, first-order transitions do not exhibit critical slowing down or diverging correlation lengths. Instead, they are marked by a discontinuity in the first derivative of the free energy with respect to an external parameter, typically temperature or pressure. The canonical description of first-order phase transitions hinges on the concept of symmetry breaking, where the system transitions from a more symmetric phase to a less symmetric one. This process is often associated with the emergence of latent heat, indicative of the energy change associated with the transition. Mathematically, the Landau theory of phase transitions provides a framework for understanding these phenomena. The free energy density f can be expressed as a function of an order parameter ϕ [89], such that:

$$f(\phi) = f_0 + \frac{r}{2}\phi^2 + \frac{u}{4}\phi^4 - h\phi^4 + \cdots , \tag{4.1}$$

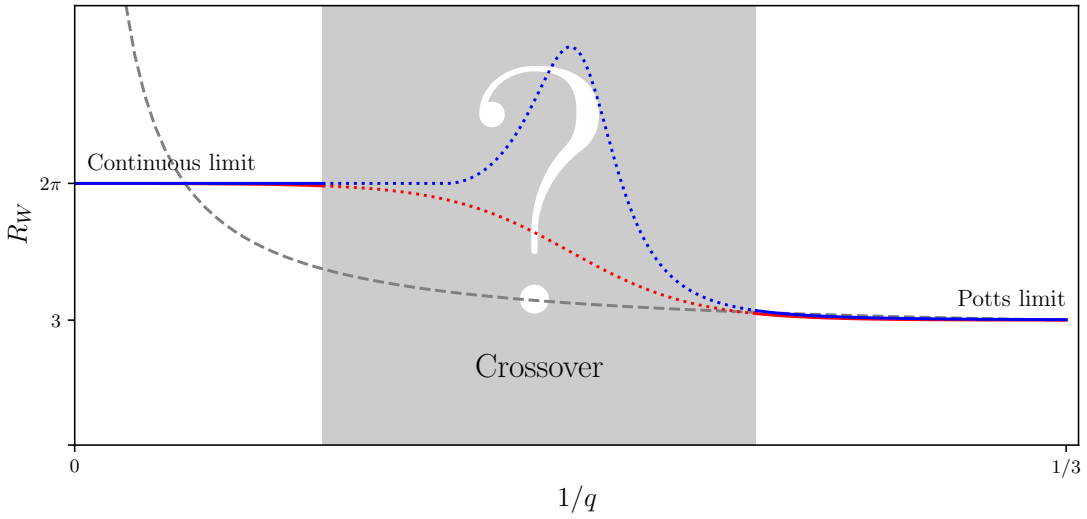

Figure 4.1: Illustration of the expected behavior as q approaches infinity. The gray dashed line shows the known behavior of the $3d$ Potts model for the relative weight R_W of the phases present at the first order transition.

where f_0 is the free energy at the reference state, and r, u are coefficients that depend on external parameters like temperature and h is an external field. For first-order transitions, the terms proportional to odd powers in ϕ become significant, leading to an asymmetric potential that facilitates the abrupt phase change. Terms proportional to ϕ can always be eliminated by a shifting the order parameter by a constant to recover the standard form, for which the first odd power is ϕ^3.

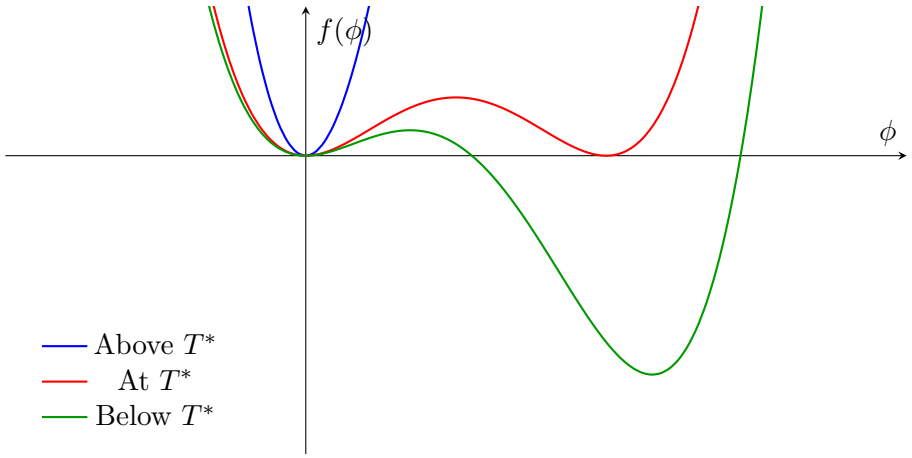

Figure 4.2: Free energy landscape of a first order transition above, at and below the transition temperature T^* as a function of the order parameter. The abrupt change in the global minimum causes the well known discontinuities and explains phenomena like latent heat.

In the thermodynamic limit, the probability distribution $p(\phi)$ is given by a delta function at the spontaneous magnetization 0 and $\pm M$ (with $h = 0$), showing phase coexistence as

the exact transition temperature is reached:

$$p(\phi) = \delta(\phi) + \delta(\phi + M) + \delta(\phi - M). \tag{4.2}$$

In the case of finite systems with linear system size L, however, it has been shown [90, 91] that the probability distribution is given by

$$p(\phi) \propto \exp[-f(\phi)L^d/(k_bT)], \tag{4.3}$$

and can be approximated near the transition point with two Guassians

$$p(\phi) \propto A_+ \exp\left[-\frac{(\phi - M - \chi h)^2}{2k_bT\chi}L^d\right] + A_- \exp\left[-\frac{(\phi + M - \chi h)^2}{2k_bT\chi}L^d\right] \tag{4.4}$$

where $\pm M = \pm\sqrt{-r/u}$ is again the spontaneous magnetization in absence of an magnetic field and $\chi = 1/(r + 3uM)$ the susceptibility. Not only is it clear that there is now a broadening of the peaks proportional to L^{-d}, but by investigating the amplitudes

$$A_\pm = \exp\left[\pm\frac{hML^d}{k_bT}\right] \tag{4.5}$$

more closely, it can be seen that the transition takes place over a range of temperatures and is no longer instantaneous. Both of these phenomena explain the general smoothing out of singular behavior observed in finite systems. Theses aspects will become important when estimating the transition temperature and analyzing the relative weights of the phases for the specific model in question.

More specifically, as has been alluded to in the introduction of this chapter, in [88] the antiferromagnetic XXZ model in $3d$ with the Hamiltonian

$$H^{\mathrm{XXZ}} = J\sum_{\langle i,j\rangle}[\Delta(S_{i,x}S_{j,x} + S_{i,y}S_{j,y}) + S_{i,z}S_{j,z}] - h\sum_i S_{i,z} \tag{4.6}$$

and classical spins $\boldsymbol{S}_i = (S_{i,x}, S_{i,y}, S_{i,z})^T$ has been studied. It exhibits a rich phase diagram, but has here been specifically chosen for its first order phase transition between a low field antiferromagnetic (AFM) phase, where the spins are aligned anti-parallel, and a spin-flop (SF) phase, in which the spins are tilted with continuous rotational symmetry. The SF phase is described by the vector $\boldsymbol{\Psi} = (\Psi_x, \Psi_y)^T$ with

$$\Psi_\alpha = \frac{1}{L^3}\left(\sum_{i\in 1} S_{i,\alpha} - \sum_{i\in 2} S_{i,\alpha}\right), \quad \alpha = (x, y) \tag{4.7}$$

where 1 and 2 refer to the two interpenetrating sublattices of the simple cubic main lattice, from which the relevant order parameter in the thermodynamic limit follows as:

$$\Psi_\infty = \sqrt{\langle\Psi_x^2 + \Psi_y^2\rangle_{T,L\to\infty}} \tag{4.8}$$

Here the $\langle\cdots\rangle$ refer to the thermal average. With the above, it was then shown that at the first order transition point the probability density in the thermodynamic limit is given by:

$$p(|\boldsymbol{\Psi}|) = 2\delta(|\boldsymbol{\Psi}|) + 2\pi\delta(|\boldsymbol{\Psi}| - \Psi_\infty) \tag{4.9}$$

Here the factor 2 in front of the first delta function arises, similarly to (4.2), because the magnetization, which was not discussed in this summary, can take two values $\pm M$ but

was already integrated out. However, the factor 2π in front of the right terms shows up because the probability distribution only depends on the absolute value of $\boldsymbol{\Psi}$, not on its angular part; and since $\boldsymbol{\Psi}$ is a $2d$ vector, integrating yields 2π and thus the relative weight of the two phases is $2\pi/2 = \pi$.

A similar observation can be made for the q-state Potts model [79, 88] with Hamiltonian

$$H^{\text{Potts}} = -J \sum_{\langle i,j \rangle} \delta(s_i - s_j) \tag{4.10}$$

where $J > 0$, $s_i = 0, 1, \ldots, q-1$ and the order parameter $\boldsymbol{m} = (m_0, m_1, \ldots, m_{q-1})^T$ with

$$m_i = \frac{1}{L^3} \frac{q}{1-q} \sum_j \delta(s_j - i) - \frac{1}{q}. \tag{4.11}$$

Here the probability distribution at the transition temperature consists of one disordered and q ordered phases with $\boldsymbol{m}_i = (0, \ldots, m_i, \ldots, 0)^T$; resulting in

$$p(\boldsymbol{m}) = \delta(\boldsymbol{m}) + \sum_{i=0}^{q-1} \delta(\boldsymbol{m} - \boldsymbol{m}_i) \tag{4.12}$$

and hence a relative weight of q. In the next chapter, a model will be introduced that has as one of its limits the 3-state Potts model, but, unlike the Potts model, is well defined as the number of possible states, q, is increased until truly continuous degrees of freedom are reached. Additionally, this model has a first order transition for all q and thus makes it possible to test the hypothesis if and how the crossover from a relative weight of q to 2π happens.

4.2 Clock model with biquadratic term

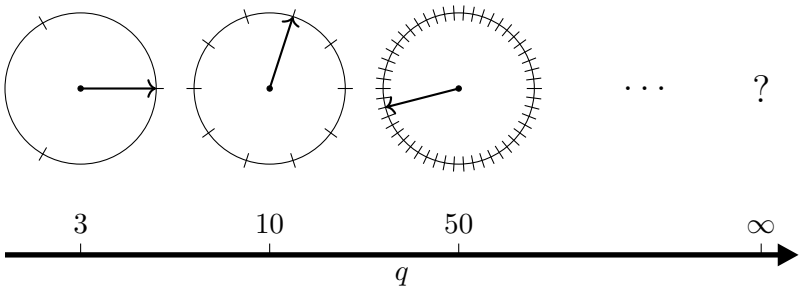

Figure 4.3: Illustration of the crossover process in the q-state clock model.

In [92] an XY-model in $3d$ with an additional biquadratic term was studied. The Hamiltonian is given by

$$H^{\text{clock}} = -J \sum_{\langle i,j \rangle} \boldsymbol{S}_i \cdot \boldsymbol{S}_j - J' \sum_{\langle i,j \rangle} (\boldsymbol{S}_i \cdot \boldsymbol{S}_j)^2, \tag{4.13}$$

where $\boldsymbol{S}_i = (S_{i,x}, S_{i,y})^T$ is a vector at lattice site i with the additional condition $|\boldsymbol{S}_i| = 1$; $\langle i, j \rangle$ denotes the sum over nearest neighbors and the couplings J, J' are non-negative. It

was found that there is first order phase transition for $0.35 < J/J' < 0.55$ between a high temperature paramagnetic (PM) and a low temperature dipole long-range ordered phase (DLRO), for $J/J' > 0.55$ the paper concludes a continuous phase transition between the same phases; however, it is possible that this actually is a weakly first order transition. In the regime $J/J' < 0.35$ the system goes from the DLRO first into a quadrupole long-range ordered phase (QLRO) before, at high temperatures, ending up in the PM phase. The order parameters of these phases are

$$M = \left[\left(\sum_i S_{i,x} \right)^2 + \left(\sum_i S_{i,y} \right)^2 \right]^{1/2} \tag{4.14}$$

$$Q = \left[\left(\sum_i \left((S_{i,x})^2 - (S_{i,y})^2 \right) \right)^2 + \left(\sum_i 2 S_{i,x} S_{i,y} \right)^2 \right]^{1/2} \tag{4.15}$$

Since in this work only the region of $0.35 < J/J' < 0.55$ is of interest, the QLRO phase will not be discussed further. As explained in the introduction, the problem of interest is the crossover from discrete to continuous variables; to this end, the above Hamiltonian is modified by changing the degrees of freedom to

$$\boldsymbol{S}_i = \begin{pmatrix} \cos(2\pi n/q) \\ \sin(2\pi n/q) \end{pmatrix} \tag{4.16}$$

where $n = 0, 1, \ldots, q-1$ and the original model is recovered at $q \to \infty$. On the other hand, in the case of $q = 3$ one finds that

$$\boldsymbol{S}_i \cdot \boldsymbol{S}_j = \cos\left[\frac{2\pi}{3} (n_i - n_j) \right] = \begin{cases} 1 & \text{if } |n_i - n_j| = 0 \\ -1/2 & \text{if } |n_i - n_j| = 1 \\ -1/2 & \text{if } |n_i - n_j| = 2 \end{cases} \tag{4.17}$$

Using this, (4.13) can be rewritten, up to an irrelevant additive constant, as

$$\begin{aligned} H_{q=3}^{\text{clock}} = & \\ & - \frac{3(J-J')}{2} \sum_{\langle i,j \rangle} \frac{2}{3} \left(\cos\left[\frac{2\pi}{3} (n_i - n_j) \right] + \frac{1}{2} \right) - \frac{9J'}{4} \sum_{\langle i,j \rangle} \frac{4}{9} \left(\cos\left[\frac{2\pi}{3} (n_i - n_j) \right] + \frac{1}{2} \right)^2 \\ = & - \frac{3}{4} \left(2J + J' \right) \sum_{\langle i,j \rangle} \delta(n_i - n_j) \end{aligned} \tag{4.18}$$

where $\delta(n)$ is the delta function which is equal one if $n = 0$ and zero otherwise; the additional J' in the left term is necessary to balance out the addition of the $+1/2$-term in the right sum under the square. After the above manipulations it is clear, that for $q = 3$ the $3d$, 3-state Potts model can be recovered from the discretized Hamiltonian (4.13), which has been shown to exhibit a first order transition [79, 93, 94].

What would one predict for the relative weight of the ordered and disordered phases in this model as $q \to \infty$? First, since this is a temperature driven transitions, as opposed to the field driven transition in the XXZ model, there is only one disordered phase where all the vectors point in random directions; second, since the order parameter is the absolute value of the magnetization (4.14), but the state is characterized by the aligned, but freely rotating $2d$ vectors, the angular part should, similarly to (4.9) be integrated out, resulting in a relative weight of 2π.

4.3 Estimating the transition point

When simulating physical systems, accurately determining the transition temperature, T^*, of first-order phase transitions is a crucial first step to gain access to the properties of interest. Traditional methods for estimating T^* from finite-size systems with volume V and at inverse temperature $\beta = 1/(k_b T)$ involve analyzing observables like the specific heat, C, or the Binder cumulant [90, 91, 95]

$$B(V,\beta) = 1 - \frac{\langle E^4 \rangle}{3\langle E^2 \rangle^2}, \tag{4.19}$$

which exhibit significant shifts and scaling behaviors due to finite-size effects. These methods necessitate extrapolations to infinite volume, leveraging the assumption of power-law finite-size scaling, a process that introduces potential inaccuracies.

A different approach, as described in [96, 97], circumvents the reliance on power-law finite-size scaling by introducing new observables that directly target the exponential corrections to finite-size scaling, which are intrinsic to first-order phase transitions. This method hinges on the analysis of the partition function's behavior and its derivatives, offering a more accurate and theoretically robust means of locating T^*.

The advantage of the above method lies in its foundational principle: instead of observing traditional metrics that require correctional scaling, it utilizes observables derived from the general form of partition functions that describe systems with q coexisting ordered phases and one disordered phase, which can be shown to be of the form [98, 99]

$$Z(V,\beta) = \left[\sum_{m=0}^{q} \exp\left(-\beta f_m(\beta) V\right)\right] \left[1 + \mathcal{O}(V e^{-L/L_0})\right], \tag{4.20}$$

where L_0 is some finite constant, $V = L^d$ the total system volume and $f_m(\beta)$ the metastable free energy density of phase m, which can be identified with the bulk free energy density $f_b(\beta)$ if m is a stable phase; and $f_m(\beta) > f_b(\beta)$ if m is unstable. Additionally, since in the thermodynamic limit and at the transition point, all free energies f_m are equal [100], the expression

$$N(\beta) = \lim_{V\to\infty} Z(V,\beta) e^{\beta f_b(\beta) V} \tag{4.21}$$

counts the number of stable phases $N(\beta^*) = q + 1$ apart from exponentially small corrections. It is thus a natural choice to select the temperature where the relative weight of the ordered and disordered phases approaches q as the transition point. As discussed further above, one observes a two peak structure in the energy or magnetization probability distributions $p(\beta, E)$, where each peak belongs to one of the two states. By comparing the areas, one can define the ratio of weights:

$$R(V,\beta) = \frac{\sum_{E<E_0} p(\beta,E)}{\sum_{E\geq E_0} p(\beta,E)} \equiv \frac{W_o}{W_d} \overset{\beta\to\beta^*}{=} q \tag{4.22}$$

Here E_0 is the energy that divides the two regions and is chosen as the minimum between the peaks, when both are of equal height. See fig. 4.4 for an illustration. However, if the number of ordered states q is not known a priori, the crossing point of the ratios at two different system sizes V_1 and V_2 can be used to estimate the transition point

$$R(V_1,\beta^*) = R(V_2,\beta^*), \tag{4.23}$$

since the number of phases is independent of system size.

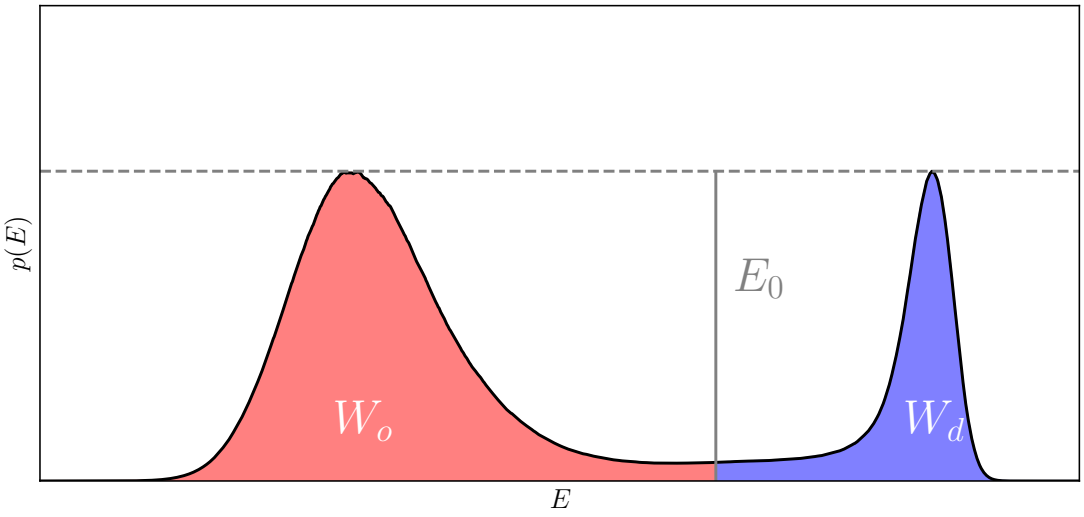

Figure 4.4: Energy histogram near a first order phase transition. The red and blue shaded areas indicate the contribution of the ordered (W_o) and disordered (W_d) states to the total statistical weight. E_0 is the energy that divides the two regions at the minimum between the peaks.

4.4 The Wang-Landau algorithm

The Wang-Landau Monte Carlo algorithm [101–103] is a powerful computational method designed to efficiently sample the energy landscape of statistical systems. Unlike traditional Monte Carlo methods that sample states according to their Boltzmann weight, the Wang-Landau algorithm aims to achieve a flat histogram in energy space, thus ensuring a uniform sampling of all energy levels. This technique is particularly useful for systems with rugged energy landscapes, such as near first order transitions, where conventional methods tend to get trapped in local minima.

In a quite general setup of a classical statistical system, with degrees of freedom ϕ and energies $E(\phi)$ at inverse temperature $\beta = 1/(k_b T)$, the partition function is given by:

$$Z = \sum_{\{\phi_i\}} e^{-\beta E(\phi_i)} = \sum_E g(E) e^{-\beta E} \tag{4.24}$$

Here, the first sum goes over all possible configurations of ϕ_i, whereas the second sum considers the energies only; to account for degeneracies, the density of states (DOS) $g(E)$, which counts the numbers of state associated with energy E, is introduced. The general idea of the algorithm is now to start from a uniform DOS and keep track of how often an energy has been visited through a histogram; every time an energy is reached, the associated DOS is increased by a factor $f > 1$, however, the probability of choosing a configuration with a larger DOS than the current one in the next step is lower. This causes the algorithm to prescribe a random walk through the energy landscape, biased towards configurations with smaller density of states. Once the histogram is flat enough, i.e., all energies have been sampled roughly equally well, the histogram is reset, f is decreased, but importantly, $g(E)$ is kept; this process is repeated until f is close to unity. More precisely, the Wang-Landau algorithm can be encapsulated in the following steps:

(1) Initialize the density of states $g(E)$, typically starting with $g(E) = 1$ for all accessible energy levels E and the set energy histogram $H(E)$ to zero.

(2) Choose an initial configuration of the system randomly or based on a specific criterion.

(3) Perform a Monte Carlo move (e.g., spin flip in the Ising model) to obtain a new configuration with energy E'.

(4) Accept the new configuration with probability

$$p(E \to E') = \min\left\{1, \frac{g(E)}{g(E')}\right\}, \tag{4.25}$$

where $g(E)$ and $g(E')$ are the DOS at the old and new energies, respectively.

(5) Update the DOS and the histogram: $g(E') \to g(E')f$, $H(E') \to H(E') + 1$, where $f > 1$ is the modification factor.

(6) Check the flatness of the histogram $H(E)$. If it is sufficiently flat, reduce the modification factor f (e.g., $f \to \sqrt{f}$) and reset the histogram.

(7) Repeat steps (3)-(6) until the modification factor f reaches a predefined threshold, e.g. $f \approx 1 + \exp(10^{-8})$, indicating convergence.

The criterion for histogram flatness is typically defined as the condition where the minimum number of entries in $H(E)$ for any energy level is not less than a certain percentage (e.g. 80%) of the average histogram height. This criterion ensures that all energy levels are sampled with roughly equal probability. Additionally, it should be noted, that the Wang-Landau algorithm does not fulfill detailed balance, since the acceptance probability is updated on the fly; however, once $f = 1$ is reached, detailed balance is restored. Moreover, to initialize the DOS and histogram, the exact energy states of the system have to be known a priori or, in the case of continuous variables, can be replaced by energy bins. If only a subset of the total energy spectrum is of interest, the sampling can be constraint by rejecting moves to states below or above an energy threshold.

After a successful run, one is left with the final density of states $g(E)$, which can also bs interpreted as the unnormalized probability density at $\beta = 0$, hence

$$p_{\beta=0}(E) = \frac{g(E)}{\sum_E g(E)}. \tag{4.26}$$

However, through the process of reweighing, the probability density at any temperature can be recovered by simply multiplying by the desired Boltzmann factor:

$$p_\beta(E) = \frac{g(E)e^{-\beta E}}{\sum_E g(E)e^{-\beta E}} \tag{4.27}$$

For the specific problem at hand, the Wang-Landau algorithm is a good choice, because a normal Monte-Carlo method, that tries to sample mostly configurations with large probability, would get stuck in one of the peaks near or at a first order transition, since moving between the two requires it to take multiple low probability steps. Again see e.g. fig. 4.4 for a visualization of the bimodal nature. This problem is exacerbate since (4.4) implies that as the system gets large, the peaks get narrower and the valley between them deeper, making sampling with more typical methods very challenging.

Finally, some technical remarks: It can be useful to not work with the density of states $g(E)$ directly, but rather with its logarithm, since continually multiply by even a small

number can lead to numerical issues. The algorithm can be parallelized by dividing the energy spectrum into overlapping regions, where the overlap is used to match the different parts after completion; alternatively, multiple simultaneous random walkers can work with the same histogram an DOS, accelerating the process.

4.5 Simulation results

The procedure to obtain the relative weight of the ordered and disordered phases and observe the crossover is as follows:

(1) Simulate model (4.13) using the Wang-Landau algorithm for a range of lattice sizes at $J/J' = 0.4$ and fixed q.

(2) Use the method from section 4.3 to estimate the transition temperature T^* by finding all the crossing point $R(L^3, \beta^*) = R((L')^3, \beta^*)$ with $L' > L$ and extrapolate to the thermodynamic limit. The error of $\beta^*(L)$ can be estimated by taking the mean and standard deviation of all crossings that had L as a partner.

(3) Compare the areas under the simulated probability density at β^* belonging to the different phases to determine their relative weight.

In figure 4.6 the histograms obtained for $q = 3$ (Potts model) and $q = 50000$ (close to continuous limit) are shown at equal height, i.e. where the temperature was tuned until both peaks are of the same height. Both figures show the expected features, like the peaks becoming more and more pronounced for larger system sizes and the large weight (area under the graph) of the low temperature ordered phase.

Using the weight ratio of the ordered to the disordered phases, shown in fig. 4.7, the transition temperature β^* can be determined by first finding the crossing points of system sizes L with L' ($L' > L$) and extrapolating to the thermodynamic limit as shown in fig. 4.8 for $q = 3$ and fig. 4.9 for $q = 3000$. Additionally, the criterion of equal heights [104, 105] to estimate the transition temperature is shown, where the temperature at which the peaks of the ordered and disordered phases have the same height for different system sizes is extrapolated to the thermodynamic limit. However, it has been shown in [104], that estimators which take the weight of the phases, instead of the peak height, into account, are superior. Ultimately, this method allows the transition temperature to be estimated to high accuracy of typically $\Delta\beta^*/\beta^* \approx 10^{-5}$; exact values can be seen in table 4.1. Histograms at the bulk transition temperature are shown in fig. 4.10.

q	β^*	$\Delta\beta^*$
3	0.1631222	0.0000025
6	0.2701395	0.0000018
300	0.3097117	0.0000088
3000	0.3096794	0.0000111
50000	0.3096792	0.0000114

Table 4.1: The extrapolated transition temperatures β^* and errors $\Delta\beta^*$ for the q under consideration.

Fig. 4.11 shows the final relative weight of the phases for a range of q and plotted as a function of $1/L^3$; for small L, the errors are well behaved, however, as the systems get

larger, the error increases rapidly. The reasons for this are two fold: As can be seen from fig. 4.12, even though the typical error of the estimated β^* is small, for large system sizes the distributions are very sensitive to temperature. Furthermore, the crossings in fig. 4.7 get steeper for larger L and, even though the corrections to the estimator are exponentially small, make it difficult to estimate the transition temperature near the thermodynamic limit. However, based on the above observations, it is possible to make at least a very basic estimate for the relative weight of the phases by only examining the smaller system sizes $L \leq 15$ of the nearly continuous system ($q = 50000$), shown in fig. 4.5, which leads to

$$\lim_{q\to\infty} \lim_{L\to\infty} R(L^3, \beta^*) \equiv R_\infty = 6.3383 \pm 0.2289 \tag{4.28}$$

or alternatively $R_\infty/(2\pi) = 1.0(1)$.

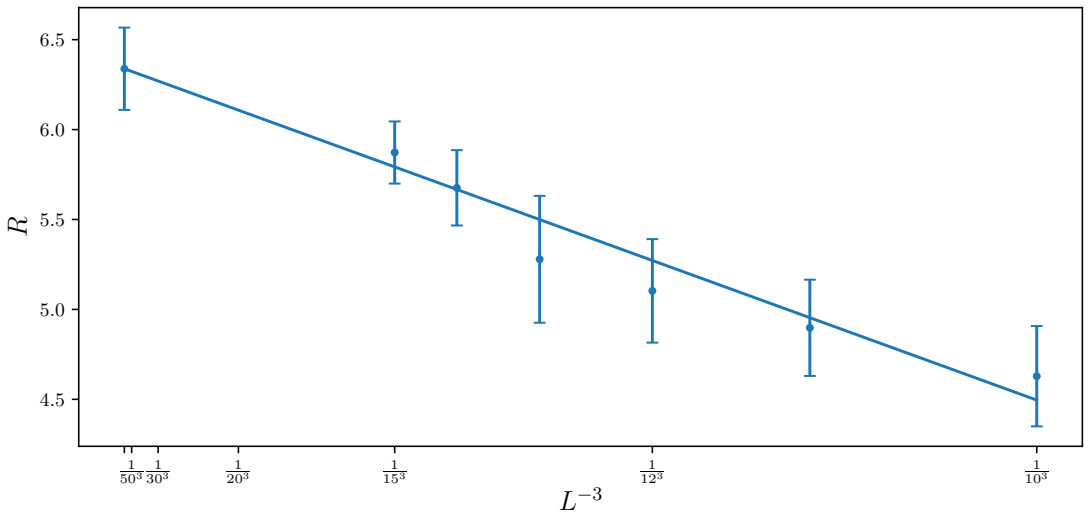

Figure 4.5: Extrapolation of the relative weight of phases for $q = 50000$ from small system sizes only. The final error bar at $L^{-3} = 0$ shows the fit uncertainty in the thermodynamic limit.

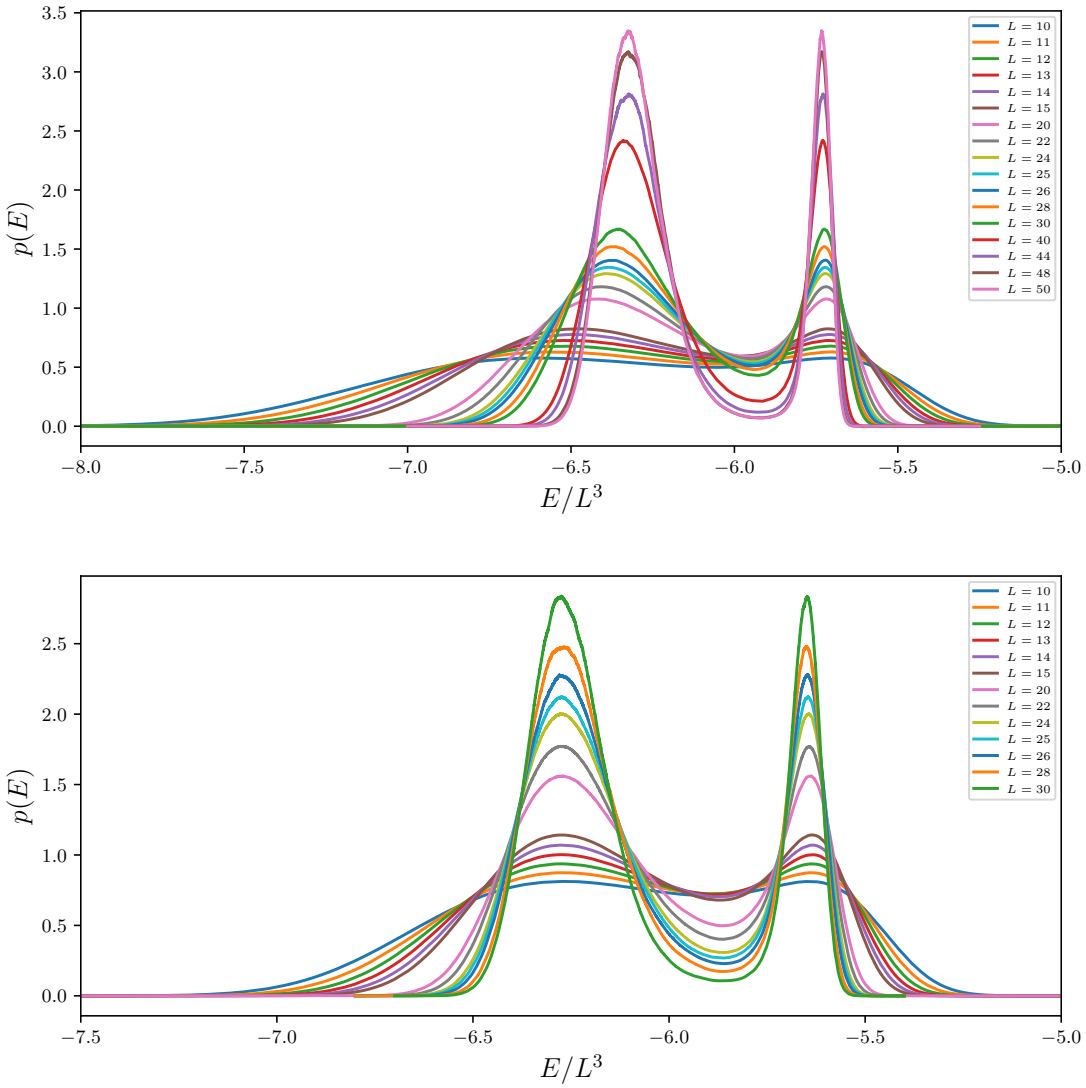

Figure 4.6: The energy histograms obtained by simulating the model (4.13) with $J/J' = 0.4$ using the Wang-Landau algorithm. As an examples the Potts model case with $q = 3$ (top) and the (nearly) continuous case with $q = 50000$ (bottom) are shown. System sizes of $L = 10, \ldots, 50$ are shown in the first case, $L = 10, \ldots, 30$ in the second case; the narrowing of the peak width and deepening of the valley between them is visible, as predicted by theory.

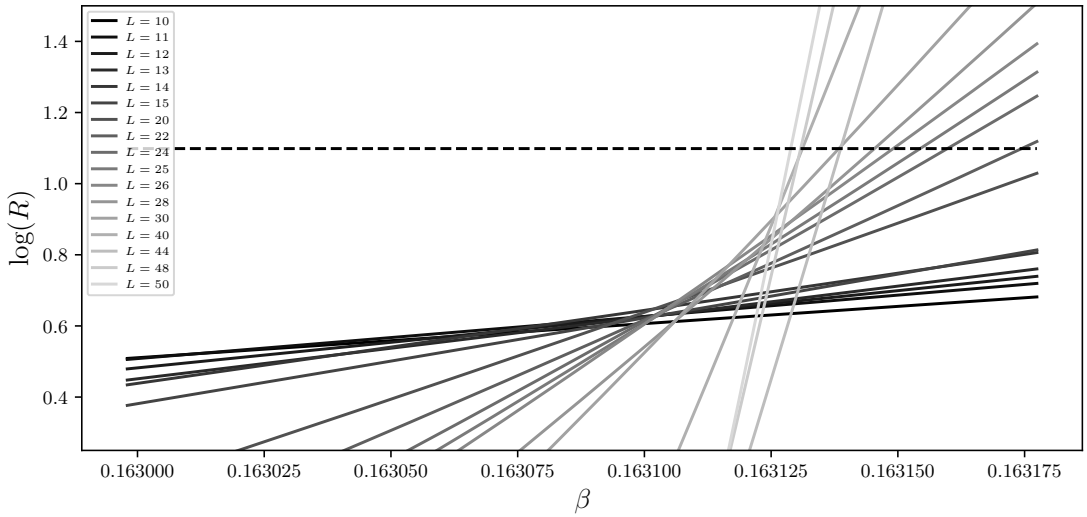

Figure 4.7: The crossings of the relative phase weights are shown for $q = 3$ and different system sizes. The fact that the number of coexisting phases is independent of L causes the lines to cross very close to each other; note the scale of the x-axis. The dashed line shows the result predicted by theory for the Potts model $\log q = \log 3$.

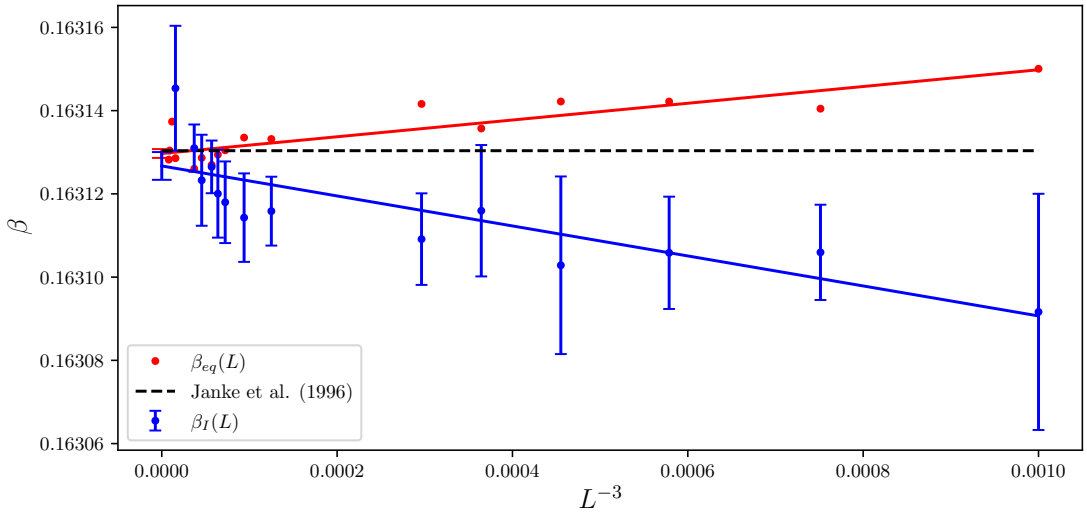

Figure 4.8: The crossing points extracted from the number of phases criterion for L and $L' > L$ (blue) and the equal height estimator (red). The solid lines show the least square fit of the data with the error bar at $L^{-3} = 0$ showing the error estimate for the thermodynamic limit. Data shown here is for the $q = 3$ Potts like model with the dashed line the predictions for β^* from [96].

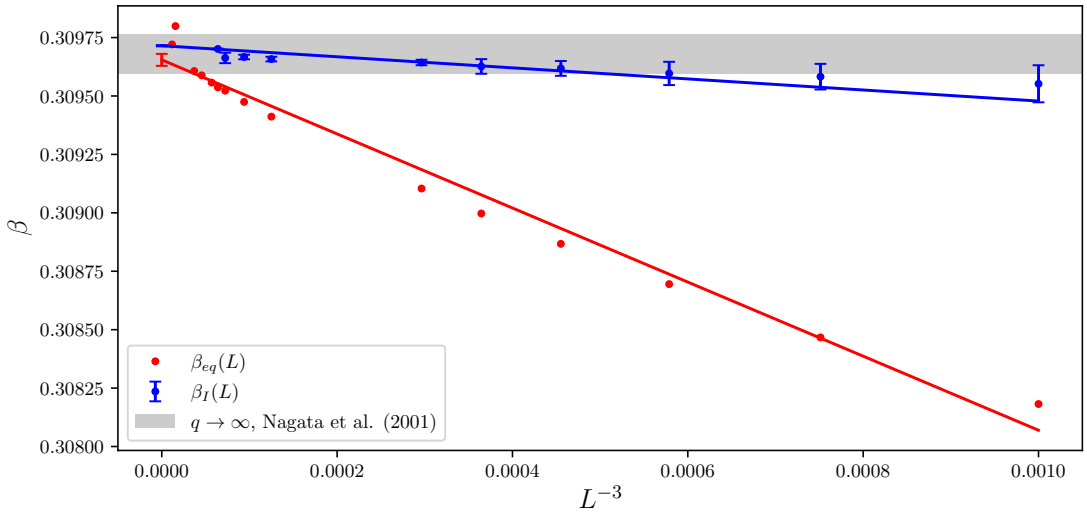

Figure 4.9: Similar to fig. 4.8 the crossing points were extracted from the number of phases criterion for L and $L' > L$ (blue) and the equal height estimator (red). The solid lines show the least square fit of the data with the error bar at $L^{-3} = 0$ showing the error estimate for the thermodynamic limit. Data shown here is for the $q = 3000$ model with the gray shaded area the prediction range for β^* from [92].

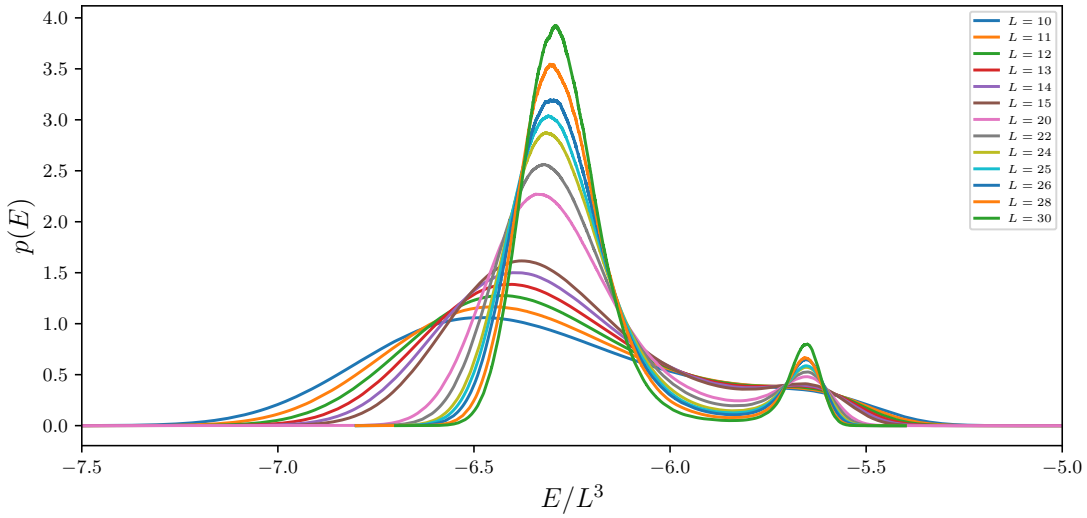

Figure 4.10: The energy histograms of the (nearly) continuous model with $q = 50000$ but now, instead of equal height, all system sizes are shown tuned to the transition temperature β^*.

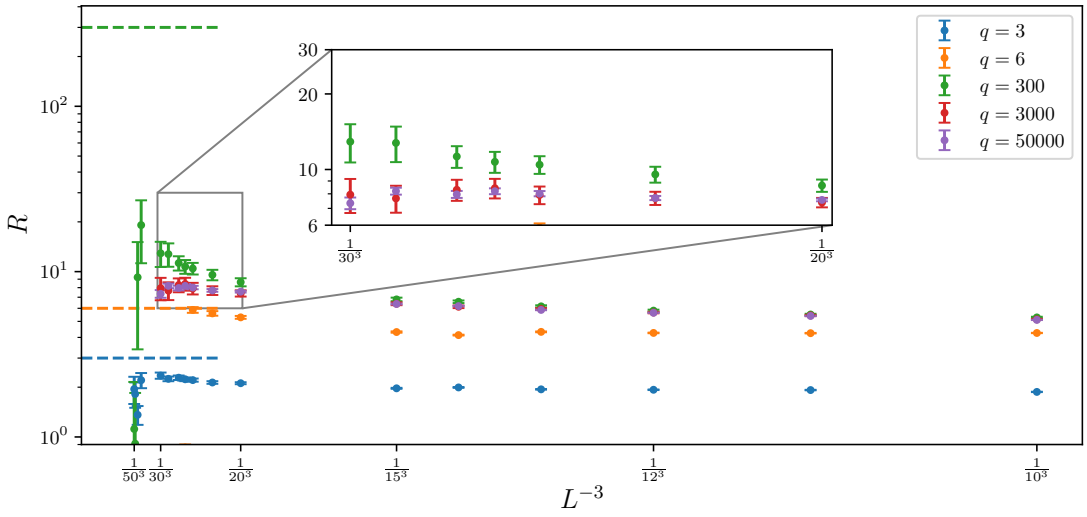

Figure 4.11: The ratio of phases at β^* shown for a range of q and as a function of $1/L^3$. The dashed lines to the left show the Potts theoretical result i.e. $R = q$, however this is only truly accurate for the model discussed here at $q = 3$. The error bars follow from the propagated error on the transition temperature β^*.

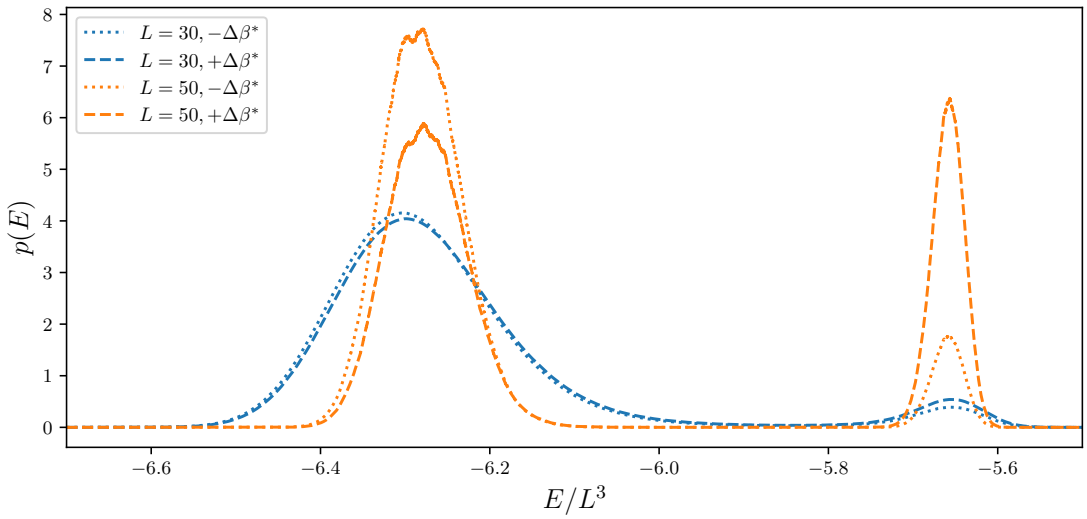

Figure 4.12: Shown are simulations of the system with $L = 30$ and $L = 50$ for $q = 50000$, but with the transition temperature shifted up or down by the estimated error on β^*. In the case of the smaller system, the change is visible but not too extreme, however, in the case of $L = 50$, the uncertainty of the transition temperature has a real impact on the measured phase weights.

4.6 Conclusions

Even though the results seem to be in agreement with the predictions, it was necessary to limit the system sizes used in the final extrapolation. It would have been preferred if all data points could have been included, however, the large sensitivity to the transition temperature would require prohibitively more computation time. In conclusion, a tentative confirmation of the initial hypothesis was obtained; in the future, a more precise estimation of the transition temperature could be able to shed more light on the case of $q \to \infty$ as well as probe the crossover region itself more carefully. Alternatively, it is possible that there is a different kind of crossover effect present, where the limits $L \to \infty$ and $q \to \infty$ do not commute, as opposed to what is shown in fig. 4.1. More specifically,

$$\lim_{L\to\infty}\lim_{q\to\infty} R = 2\pi \quad \text{or} \quad \lim_{q\to\infty}\lim_{L\to\infty} R = \infty, \tag{4.29}$$

however, this kind of behavior might be difficult to probe using numerical methods. The general idea is shown in the figure below, where there is a region of intermediate L with expected weight of $R = 2\pi$ for continuous degrees of freedom, which is replaced by divergent behavior as the thermodynamic limit is approached.

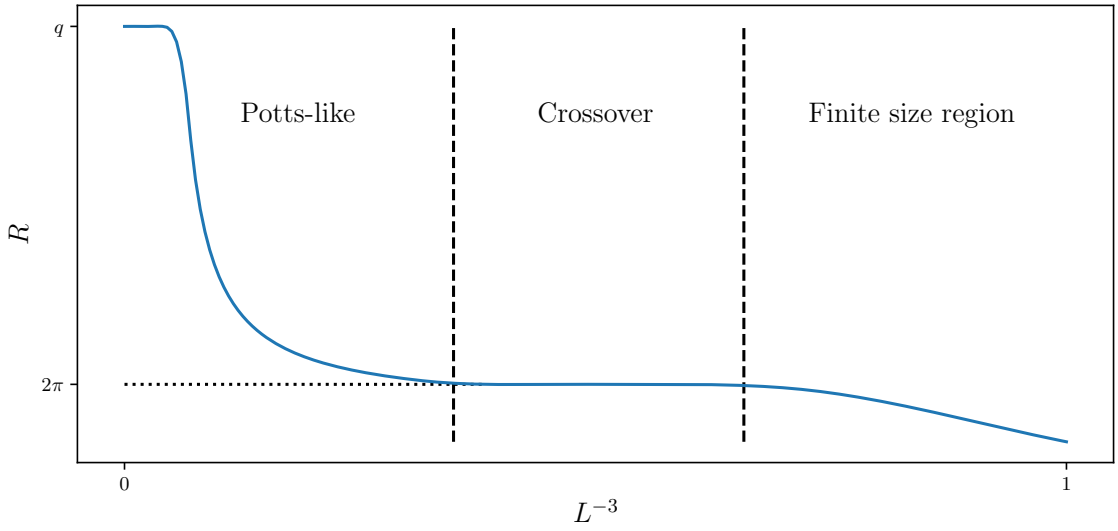

Figure 4.13: Possible alternative crossover effect that could explain the observed behavior.

Publications

[1] V. Dohm, F. Kischel, and S. Wessel, "Multiparameter universality of exact self-similar finite-size scaling functions at and away from criticality of anisotropic systems", in preparation (2024).

[2] F. Kischel and S. Wessel, "Critical Phenomena and Universality in the Ising Model: Insights from Anisotropic Lattice Configurations and Finite-Size Effects", in preparation (2024).

[3] F. Kischel and S. Wessel, "Quantifying nonuniversal corner free-energy contributions in weakly anisotropic two-dimensional critical systems", Phys. Rev. E **110**, 024106 (2024).

Bibliography

[4] J. D. Van der Waals, *Over de Continuiteit van den Gas - en Vloeistoftoestand*, Vol. 1 (Sijthoff, 1873).

[5] L. D. Landau, "On the theory of phase transitions", Zh. Eksp. Teor. Fiz. **7**, edited by D. ter Haar, 19–32 (1937).

[6] K. Mosofuji, K. Fujii, M. Uematsu, K. Watanabe, H. J. Hanley, and A. Cezairliyan, "Precise measurements of critical parameters of sulfur hexafluoride by laser interferometry", International Journal of Thermophysics (1986).

[7] L. de Jongh and A. Miedema, "Experiments on simple magnetic model systems", Advances in Physics **23**, 1–260 (1974).

[8] N. Goldenfeld, *Lectures On Phase Transitions And The Renormalization Group* (Basic Books, 1992).

[9] B. Widom, "Equation of State in the Neighborhood of the Critical Point", The Journal of Chemical Physics **43**, 3898–3905 (1965).

[10] J. J. Rehr and N. D. Mermin, "Revised Scaling Equation of State at the Liquid-Vapor Critical Point", Physical Review A **8**, 472–480 (1973).

[11] L. P. Kadanoff, "Scaling laws for Ising models near T_c", Physics Physique Fizika **2**, 263 (1966).

[12] L. P. Kadanoff, W. Götze, D. Hamblen, R. Hecht, E. Lewis, V. V. Palciauskas, M. Rayl, J. Swift, D. Aspnes, and J. Kane, "Static phenomena near critical points: theory and experiment", Reviews of Modern Physics **39**, 395 (1967).

[13] K. G. Wilson, "Renormalization group and critical phenomena. I. Renormalization group and the Kadanoff scaling picture", Physical review B **4**, 3174 (1971).

[14] C. Domb, M. Green, and J. Lebowitz, *Phase Transitions and Critical Phenomena*, Phase Transitions and Critical Phenomena Vol. 14 (Academic Press, 1991).

[15] M. E. Fisher and M. N. Barber, "Scaling Theory for Finite-Size Effects in the Critical Region", Physical Review Letters **28**, 1516–1519 (1972).

[16] E. Brézin, "An investigation of finite size scaling", Journal de Physique **43**, 15–22 (1982).

[17] V. Privman, *Finite Size Scaling and Numerical Simulation of Statistical Systems* (World Scientific, 1990).

[18] A. D. Bruce, "On the critical behaviour of anisotropic systems", Journal of Physics C: Solid State Physics **7**, 2089 (1974).

[19] A. Aharony and M. E. Fisher, "University in Analytic Corrections to Scaling for Planar Ising Models", Physical Review Letters **45**, 679–682 (1980).

[20] J. A. Plascak and N. P. Silva, "Mean-field renormalisation group study of the anisotropic Ising model", Journal of Physics C: Solid State Physics **19**, 4493 (1986).

[21] R. M. Z. dos Santos and R. R. dos Santos, "Anisotropy effects in the 2D transverse Ising model", Journal of Physics C: Solid State Physics **21**, 1983 (1988).

[22] X. S. Chen and V. Dohm, "Nonuniversal finite-size scaling in anisotropic systems", Physical Review E - Statistical Physics, Plasmas, Fluids, and Related Interdisciplinary Topics **70**, 7 (2004).

[23] V. Dohm, "Anisotropy and restricted universality of critical phenomena", Journal of Physics A: Mathematical and General **39**, L259–L266 (2006).

[24] V. Dohm, "Diversity of critical behavior within a universality class", Physical Review E - Statistical, Nonlinear, and Soft Matter Physics **77**, 1–38 (2008).

[25] V. Dohm, "Critical Casimir force in slab geometry with finite aspect ratio: Analytic calculation above and below Tc", EPL **86**, 20001 (2009).

[26] V. Dohm, "Crossover from goldstone to critical fluctuations: Casimir forces in confined O(n)-symmetric systems", Physical Review Letters **110**, 1–5 (2013).

[27] V. Dohm, "Crossover from low-temperature to high-temperature fluctuations: Universal and nonuniversal Casimir forces of isotropic and anisotropic systems", Physical Review E **97**, 1–30 (2018), arXiv:1708.06272.

[28] V. Dohm, "Multiparameter universality and directional nonuniversality of exact anisotropic critical correlation functions of the two-dimensional Ising universality class", Physical Review E **100**, 1–6 (2019).

[29] V. Dohm and S. Wessel, "Exact Critical Casimir Amplitude of Anisotropic Systems from Conformal Field Theory and Self-Similarity of Finite-Size Scaling Functions in $d \geq 2$ Dimensions", Physical Review Letters **126**, 60601 (2021).

[30] V. Dohm, "Multiparameter universality and intrinsic diversity of critical phenomena in weakly anisotropic systems", Phys. Rev. E **108**, 044149 (2023).

[31] V. Dohm, to appear in *50 Years of the Renormalization Group*, edited by A. Aharony, O. Entin-Wohlman, D. A. Huse, and L. Radzihovsky (World Scientific, 2024), arXiv:2311.02720 [cond-mat.stat-mech].

[32] H. G. Vaidya, "The spin-spin correlation functions and susceptibility amplitudes for the two-dimensional Ising model; triangular lattice", Physics Letters A **57**, 1–4 (1976).

[33] P. Di Francesco, P. Mathieu, and D. Sénéchal, *Conformal Field Theory*, Graduate Texts in Contemporary Physics (Springer New York, New York, NY, 1997).

[34] L. Onsager, "Crystal Statistics. I. A Two-Dimensional Model with an Order-Disorder Transition", Physical Review **65**, 117–149 (1944).

[35] B. Kaufman, "Crystal Statistics. II. Partition Function Evaluated by Spinor Analysis", Physical Review **76**, 1232–1243 (1949).

[36] V. N. Plechko, "Simple solution of two-dimensional Ising model on a torus in terms of Grassmann integrals", Theoretical and Mathematical Physics **64**, 748 (1985).

[37] V. N. Plechko, "Grassman path-integral solution for a class of triangular type decorated Ising models", Physica A: Statistical Mechanics and its Applications **152**, 51–97 (1988).

[38] V. N. Plechko, "Fermionic Path Integrals and Analytic Solutions for Two-Dimensional Ising Models", Journal of Physical Studies **1**, 554–563 (1996), arXiv:9609044 [hep-th].

[39] D. Boyanovsky, "Field theory of the two-dimensional Ising model: Conformal invariance, order and disorder, and bosonization", Physical Review B **39**, 6744–6756 (1989).

[40] V. Privman and M. E. Fisher, "Universal critical amplitudes in finite-size scaling", Physical Review B **30**, 322–327 (1984).

[41] V. Dohm, "Critical free energy and Casimir forces in rectangular geometries", Physical Review E **84**, 021108 (2011).

[42] F. A. Berezin, "The plane Ising model", Russian Mathematical Surveys **24**, 1–22 (1969).

[43] F. Kischel, "Casimir effects in anisotropic 2D systems", MA thesis (RWTH Aachen, Nov. 2020).

[44] A. N. Berker and K. Hui, "Phase diagram of the Ising model on the square lattice with crossed diagonal bonds", Physical Review B **48**, 12393–12398 (1993).

[45] V. N. Popov, *Functional Integrals in Quantum Field Theory and Statistical Physics* (Springer Dordrecht, 1983).

[46] V. Dohm, "Private correspondence", Dec. 2020.

[47] D. Stauffer, M. Ferer, and M. Wortis, "Universality of Second-Order Phase Transitions: The Scale Factor for the Correlation Length", Physical Review Letters **29**, 345–349 (1972).

[48] P. M. Morse and H. Freshbach, *Methods of theoretical physics* (McGraw-Hill, 1953).

[49] *NIST Digital Library of Mathematical Functions*, http://dlmf.nist.gov/, Release 1.1.2 of 2021-06-15, F. W. J. Olver, A. B. Olde Daalhuis, D. W. Lozier, B. I. Schneider, R. F. Boisvert, C. W. Clark, B. R. Miller, B. V. Saunders, H. S. Cohl, and M. A. McClain, eds.

[50] C. Nash and D. O' Connor, "Modular Invariance, Lattice Field Theories, and Finite Size Corrections", Annals of Physics **273**, 72–98 (1999).

[51] N. Koblitz, *Introduction to elliptic curves and modular forms*, Vol. 97 (Springer New York, 1993).

[52] D. B. Ray and I. M. Singer, "Analytic Torsion for Complex Manifolds", Annals of Mathematics **98**, 154–177 (1973).

[53] H. Bateman, *Tables of integral transforms* (McGraw-Hill, London, 1954).

[54] A. Hucht, D. Grüneberg, and F. M. Schmidt, "Aspect-ratio dependence of thermodynamic Casimir forces", Physical Review E **83**, 051101 (2011).

[55] V. Dohm and S. Wessel, "Supplemental Material: Exact Critical Casimir Amplitude of Anisotropic Systems from Conformal Field Theory and Self-Similarity of Finite-Size Scaling Functions in $d \geq 2$ Dimensions", Physical Review Letters **126**, 60601 (2021).

[56] A. Hucht, D. Grüneberg, and F. M. Schmidt, "Aspect-ratio dependence of thermodynamic Casimir forces", Physical Review E **83**, 051101 (2011).

[57] H. Hobrecht and F. Hucht, "Anisotropic scaling of the two-dimensional Ising model I: the torus", SciPost Physics **7**, 026 (2019).

[58] H. Hobrecht and A. Hucht, "Anisotropic scaling of the two-dimensional Ising model II: surfaces and boundary fields", SciPost Phys. **8**, 32 (2020).

[59] T. Nishino and K. Okunishi, "Corner Transfer Matrix Renormalization Group Method", Journal of the Physical Society of Japan **65**, 891–894 (1996).

[60] T. Nishino and K. Okunishi, "Corner Transfer Matrix Algorithm for Classical Renormalization Group", Journal of the Physical Society of Japan **66**, 3040–3047 (1997).

[61] R. J. Baxter, H. Temperley, and S. E. Ashley, "Triangular Potts model at its transition temperature, and related models", Proceedings of the Royal Society of London. A. Mathematical and Physical Sciences **358**, 535–559 (1978).

[62] R. J. Baxter, "Potts model at the critical temperature", Journal of Physics C: Solid State Physics **6**, L445 (1973).

[63] R. Baxter, "Corner transfer matrices", Physica A: Statistical Mechanics and its Applications **106**, 18–27 (1981).

[64] R. Baxter, *Exactly Solved Models in Statistical Mechanics* (Academic Press, 1982).

[65] S. Ran, E. Tirrito, C. Peng, X. Chen, L. Tagliacozzo, G. Su, and M. Lewenstein, *Tensor Network Contractions: Methods and Applications to Quantum Many-Body Systems*, Lecture Notes in Physics (Springer International Publishing, 2020).

[66] F. van der Ploeg, "Simulation of the two-dimensional Ising model using the Corner Transfer Matrix Renormalisation Group method on the square, honeycomb and triangular lattice", Bachelor's Thesis (University of Amsterdam, 2018).

[67] H.-H. Zhao, Z.-Y. Xie, Q. N. Chen, Z.-C. Wei, J. W. Cai, and T. Xiang, "Renormalization of tensor-network states", Physical Review B **81**, 174411 (2010).

[68] P. Corboz, S. R. White, G. Vidal, and M. Troyer, "Stripes in the two-dimensional t-J model with infinite projected entangled-pair states", Physical Review B **84**, 041108 (2011).

[69] L. Wang, I. Pižorn, and F. Verstraete, "Monte Carlo simulation with tensor network states", Physical Review B **83**, 134421 (2011).

[70] Y.-K. Huang, P. Chen, and Y.-J. Kao, "Accurate computation of low-temperature thermodynamics for quantum spin chains", Physical Review B **86**, 235102 (2012).

[71] P. Corboz, T. M. Rice, and M. Troyer, "Competing States in the t-J Model: Uniform d-Wave State versus Stripe State", Physical Review Letters **113**, 046402 (2014).

[72] P. Corboz, T. M. Rice, and M. Troyer, "Competing States in the t-J Model: Uniform d-Wave State versus Stripe State: Supplemental Material", Physical Review Letters **113**, 046402 (2014).

[73] H. N. Phien, J. A. Bengua, H. D. Tuan, P. Corboz, and R. Orús, "Infinite projected entangled pair states algorithm improved: Fast full update and gauge fixing", Physical Review B **92**, 035142 (2015).

[74] J. M. Yeomans, *Statistical Mechanics of Phase Transitions* (Oxford University Press, May 1992).

[75] M. M. Rams, P. Czarnik, and L. Cincio, "Precise extrapolation of the correlation function asymptotics in uniform tensor network states with application to the Bose-Hubbard and XXZ models", Physical Review X **8**, 041033 (2018).

[76] T. Burkhardt and B. Southern, "Exact critical surface of the s-state Potts model with anisotropic interactions on the triangular and honeycomb lattices", Journal of Physics A: Mathematical and General **11**, L247 (1978).

[77] M. Den Nijs, "A relation between the temperature exponents of the eight-vertex and q-state Potts model", Journal of Physics A: Mathematical and General **12**, 1857 (1979).

[78] J. Black and V. Emery, "Critical properties of two-dimensional models", Physical Review B **23**, 429 (1981).

[79] F.-Y. Wu, "The Potts model", Reviews of modern physics **54**, 235 (1982).

[80] H. Hu, R. M. Ziff, and Y. Deng, "Universal Critical Behavior of Percolation in Orientationally Ordered Janus Particles and Other Anisotropic Systems", Physical Review Letters **129**, 278002 (2022).

[81] H. Hu, R. M. Ziff, and Y. Deng, "Supplemental Material: Universal Critical Behavior of Percolation in Orientationally Ordered Janus Particles and Other Anisotropic Systems", Physical Review Letters **129**, 278002 (2022).

[82] H. Duminil-Copin, J.-H. Li, and I. Manolescu, "Universality for the random-cluster model on isoradial graphs", Electronic Journal of Probability **23**, 1–70 (2018).

[83] N. Izmailian, "Finite size and boundary effects in critical two-dimensional free-fermion models", European Physical Journal B **90**, 160 (2017).

[84] X. Wu, N. Izmailian, and W. Guo, "Shape-dependent finite-size effect of the critical two-dimensional Ising model on a triangular lattice", Physical Review E - Statistical, Nonlinear, and Soft Matter Physics **87**, 1–7 (2013).

[85] J. L. Cardy and I. Peschel, "Finite-size dependence of the free energy in two-dimensional critical systems", Nuclear Physics, Section B **300**, 377–392 (1988).

[86] J. L. Cardy, "Theory of Finite-Size Scaling", in *Current Physics–Sources and Comments, Volume 2*, edited by J. L. Cardy (North-Holland, 1988) Chap. 1, pp. 1–7.

[87] G. Delfino and E. Tartaglia, "Classifying Potts critical lines", Physical Review E **96**, 042137 (2017).

[88] J. Xu, S.-H. Tsai, D. Landau, and K. Binder, "Finite-size scaling for a first-order transition where a continuous symmetry is broken: The spin-flop transition in the three-dimensional XXZ Heisenberg antiferromagnet", Physical Review E **99**, 023309 (2019).

[89] K. Binder and D. P. Landau, "Finite-size scaling at first-order phase transitions", Physical Review B **30**, 1477–1485 (1984).

[90] K. Binder, "Critical properties from Monte Carlo coarse graining and renormalization", Physical Review Letters **47**, 693 (1981).

[91] K. Binder, "Finite size scaling analysis of Ising model block distribution functions", Zeitschrift für Physik B Condensed Matter **43**, 119–140 (1981).

[92] H. Nagata, M. Žukovič, and T. Idogaki, "Monte Carlo simulation of the three-dimensional XY model with bilinear–biquadratic exchange interaction", Journal of magnetism and magnetic materials **234**, 320–330 (2001).

[93] B. Nienhuis, E. Riedel, and M. Schick, "q-state Potts model in general dimension", Physical Review B **23**, 6055 (1981).

[94] H. Blöte and R. H. Swendsen, "First-order phase transitions and the three-state Potts model", Physical Review Letters **43**, 799 (1979).

[95] K. Binder, D. W. Heermann, and K. Binder, *Monte Carlo simulation in statistical physics*, Vol. 8 (Springer, 1992).

[96] W. Janke, "Accurate first-order transition points from finite-size data without power-law corrections", Physical Review B **47**, 14757 (1993).

[97] W. Janke and R. Villanova, "Three-dimensional 3-state Potts model revisited with new techniques", Nuclear Physics B **489**, 679–696 (1997).

[98] C. Borgs and R. Kotecký, "A rigorous theory of finite-size scaling at first-order phase transitions", Journal of Statistical Physics **61**, 79–119 (1990).

[99] C. Borgs and R. Kotecký, "Finite-size effects at asymmetric first-order phase transitions", Physical Review Letters **68**, 1734 (1992).

[100] C. Borgs and W. Janke, "New method to determine first-order transition points from finite-size data", Physical Review Letters **68**, 1738 (1992).

[101] F. Wang and D. Landau, "Determining the density of states for classical statistical models: A random walk algorithm to produce a flat histogram", Physical Review E **64**, 056101 (2001).

[102] F. Wang and D. P. Landau, "Efficient, multiple-range random walk algorithm to calculate the density of states", Physical Review Letters **86**, 2050 (2001).

[103] D. Landau and K. Binder, *A guide to Monte Carlo simulations in statistical physics* (Cambridge University Press, 2021).

[104] C. Borgs and S. Kappler, "Equal weight versus equal height: a numerical study of an asymmetric first-order transition", Physics Letters A **171**, 37–42 (1992).

[105] M. S. Challa, D. P. Landau, and K. Binder, "Finite-size effects at temperature-driven first-order transitions", Physical Review B **34**, 1841 (1986).

Acknowledgments

Firstly, I would like to thank my supervisor, Stefan Wessel, for the continued support and great discussions during my studies. I also owe great thanks to my family, friends, and colleagues, especially from the Institute for Theoretical Solid State Physics and the Institute for Theory of Statistical Physics for the fun exchanges and conversation, not only about physics, during lunch and the coffee breaks. I would also like to thank my other collaborator, Volker Dohm, for the interesting debates about the different projects we worked on together.

I acknowledge funding through the Deutsche Forschungsgemeinschaft (DFG) research training group RTG 1995 and thank the IT Center at RWTH Aachen University for the computation time.